Oxygen- and Nitrogen-Group Transfers in Aryl-Nitroso Iron Complexes

Maryam Habibian

A Thesis
in
The Department
of
Chemistry and Biochemistry

Presented in Partial Fulfillment of the Requirements
for the Degree of Master of Science (Chemistry) at
Concordia University
Montreal, Quebec, Canada

January 2011

CONCORDIA UNIVERSITY

School of Graduate Studies

This is to certify that the thesis prepared

By: Maryam Habibian

Entitled: Oxygen- and Nitrogen-Group Transfers in Aryl-Nitroso Iron Complexes

and submitted in partial fulfillment of the requirements for the degree of

Master of Science (Chemistry)

complies with the regulations of the University and meets the accepted standards with respect to originality and quality.

Signed by the final examining committee:

Dr. Ann English	Chair
Dr. Pat Forgione	Examiner
Dr. Cerrie Rogers	Examiner
Dr. Xavier Ottenwaelder	Supervisor

Approved by ______________________________
Chair of Department or Graduate Program Director

January 6th, 2011 ______________________________
Dean of Faculty

Abstract

Oxygen- and Nitrogen-Group Transfers in Aryl-Nitroso Iron Complexes

Maryam Habibian

Transition metal complexes containing imido ligands (M=NR) are an important class of coordination compounds implicated in nitrogen-group-transfer reactions such as aziridination. The present thesis investigates the formation of iron-imido complexes via deoxygenation of iron-nitroso complexes that have a nitroso (RN=O) functionality tethered to their main ligand framework. This process is at the heart of important oxygen-atom-transfer (OAT) reactions such as the epoxidation of alkenes or the hydroxylation of organic substrates.

For this purpose, the new pentadentate monoanionic ligand $\mathrm{BPAEB_{NHOH}}$ was synthesized and disproportionated by Fe(II) salts to yield N-bonded monomeric iron-nitroso complexes $[\mathrm{Fe^{(II)}BPAEB_{NO}(OAc)}]$ **(1)** and $[\mathrm{Fe^{(II)}BPAEB_{NO}(MeCN)}](\mathrm{OTf})$ **(2)** as well as the iron-amine complex $[\mathrm{Fe^{(II)}BPAEB_{NH_2}(OAc)}]$. These complexes were characterized by X-ray crystallography and spectroscopic techniques. Complexes **(1)** and **(2)** were found to be able to perform OAT to phosphine reagents ($\mathrm{PR_3}$) in moderate to high yields. Although not isolated, iron-iminophosphorane ($\mathrm{M{-}N{=}PR_3}$) compounds were identified as the main products of the reaction. Detailed kinetic and mechanistic studies of this reaction suggest that the mechanism does not involve a simple rate law. Control experiments and comparisons with the literature suggest that the mechanism involves the replacement of acetate and acetonitrile ligands with a phosphine ligand, before the nitroso group is deoxygenated. These results suggest the formation of an iron-imido intermediate, prior to its trapping by phosphine reagents.

Acknowledgements

There are numerous individuals I would like to acknowledge for helping me during my studies at Concordia University. First and foremost, I would like to express my sincere gratitude to my research supervisor, Dr. Xavier Ottenwaelder for his guidance, dedication, and support. It was through his detailed and constructive comments that I developed the critical mindset to undertake scientific challenges. I am also greatly indebted to him for helping me during my early years of transition as an international student. I am very grateful to my committee members, Dr. Pat Forgione and Dr. Cerrie Rogers for their continuous guidance and support. I owe my deep gratitude to my good friends at the XoRG, Laura Chaloner and Mohammad Askari, for their help, understanding, friendship, and for keeping me grounded. The joyful moments that we created together are unforgettable.

I would like to thank many individuals who helped me at various stages of this project: Dr. Sébastien Robidoux, Dr. Louis Cuccia, Dr. Heidi Muchall, Dr. Hein Schaper at the University of Montreal, Alain Tessier at CBAMS at the Concordia University, Francine Bélanger at the crystallography center at the University of Montreal, all my friends at Concordia University: Maria Kaltcheva, John Chin, Paknoosh Pakarian, Badr Benasilla, Dirk Ortgies, Avid Hassanpour, Stephane Sevigny, Michel Boisvert, and everyone else in the department for creating a nurturing and friendly working atmosphere throughout my time as a graduate student in the Chemistry and Biochemistry department. I am very grateful to my parents who have supported and encouraged me my entire life. Last but certainly not least, my special appreciation goes to my true friend and husband, Ali, for

his unconditional support, understanding, and endurance. His love, friendship, and respect has always kept my spirits high and motivated me to learn and work harder.

My love and this thesis are dedicated to him.

Table of Contents

List of Figures

List of Tables

List of Abbreviations

Ad: Adamantyl

B.M: Bohr magneton

BPA: Bis(2-pyridyl)amine

BPMEN: *N,N'*-dimethyl-*N,N'*-bis(2-pyridylmethyl)ethane-1,2-diamine

DFT: Density Functional Theory

ESI-MS: Electron spray ionization-mass spectrometry

ESR: Electron Spin Resonance

Me_3tacn: 1,4,7-trimethyl-1,4,7-triazacyclononane

MMOH: Methane monooxygenase hydroxylase

MMOR: Methane monooxygenase reductase

NGT: Nitrogen-group-transfer

Ns: *p*-Nitrobenzenesulfonyl

NTB: tris(2-benzimidazolymethyl)amine

OAT: oxygen atom transfer

PhTPA: (6-Phenyl-pyridin-2-ylmethyl)-bis-pyridin-2-ylmethyl-amine

sMMO: Soluble methane monooxygenase

SQUID: superconducting quantum interference device

TMS: tetramethylsilane

TPA: tris(2-pyridylmethyl)amine

TPP: 5,10,15,20-tetraphenylporphyrinate

Ts: *p*-Toluenesulfonyl

Por: Porphyrin

1. Introduction

The aim of this project is to study new methods in the synthesis of complexes with reactive metal-imido/nitrenoid structures. In the following thesis we investigate iron-nitroso complexes as novel reagents that could result in the formation of such structures by transferring the oxygen-atom at the nitroso group to a substrate. The resultant iron-imido/nitrenoid complexes are then studied in nitrogen-group-transfer reactions. This chapter is to review the literature on the methods of metal-catalyzed oxygen-atom and nitrogen-group transfer reactions, as well as explain the nature of intermediates in these reactions. At first, the significance of each of these reactions in organic synthesis is described, followed by a review on important or relevant examples of metal-catalyzed oxygen-atom/nitrogen-group transfer reactions. In the end the nature of metal-oxo/imido/nitrenoid species, the intermediates of such reactions, and their reactivity and synthesis are presented.

1.1 Oxygen Atom Transfer Reactions in Organic Synthesis

Oxidation/reduction of generalized molecule X/XO by formal gain or loss, respectively, of an oxygen atom is a widespread process known as oxygen atom transfer (OAT) reaction. In it, the oxygen donor is reduced and the oxygen acceptor is oxidized with the result that the atom transferred is maintained as an oxide in reactant and product (Figure 1).

$$\mathrm{X} + \mathrm{AO} \rightleftharpoons \mathrm{XO} + \mathrm{A}$$

Figure 1. Oxygen-atom transfer equation

OAT reactions constitute an important class of reactions that have been extensively used in organic synthesis.[1,2] Being a key step in converting petroleum-based hydrocarbons to useful chemicals in higher oxidation state such as alcohols, carbonyl compounds, and epoxides, OAT reactions have attracted a considerable amount of interest in the recent years. Products from these reactions are produced annually in million ton scale and find applications in all areas of chemical industries, ranging from pharmaceutical to large-scale commodities.[1] However, due to the relative inertness of hydrocarbons, selective, one-step transfer of an oxygen atom to a hydrocarbon is difficult to achieve under mild conditions. Commercial synthesis of propylene oxide, as an example, involves epoxidation of propylene with oxygen-containing oxidants such as t-butyl hydroperoxide or ethylbenzene hydroperoxide (Figure 2).[3] Nevertheless, involvement of elevated temperature and pressure (100-200˚ C, 10-50 bar) during the reaction, formation of stoichiometric amounts of by-products and low reaction yields has motivated scientists to find better catalytic oxidation alternatives such as metal-catalyzed oxidation techniques.[3]

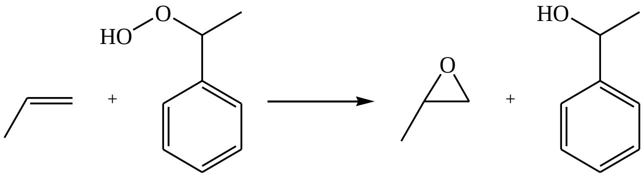

Figure 2. Epoxidation of propylene with ethylbenzene hydroperoxide

While alkene epoxidation methods are many,[4] selective CH bond functionalization such as CH bond hydroxylation is arguably more valuable and challenging. Considering the high abundance of CH bonds, this transformation has broad potential in synthesis,[5] such as allylic or benzylic oxidation, aromatic CH bond hydroxylation, and so on.[6] Achieving selectivity among many different CH bonds, still, remains a challenge.

Several methods exist for hydroxylation of unactivated CH bonds, which mostly involve the use of a transition metal catalyst[6] such as: use of Pt complexes in strongly acidic media,[7-10] organometallic catalysis through CH insertion followed by oxidation,[11-13] autoxidation (Fenton chemistry).[14] Other methods use organic oxidants such as dioxiranes[15] or oxaziridines (Figure 3).[16] Most of these methods rely on the strong electrophilic character of the active species in order to counter the high CH bond strength, low acidity, and low nucleophilicity of hydrocarbon substrates.

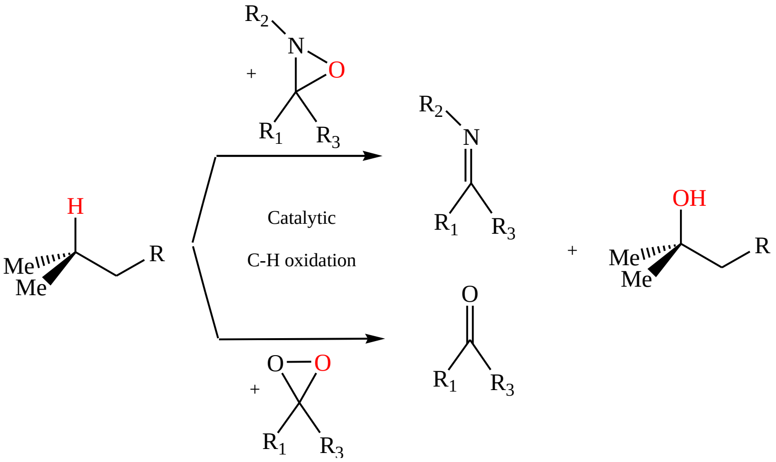

Figure 3. Proposed oxaziridine (top) and dioxirane (bottom) -catalyzed CH hydroxylations.[16,17]

Whereas most of these methods employ diverse transition metals and oxidants, some being harmful, nature has developed mild and selective oxygenation processes using only benign Fe and Cu ions and dioxygen (O_2) as terminal oxidant. The active species in most cases is an electrophilic oxygen bonded to the metal, as seen in cytochrome P450[18-20] or in non-heme Fe monoxygenase enzymes.[21] Endeavours to overcome the shortcomings of non catalytic OAT systems as well as mimicking the efficiency of natural OAT systems have resulted in the highly progressive field of “Metal-catalyzed oxygen-atom-transfer”. Extensive work done in this field is highlighted in the next section.

1.2 Metal-Catalyzed Oxygen-Atom Transfer Reactions

1.2.1 Biological Inspiration

The selective oxidation of organic molecules in biological systems can happen through redox processes mediated by metalloenzymes and molecular oxygen. These reactions can be divided into two classes: oxygenases and oxidases. Oxygenases catalyze the transfer of one (monooxygenases) or two (dioxygenases) oxygen atoms to organic substrates through an inner-sphere mechanism. This mechanism involves coordination of an oxygen atom to the metal, increasing the oxidation state of the metal by the number of two, to form a metal-oxo intermediate (**1**) (Figure 4). This intermediate then transfers the coordinated oxygen-atom to the substrate, resulting in a reduced metal center (**2**) (Figure 4). The redox mechanism happens in the inner coordination sphere of the metal complex. Reoxidation by molecular oxygen, two protons, and two electrons regenerates the metal-oxo and yields water as a by-product. Oxidases, on the other hand, do not involve oxygen-atom transfer to the substrate. Instead, the metal oxidant (**3**) catalyzes a formal dehydrogenation, resulting in the loss of two electrons and two protons from the substrate and the formation of a reduced metal species (**2**). Molecular oxygen then acts as an electron acceptor, regenerating the oxidized metal species (**3**). Water or hydrogen peroxide is the by-product of these oxidations.[22]

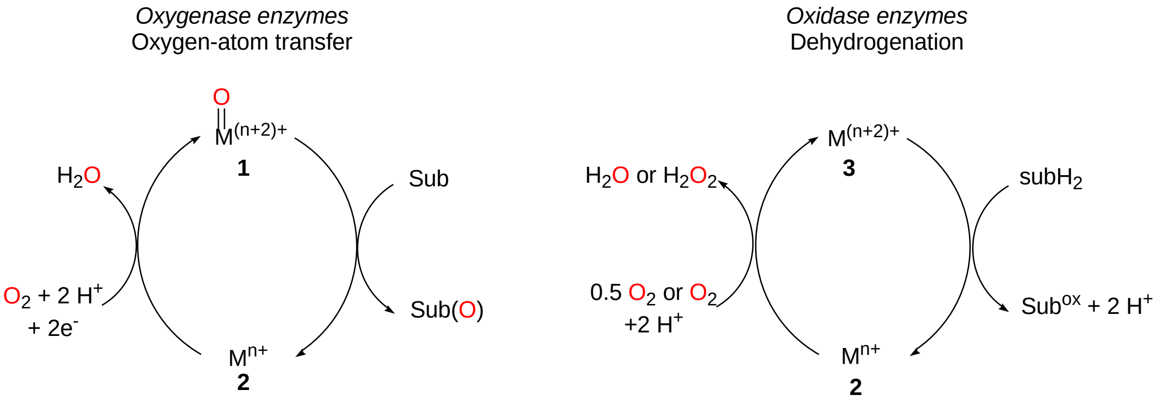

Figure 4. Oxygenase vs. Oxidase enzymatic mechanisms [22]

Oxygenase-type enzymes, performing metal-catalyzed OAT, are of interest in this thesis. Some of the most important examples of such enzymes are cytochrome P450 enzymes and none-heme Fe monooxygenases.

Cytochrome P450 enzymes constitute a large family of cysteinato-heme enzymes which are present in all forms of life. In all these enzymes the prosthetic group is constituted of an iron(III) protoporphyrin IX coordinated to the thiolate group of a proximal cysteine amino acid of the protein (Figure 5). More than fifty years after the first isolation and characterization of these enzymes, the nature of the active species in the oxygen insertion step of the mechanism is still a matter of intense debate, though it is believed to proceed through formation of high oxidation state iron-oxo intermediates.[22,23] The proposed mechanism, outlined in Figure 5, represents various intermediates formed in the catalytic cycle before leading to the formation of “compound I” which is believed to be the key intermediate in charge of OAT in this cycle. This compound is a reactive iron(IV)-oxo intermediate with a radical cation porphyrin ligand (F). The exact nature of this intermediate is still a matter of debate and recently it has also been suggested to be more of an iron(V)-oxo complex.[24] This intermediate species then quickly transfers the activated oxygen to the substrate and returns to the water-bound iron(III) resting state (A) (Figure 5).[18,22,23]

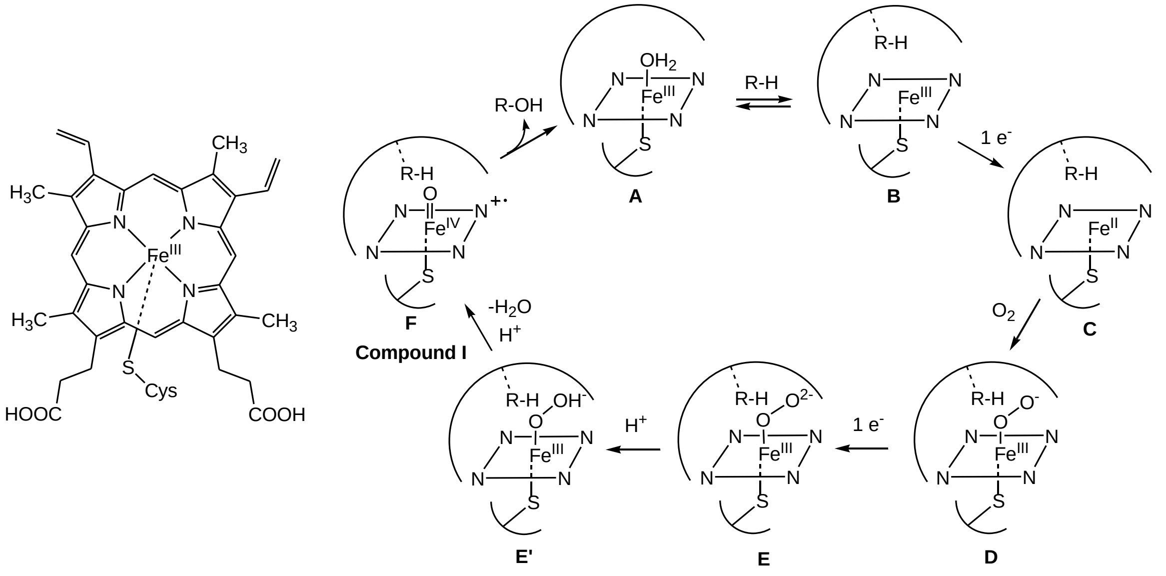

Figure 5. Left: Protoporphyrin IX in a human cytochrome P450 enzyme Right: Schematic representation of the different intermediates generated during the catalytic cycle of cytochrome P450.

Soluble methane monooxygenase (sMMO) enzyme is a non-heme iron monooxygenase extracted from methanotrophic bacteria. This enzyme catalyzes the remarkable oxidation of methane to methanol at ambient temperatures and pressures via diiron(III)–peroxo and diiron(IV) intermediates.[25] Three protein components are required for efficient catalysis of this enzyme: a dimeric hydroxylase (MMOH) with two carboxylate-bridged diiron active sites, a reductase (MMOR) which acquires electrons from NADH and transfers them to the hydroxylase, and a regulatory protein that couples electron consumption to substrate oxidation.[26] The proposed catalytic cycle of this enzyme is shown in Figure 6a. Upon two-electron reduction, the resting state of the hydroxylase (H_{ox}) active site, which is a bis(μ-hydroxo)bis(μ-carboxylato)diiron(III), is reduced to the diiron(II) form (H_{red}).

The bridging hydroxide ligands then dissociate, and in the presence of the regulatory protein the diiron center reacts rapidly with dioxygen. Following this reaction a sequence of intermediates is formed which rapidly convert to each other in a proton-driven processes, ending up as intermediate Q.[27,28] Spectroscopic characterization of this intermediate revealed it to be a diiron(IV) cluster with a diamagnetic ground state due to antiferromagnetic coupling between the iron atoms (Figure 6b).[29,30] The reactivity of this intermediate has been extensively investigated with different substrates, verifying that this species is responsible for methane oxidation.[31,32] The mechanism of methane hydroxylation by Q is not very well known but Density Functional Theory (DFT) studies suggest that it is initiated by a proton-coupled outer-sphere electron transfer from a methane C-H bond and a bridging oxygen atom to one of the iron atoms.[33] This results in the formation of a transiently bound, substrate-derived radical intermediate that reacts further with the other iron-oxygen bond to generate methanol and continue the catalytic cycle towards the resting state (Figure 6c).[33] In the absence of substrate, Q decays slowly to H_{ox} by a mechanism that proceeds through a recently identified intermediate Q* of unknown composition.[26] Most of the literature on the hydroxylation mechanisms of MMOH has focused on reactions of Q intermediate, but recent findings suggest that H_{peroxo} can also react with hydrocarbon substrates.[28,29]

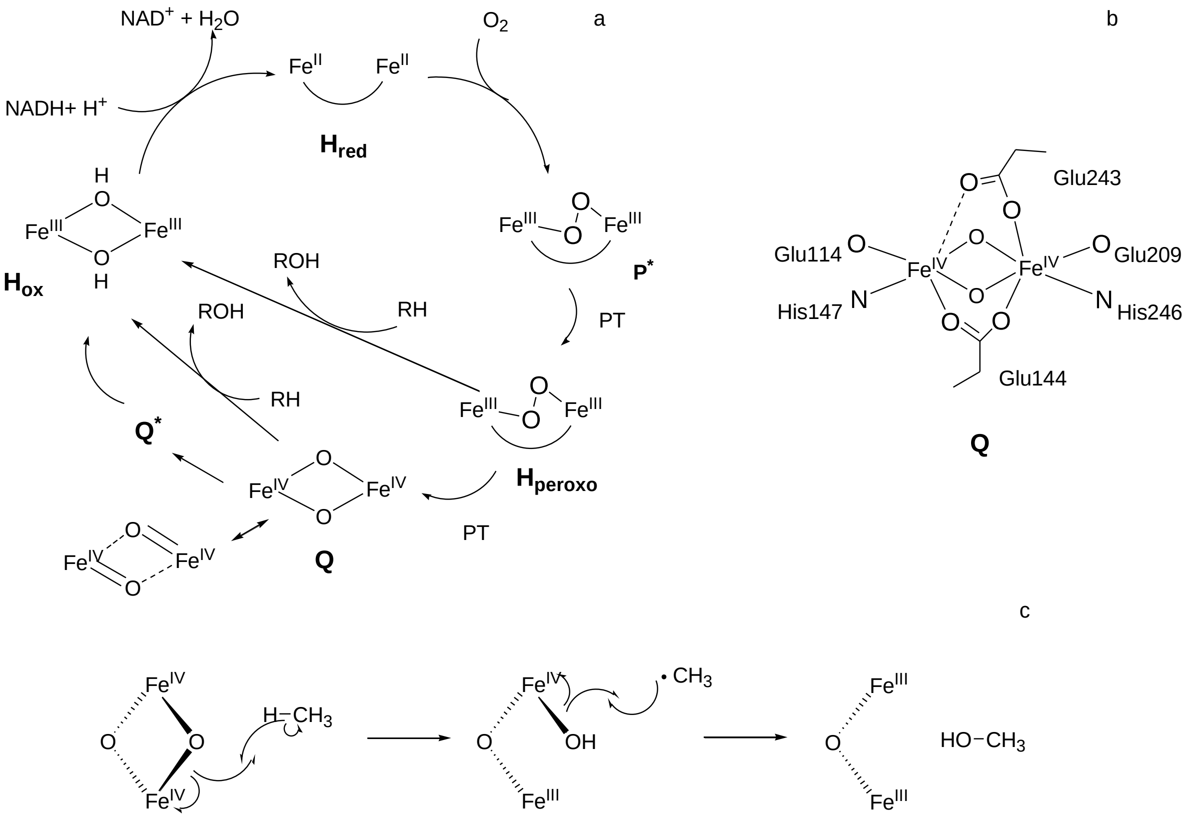

Figure 6. a) Current working model of catalysis by the MMOH diiron center[34] b) Proposed structure of Q intermediate in MMOH catalytic cycle[25] (PT: proton transfer) c) Proposed mechanism of methane hydroxylation by Q intermediate[34]

Mononuclear non-heme iron enzymes such as α-ketoglutarate-dependent enzymes or rieske-type dioxygenases also function based on the activation of dioxygen. The catalytic cycle in these enzymes also involve formation of Fe(IV)-oxo species as key intermediates in the OAT processes.[35,36]

In the past few years vast studies have been focused on revealing the exact mechanism of OAT in enzymatic systems. Successes in the synthesis and catalytic studies of synthetic analogues of these enzymes have also greatly helped to resolve the unknown mechanistic pathways in biological systems. [37,38] Examples of such synthetic analogues are discussed in the following section.

1.2.2 Synthetic Catalysts

Many useful catalysts that mediate selective OAT have been inspired by the mechanism of oxidation seen in the monooxygenase family of enzymes. In their pioneering work, Breslow *et al*. used synthetic porphyrins for OAT to both saturated and unsaturated systems (Figure 7a).[39] Porphyrins (also called heme-type ligands) are macrocyclic aromatic ligands that are doubly deprotonated to make a tetradentate planar ligand environment, bringing exceptional stability to the metal complex. The chiral salen epoxidation catalysts, which were first developed by Jacobsen, contain a manganese ion in the center of a small-molecule ligand that incorporates heme characteristics such as being tetradentate, negatively charged, planar and aromatic (Figure 7b).[40] The parallels with the cytochrome P450 active site can be seen from the structures of these synthetic catalysts.[41]

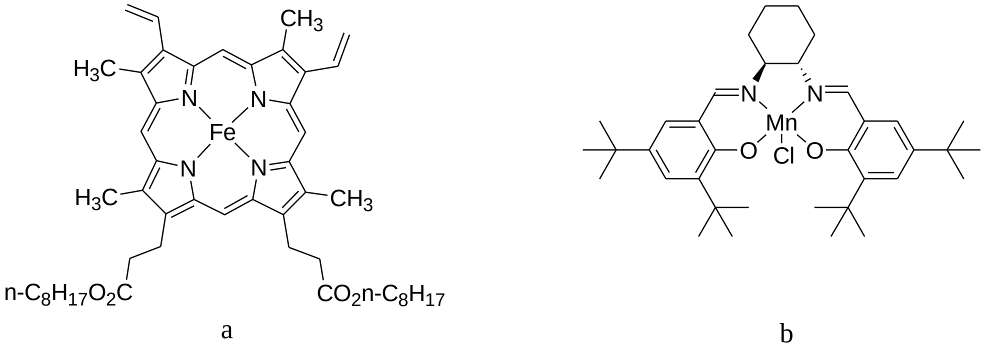

Figure 7. (a) Synthetic iron porphyrin catalyst used by Breslow for oxygen transfer reactions. [39] (b) Manganese salen epoxidation catalyst developed by Jacobsen for oxygen transfer to olefins [40]

An improved procedure with Jacobsen's catalyst is used now as a commercial method in enantioselective epoxidation of alkenes. This method allows the enantioselective formation of epoxides from various *cis*-substituted olefins by using a chiral Mn-salen catalyst and a stoichiometric oxidant such as bleach (Figure 8).[42]

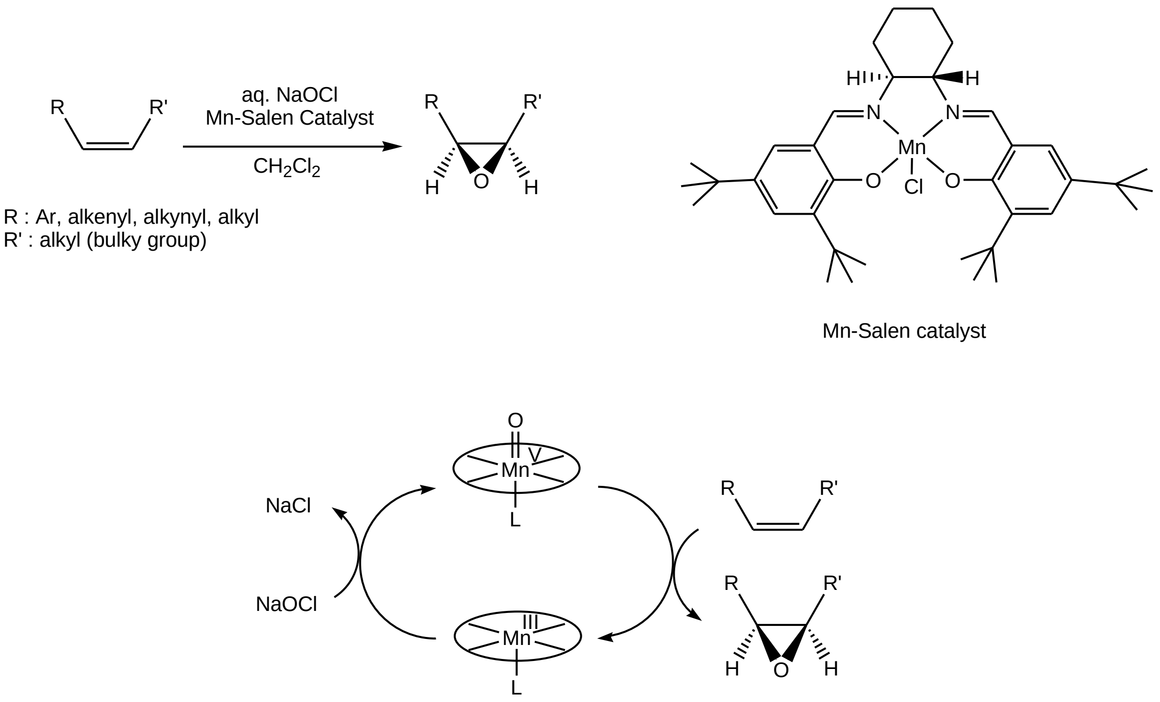

Figure 8. Top: Use of Jacobsen catalyst in enantioselective epoxidation of cis-substituted olefins. Bottom: Mechanism of Jacobsen epoxidation [42]

Sharpless and Katsuki have also developed one of the first widely applicable processes, utilizing readily available reagents to selectively epoxidize allylic alcohols with *tert*-butyl hydroperoxide as the stoichiometric oxygen atom donor.[43] Later, Sharpless was able to achieve the asymmetric dihydroxylation of olefins with an osmium catalyst and potassium ferricyanide as the terminal oxidant (Figure 9).[43] Sharpless was awarded the Noble prize in chemistry in 2001 for his work on chirally catalyzed oxidation reactions.

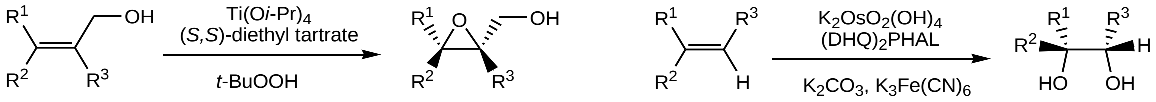

Figure 9. Left: Sharpless-Katsuki asymmetric epoxidation Right: Sharpless asymmetric dihydroxylation

During the past decades, extensive work has been done to design better synthetic metal catalyzed OAT systems with various ligand sets.[44] The catalytic activity of iron, for instance, has been screened with various non-heme polyamine ligand systems in the presence of different peroxides for alkane hydroxylation.[44] Some examples of the ligands used in these OAT iron catalysts are shown in Figure 10.

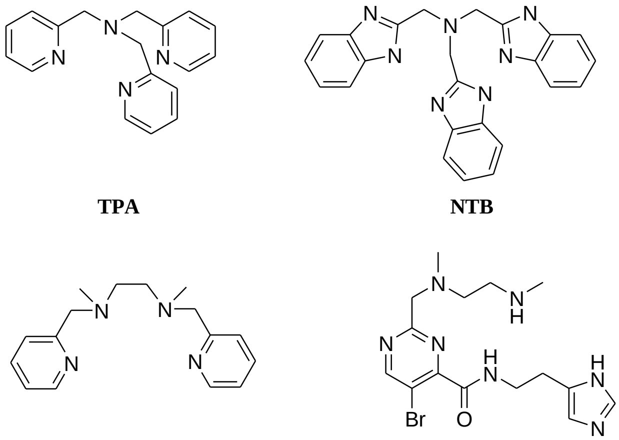

TPA

NTB

BPMEN

PMC-H

Figure 10. Ligands used in preparation of OAT iron catalysts: $[FeCl_2(TPA)](ClO_4)$ [45], $[Fe_2O(OAc)(NTB)_2](ClO_4)_3$ [46], $[Fe_2O(OAc)(BPMEN)_2](ClO_4)_3$ [47], $[Fe(PMC)]^{2+}$ [48]

1.3 Nitrogen-Group Transfer in Organic Synthesis

Nitrogen-group (nitrene) -transfer (NGT) reactions, analogous to OAT reactions, are used to incorporate nitrogen-containing functional groups into organic systems. These reactions have found vast application in aziridination and amination of organic compounds. The nature of nitrene species and their application in NGT reactions are explained in the following sections.

1.3.1 Nitrenes: Structure and Synthesis

Nitrenes are uncharged, electron-deficient molecular species that contain a monovalent nitrogen atom formally surrounded by only six electrons (Figure 11). Nitrenes, being nitrogen analogues of carbenes, are found in singlet or triplet electronic states. In a singlet nitrene the electrons are arranged as two lone pairs, whereas in triplet nitrenes these electrons are present in three orbitals, one filled and two half-filled (Figure 11).[49] Triplet nitrenes, therefore, show diradical behavior. Given that nitrenes have four non-bonded electrons and lack two electrons to form a stable octet, they are considered to be very reactive electrophilic species. Whether singlet or triplet, nitrenes are not stable molecules and react readily with a great variety of organic substrates as soon as they are formed.[49]

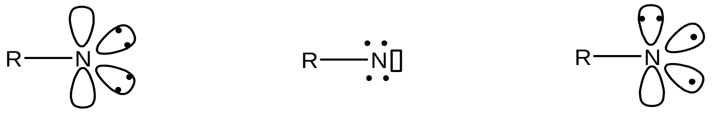

Figure 11. Singlet (left) and triplet (right) states of nitrenes

There are a few methods for *in situ* preparation of nitrenes (Figure 12). These include thermolysis or photolysis of (a) azides with expulsion of nitrogen gas (analogous to the formation of carbenes from diazo compounds) and (b) isocyanates with expulsion of carbon monoxide (analogous to carbene formation from ketenes). The most commonly employed nitrene source is iminophenyliodinanes (PhI=NR). Recently, new nitrogen source alternatives have also been investigated, such as chloramine-T (TsN(Cl)Na), or bromamine-T (TsN(Br)Na).[49]

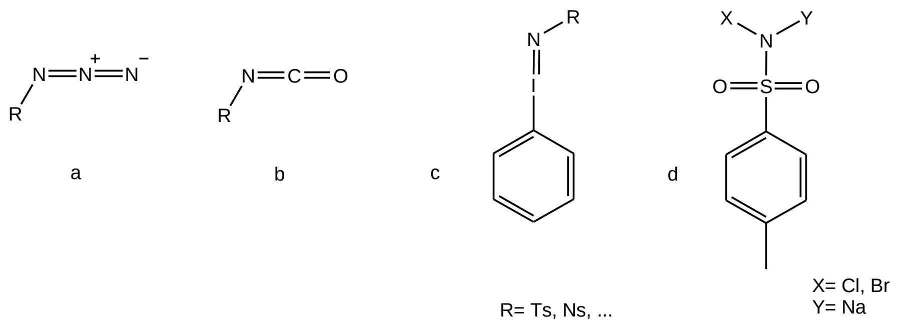

Figure 12. Common sources of nitrene. a) Azides b) Isocyanates c) Imidophenyl iodinanes (Ts: *p*-toluenesulfonyl, Ns: *p*-nitrobenzenesulfonyl) d) Chloramine and Bromamine -T

These reagents are generally used in combination with a transition metal catalyst to promote the formation of the “NR” moiety as well as to selectively drive the nitrene transfer towards organic molecules (Figure 13).[49-52]

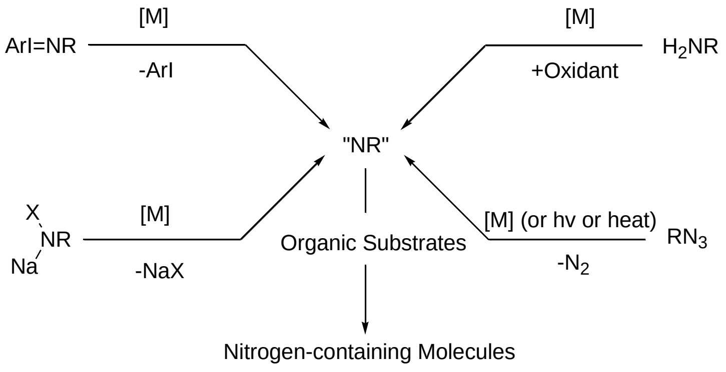

Figure 13. General scheme for nitrene formation and transfer catalyzed by metals [49]

1.3.2 Reactions

Nitrene transfer reactions are fundamental tools in organic synthesis. In contrast to the apparent lack of biosynthetic schemes for nitrogen group transfer, synthetic systems that deliver nitrene fragments to organic molecules in a direct fashion do exist. These reactions encompass (i) aziridination and (ii) amination, and have been used to synthesize new compounds and to streamline existing synthetic routes.[53]

The type of aziridination reaction that involves a nitrogen-group transfer is usually by metal-catalyzed transfer of a nitrene to an alkene. The product of this reaction, an aziridine, is a three membered ring incorporating the nitrogen of the “NR” group and two methylene groups (Figure 14).

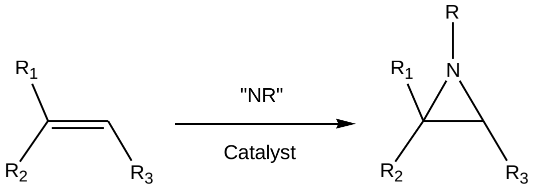

Figure 14. General scheme for catalytic aziridination of olefins through nitrene transfer

Aziridines are the nitrogen analogues of epoxides and exhibit similar reactivity patterns as electrophilic reagents. They undergo highly regio- and stereoselective ring-opening transformations and hence are very useful building blocks for organic synthesis (Figure 15). This versatile reactivity has led to continuous efforts to discover new and efficient methods that can produce aziridines from simple olefins.[53-55] In addition, aziridines may exhibit antitumor or antibiotic activity or some other biological properties, which makes them attractive synthetic targets in their own right.[56,57]

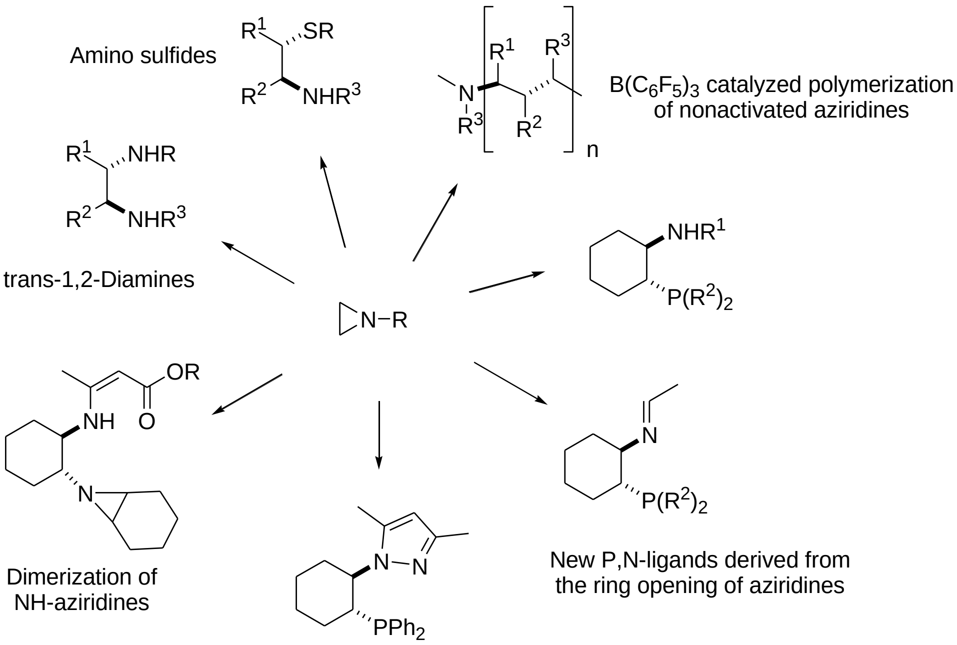

Figure 15. Aziridines ring opening products [50]

The formal insertion of a nitrene unit into a saturated CH bond, which constitutes a strategy for CH bond functionalization, and the concomitant formation of an amine is called amination (Figure 16).

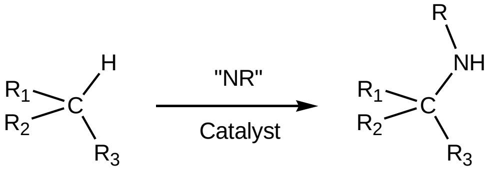

Figure 16. General scheme for catalytic C-H amination of hydrocarbons through nitrene transfer

It is also called “oxidative amination” due to some one-pot examples in which the nitrene source is generated from an iminoiodane which itself is prepared *in situ* from an amine and an oxidant such as PhI(OAc)$_2$.[54] This direct use of amines makes CH amination very attractive for organic synthesis purposes, since it makes an easy protocol for the formation of the desired nitrene reagents directly from readily available amine sources and in a one-pot with the olefin and the proper metal catalyst (Figure 17).[58]

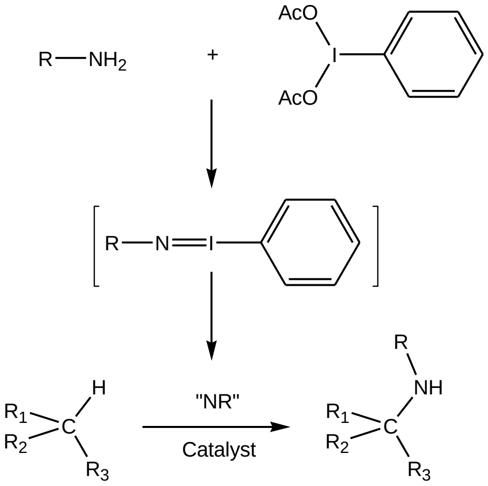

Figure 17. *In situ* synthesis of the nitrene source by oxidation

Compared to aziridination methods, the amination methodology is less explored, probably due to the more inert nature of CH bonds. Only recently has some research been done in this field by utilization of metal catalysts.[41,49,52,53,59] Progress in this field is discussed in detail in the next section.

Due to their highly electrophilic nature, nitrenes may also react with any other nucleophiles other than hydrocarbons. This feature has been used to study the mostly unclear pathways that are involved in the formation and reaction of nitrenes. Reagents such as phosphines (PR_3), phosphates ($P(OR)_3$), and carbon monoxide (CO) have been used to “trap” nitrene intermediates. Such reactions have been used readily as an indirect proof of nitrene formation based on the nitrene transferred products. These reactions also act as a termination point for chains of reactions that occur upon release of a very reactive nitrene intermediate in the reaction mixture. Phosphines (PR_3, R: aryl and/or alkyl) and carbon monoxide, for example, have been used as nitrene trapping reagents to form iminophosphoranes (phosphorimidates)[60] and isocyanates,[61] respectively (Figure 18).

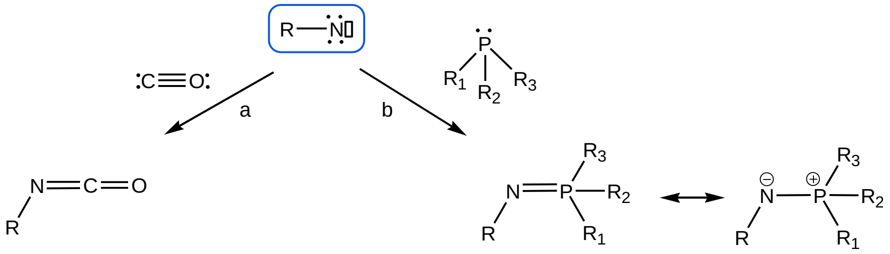

Figure 18. Formation of a) isocyanates and b) iminophosphoranes by reaction of nitrene reagents with carbon monoxide and phosphines, respectively

1.4 Metal-Catalyzed Nitrogen-Group Transfer

As mentioned before, the use of proper transition metal catalysts is the key to achieving selective nitrene transfer processes. A transition metal catalyst both assists the nitrene formation and selectively drives the nitrene moiety towards the desired reaction site. This mechanism is fundamentally possible through two pathways: the non-redox pathway and the redox pathway, both of which involve two steps (Figure 19).

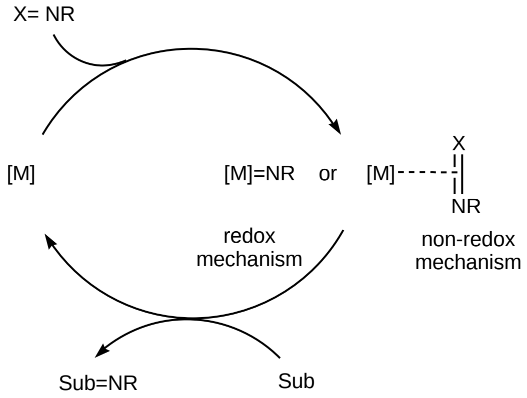

Figure 19. General metal catalyzed nitrene transfer mechanism (Sub=substrate, X=Ts, Ns,...)

In the non-redox pathway, the first step involves the formation of a complex between the metal catalyst and the nitrene precursor (metal-nitrenoid), without oxidative transfer of the nitrene group to the catalyst. This complex then transfers the nitrene group to a substrate. In the redox pathway, the first step is nitrene transfer to the metal complex with formal oxidation of the metal center, to form a metal-imido/nitrenoid complex (more details in section 1.5). This oxidized metal complex then transfers the nitrene group to a substrate. When the mechanism follows the redox pathway, the reactivity of the catalyst is greatly influenced by the stability of the metal nitrenoid complex. This point stands out because overly stable complexes are often unreactive to perform efficient catalytic nitrene transfer, wheras unstable complexes can undergo several undesired side-reactions and hence would not be useful.[62]

In the following sections, selected examples of mid- to late- transition metal catalyzed nitrene transfer reactions are presented with an emphasis on the nature of the intermediate. For brevity, the scope of this section concentrates on nitrene transfer reactions catalyzed by group 8 transition metal (Os, Ru, Fe) complexes. Important cases of Mn- and Rh- catalyzed nitrene transfer reactions are also discussed.

1.4.1 Osmium-Catalyzed Nitrene Transfer Complexes: An Early Example

One of the first examples of metal-catalyzed nitrene transfer is the osmium-catalyzed oxyamination of olefins by Chloramine-T introduced by Sharpless and co-workers (Figure 20).[63] This reaction is proposed to proceed by an $Os(O)_3(Ts)$ intermediate (Ts = *p*-toluenesulfonyl) in analogy to an earlier work by the same group utilizing $Os(O)_3(NR)$ [R = *t*-Bu, 1-adamantyl (Ad)] for a stoichiometric oxyamination.[64]

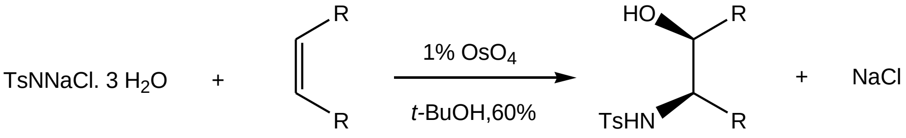

Figure 20. General metal-catalyzed nitrene transfer mechanism

1.4.2 Manganese- and Iron-Catalyzed Nitrene Transfer

In 1982 Breslow and co-workers reported that 5,10,15,20-tetraphenylporphyrinato (TPP) complexes of manganese and iron could catalyze the electrophilic sulfonamidation of cyclohexane by *N*-(*p*-toluenesulfonyl)iminophenyl iodinane (PhINTs).[65-67] This work was based on an earlier hydroxylation reaction catalyzed by an analogous iron porphyrin complex with iodosobenzene (PhIO).[39,68] Intramolecular amidation of benzylic positions was found to have the highest reaction yields. Dawson and Breslow[66] discovered that microsomal cytochrome P450-LM2 purified from rabbit liver catalyzed both intermolecular and intramolecular sulfonamidation in high yields. Based on this observation it was proposed that amidation reactions with this catalytic system proceeded via formation of iron or manganese porphyrin high oxidation state intermediates, analogous to high oxidation state oxo intermediates in hydroxylation reactions in living systems. Mansuy and co-workers developed [Fe(TPP)Cl] and [Mn(TPP)Cl] as nitrene transfer reagents to olefins.[69-72] Different substrates led to the formation of different product stereochemistry, suggesting that aziridination and epoxidation may not proceed through analogous mechanisms. Another challenge with such catalytic systems is to select between aziridination and amination on demand. This was made possible by altering the substituents on the porphyrin ring.[70,71,73] Nitrene transfer via iron- and manganese- porphyrin complexes and by PhINTs is proposed to proceed through the following mechanistic pathway (Figure 21).

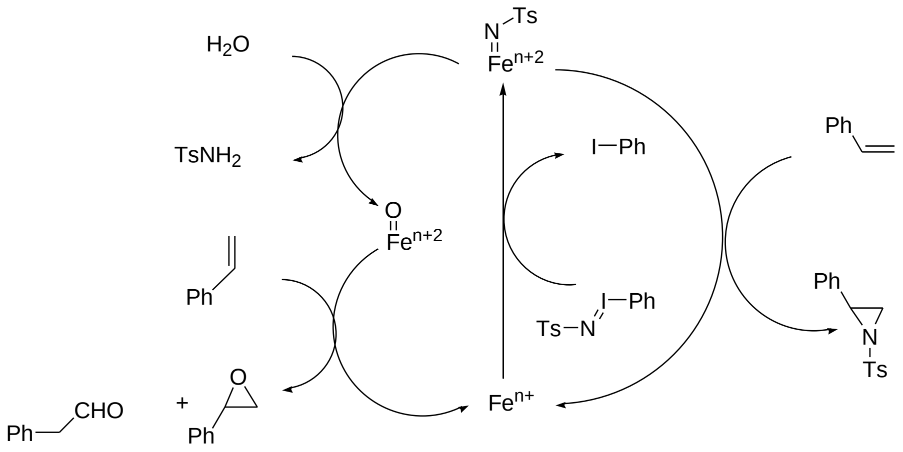

Figure 21. Proposed catalytic cycles for iron and manganese complexes catalyzed reaction of styrene with PhINTs. [74]

More recently, iron-corrole complexes were studied as nitrene-transfer reagents with chloramines-T and proved to have an incresed selectivity for aziridination of olefins compared to iron-porphyrin analogues. This finding was justified as corroles stabilize high oxidation state metals significantly better than porphyrins. [74]

While there is still a great deal of interest focused on iron and manganese porphyrin systems, iron complexes with ligands that are easier to synthesize have been made and proved to be able to perform arene amination intramolecularly. Que and co-workers investigated the reactivity of $[(6\text{-PhTPA})\text{Fe}^{II}(\text{NCCH}_3)_2](\text{ClO}_4)_2$ (PhTPA = *o*-phenyl tris(2-pyridylmethyl)amine) with PhINTs. The formation of an iron-nitrenoid intermediate was postulated based on the observed efficient and selective *ortho*-amination of the phenyl substituent on the ligand (Figure 22).[75] This example was the first example of amination at a non-activated aromatic CH bond, which is believed to proceed due to the very reactive and unstable nature of the iron-nitrenoid species in a non-heme ligand system.

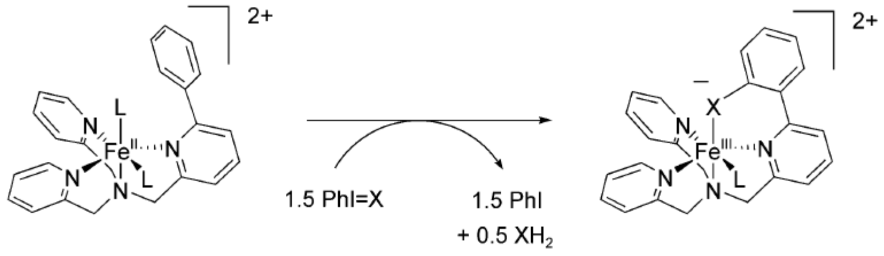

Figure 22. Overview of the amination reaction; (X=NTs) L is presumably MeCN (Picture adapted from[75]).

Despite the significant instability of iron-nitrenoids, Holland[76,77] and Peters[78] have recently succeeded in stabilizing and isolating iron(III) -imido complexes in low coordination numbers using organic azides as the nitrene source (Figure 23). These complexes were shown to transfer the electrophilic nitrene group to different nucleophiles such as carbon monoxide, *t*-butyl isocyanide and trimethylphosphine. Good electron-donor ability and high crowding of the ligands (e.g. β-diketiminates or tripodal phosphines) are addressed as the main reasons in stabilization of the metal-imido intermediate.[77] Isolation of these complexes and complete evaluation of their metal-imido bonding has also greatly helped to clarify the mechanism of nitrene transfer from these complexes.

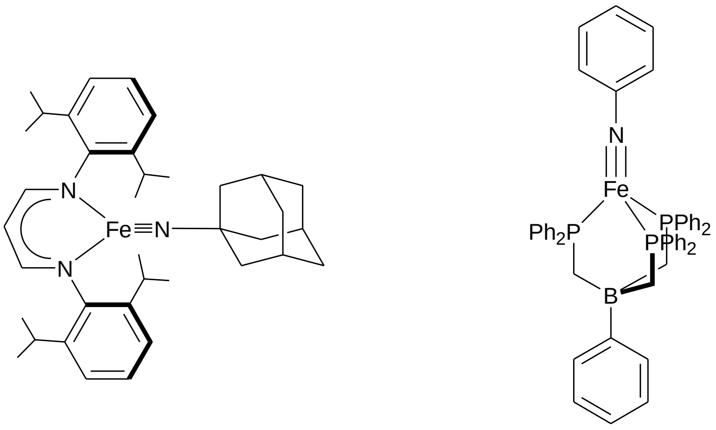

Figure 23. Isolated low-valent iron-imido complexes[76,78]

1.4.3 Ruthenium- and Rhodium- Catalyzed Nitrene-Transfer

Che and co-workers discovered that $[Ru(Me_3tacn)(CF_3CO_2)_3]$ (Me_3tacn = 1,4,7-trimethyl- 1,4,7-triazacyclononane) and *cis*-$[Ru(6,6'\text{-}Cl_2bpy)_2Cl_2]$ (6,6'-Cl_2bpy = 6,6'-chloro-2,2'-bipyridine) can catalyze amination on a variety of substrates using PhINTs with yields greater than 80%.[79,80] It was proposed that these reactions proceeded through ruthenium-nitrenoid intermediates. A general scheme showing two possible mechanisms is given below (Figure 24). These mechanisms proposed that nitrene insertion into C-H bond using PhINTs could proceed either through concerted addition of CH bond to the M-nitrenoid species or through radical pathways involving metal-nitrenoid and alkyl radical species.

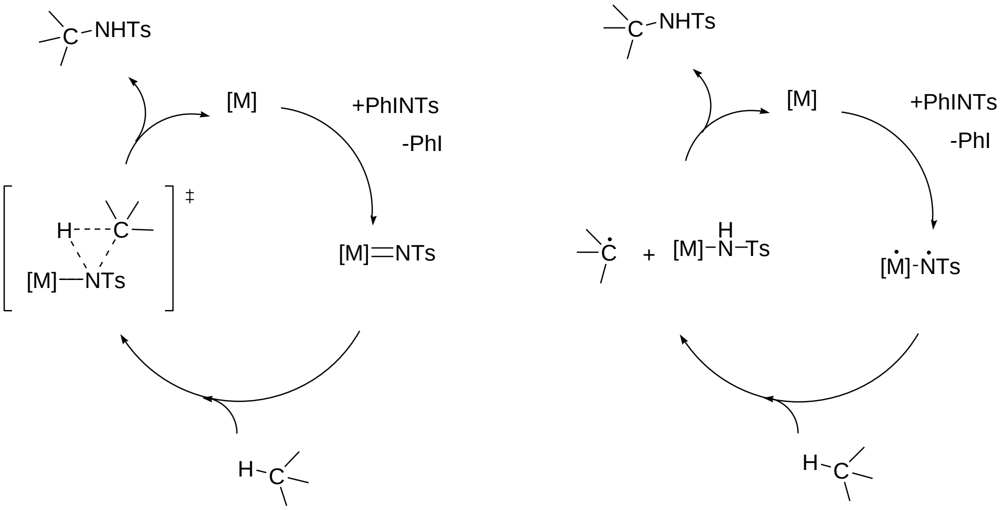

Figure 24. Proposed possible mechanisms for metal catalyzed nitrene insertion reactions, Left: Concerted pathway, Right: Radical pathway [51]

The same group also reported benzylic and allylic amination reactions catalyzed by ruthenium-imido complexes with substituted porphyrin (por) systems. They were able to isolate [Ru(por)($NSO_2C_6H_4R)_2$], which suggested that the redox nitrene transfer mechanism (Figure 17) was operative. Rates of aziridination or amination, as well as ratios of amination/aziridination, by this ruthenium-imido complex were significantly affected by varying the R group in the imido group or on the porphyrin substituents. Generally, electron-withdrawing substituents increased the rates of both aziridination and amination in these porphyrin systems.[81]

Rhodium complexes were a breakthrough in nitrene transfer catalysis. Dimeric Rh(II) complexes have been used in a variety of nitrene transfer reactions. Breslow and co-workers were the first to find out that simply $Rh(OAc)_4$ could catalyze the intramolecular benzylic amination of *N*-(2,6-diisopropylbenzenesulfonyl)iminophenyliodinane in excellent yields.[66] This standard was developed more by Muller and co-workers to Rh-catalyzed aziridination, intermolecular allylic/benzylic/ethereal amination, and intramolecular amination.[82-86] It was also found that changing the nitrene-transfer reagent from PhINTS to PhINNs (Ns = *p*-nitrobenzenesulfonyl) resulted in a large increase in aziridination yields.[83] A metal-bound nitrene intermediate has been proposed to be involved in this reaction since the stereospecificity was maintained during the aziridination.

Finally, Du Bois and co-workers discovered the [$Rh_2(OAc)_4$]-catalyzed intramolecular amination of carbamates to oxazolidinones in a mild, regio- and stereoselective process.[87] The commercially available, inexpensive iodosobenzene diacetate [$PhI(OAc)_2$] is used as the oxidant in conjunction with MgO and H_2NR in order to generate PhI=NR species *in situ.* The product oxazolidinones (Figure 25) are versatile materials that are easily hydrolyzed to furnish 1,2-amino alcohols. This convenient method has been subsequently extended to intramolecular aziridination, intermolecular allylic amination, intramolecular amination, enantioselective intramolecular aziridination, and intermolecular amination of *p*-ethylanisole cyclooctane.[87]

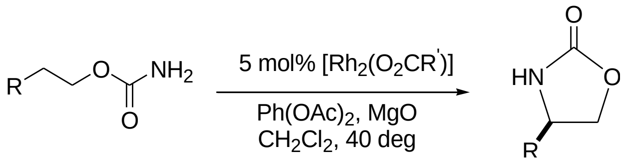

Figure 25. Rhodium-catalyzed nitrene insertion in to C-H bond of carbamates to yield oxazolidinones[87]

1.5 Nature of the M=X Bond (X = O or NR)

1.5.1 Overview

Oxo and imido (also referred to as nitrenes or imides) species are common ligands in high oxidation state transition metal chemistry that form multiple bonds with metal centers. Metal-oxo and metal-imido/nitrenoid compounds are often reactive reagents involved in metal-catalyzed oxygen-atom and nitrogen-group transfer reactions, respectively. A detailed overview of their structures is thus required to gain a better understanding of the mechanism of these reactions. The following sections of this chapter will discuss the nature of these species, as well as their synthesis and reactivity, and the factors that affect this reactivity.

Metal-imido and metal-oxo classes of compounds are isoelectronic in nature and their bonding is considered to consist of one σ bond plus one or two π bonds. In metal-imido species the π donation from filled p orbitals of nitrogen to d orbitals of the transition metal results in formation of two different geometries: linear metal-imido bonding which has two π bonds and therefore a bond order of three (sp hybridization of nitrogen orbitals), and bent metal-imido bonding which has one π bond and one lone pair centered on the nitrogen atom (sp^2 hybridization of nitrogen orbitals), resulting in a metal-nitrogen bond order of two (Figure 26). Whether linear or bent, the formal oxidation state of the metal and the imido species are generally considered as (M^{2+}) and (NR^{2-}), although different interpretations such as $(NR)^{\cdot -}$ and M^{+} have also been postulated recently.[88] Metal-oxo complexes, however, appear to be able to form bond orders from three to as low as one (examples in section 1.5.4). This is due to the high electronegativity of oxygen relative to nitrogen that allows oxygen to bear up to three non-bonded electrons pairs.

Bond order, in this case, is governed by the ability of the transition metal to accept π bonds. In metal-imido species the M-N-R bond angle can mostly be considered as an indicator of the degree of π-donation from nitrogen. Imido ligands are such good π-donors that the overwhelming majority of imido complexes are triply bonded (M-N-R bond angles from 150° to 180°) to the metal. The only circumstances under which an imido ligand has less than three bonds to the metal and hence is not linear are cases in which: (i) there is no empty d orbital on the metal that has the proper symmetry to overlap with the nitrogen lone pair sp orbital; (ii) the metal electron count is already 18 electrons; (iii) the imido ligand is part of a rigid structure which physically constrains it in a bent geometry.[88,89]

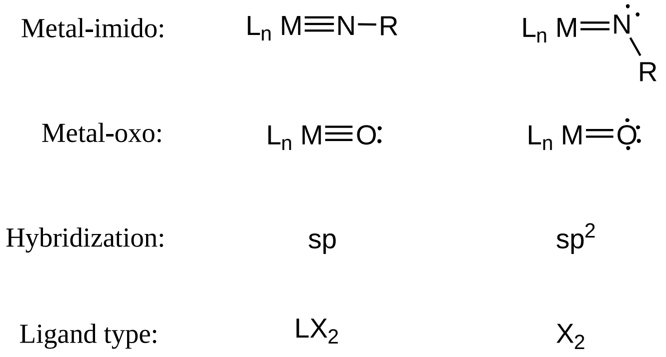

Figure 26. Metal -oxo and -imido bonding information and electron donation of imido and oxo ligands in different formalisms

Another important point about metal-imido and metal-oxo bonds is that the high electronegativity of oxygen and nitrogen polarizes their bonds with the metal (Figure 27). This fact greatly affects the reactivity of these bonds (resembling the reactivity of isoelectronic metal carbenes and its consequences in organic chemistry and catalysis) and is therefore accountable for transferability of these units as we have previously seen in oxygen-atom and nitrogen-group transfer reactions.

Figure 27. Systematic polarization of metal -oxo (left) and -imido (right) bonds

Finally, though having essentially the same nitrogen group functionality, metal-nitrenoid and metal-imido species are greatly differentiated based on the transition metal and its electronic environment. When working with high oxidation state transition metal complexes, imido units are usually considered to be NR^{2-} (M=NR, imido form), whereas those who work with low oxidation state metal complexes tend to consider it a neutral ligand (M-NR, nitrene form).[90] Metal-nitrenoids are considered to be an intermediate situation between these two extreme states (Figure 28) (see 1.5.4.).

Figure 28. Metal-imido (left) and metal-nitrenoid (right) schematic notation

1.5.2 Orbitals

Metal-imido and -oxo multiple bonds consist of one σ and one or two π bonds. These π interactions involve overlap of metal d orbitals with p orbitals of oxo/imido ligands. If the z axis is taken along the metal -N/-O bond, this π overlap would occur between d_{xz} and p_x orbitals and/or between d_{yz} and p_y orbitals to form bonding (π) and anti bonding (π*) molecular orbitals. As closed-shell anions, both oxo and imido have filled p orbitals, a consequence of the higher electronegativity of oxygen and nitrogen, and these p orbitals are lower in energy than the d orbitals of the metal (Figure 29). Therefore, in order for a productive π bonding to happen, there should be enough empty d orbitals on the metal and these empty d orbitals should have the proper symmetry for π interaction. In other words, the metal should either have low electron count or high oxidation state.[91]

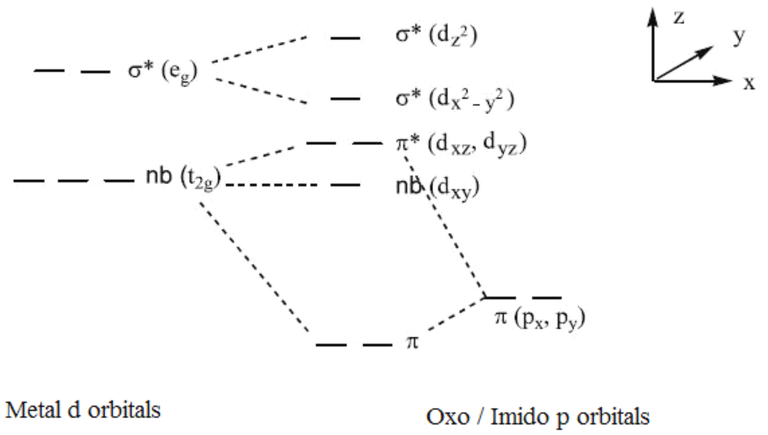

Figure 29. Partial molecular orbital diagram for an octahedral complex with one oxo or imido (linear) ligand (picture adapted from[89])

The bonding in metal-imido complexes can be properly explained by molecular orbital theory. A simplified molecular diagram for metal-imido/oxo complexes in octahedral geometry is shown in Figure 29. The majority of complexes with multiply bonded ligands are six-coordinate and adopt a geometry best described as octahedral.[91] Since the complexes synthesized in this project also adapt octahedral geometry this section will focus on the molecular orbital system in this geometry. Productive π interactions between metal d orbitals and p orbitals of oxo/imido ligands happen when these interaction result in the stabilization of the metal-ligand bond. The result of such productive π interactions is a linear metal-imido bonding. However, if the metal d orbitals are filled, depending on the geometry and the resulting molecular orbitals, electrons would occupy the π* molecular orbitals. As a consequence of these occupied antibonding orbitals, the metal-imido bonding would be destabilized and bent metal-imido bonding or, in extreme cases, metal-nitrenoids will be formed. The substantial effect of π antibonding interactions on the stability and reactivity of metal -imido and -oxo compounds stands out when we see that the abundance of stable metal -oxo and -imido complexes significantly drops when the number of d electrons increases by moving to the right in a row in transition metal series.[92] This subject is elaborated in the next section (1.5.3).

All deviations from a high symmetry structure, whether due to bond or angle distortions or because of differences in ligand strengths, will affect the molecular orbital and consequently the bonding and reactivity of the metal imido-bond. In other words, changes in the symmetry of the metal and ligand orbitals can disrupt their overlap ability and thus lead to variations between triply bonded metal imidos (stable) to singly-bonded nitrenoids (very reactive). In total, the metal-imido bonding is governed by a combination of the type of transition metal, its oxidation state, the type of the ancillary ligands, the substitutions on the imido group, the number of ligands, and the coordination geometry of the complex.[89] The same argument is valid for metal-oxo bonds, affecting the degree of the bonding (single to triple).

1.5.3 Periodic Trends

According to the molecular orbital diagram of metal-oxo and -imido complexes, the more electron-deprived the d orbitals of the transition metal are, the stronger and more stabilizing the π bonding. As a result, transition metals in groups 3-7, particularly those in high formal oxidation states, receive strong π-donation from the two filled nitrogen p orbitals into their empty d orbitals, resulting in a formal metal-imido bond order of up to three. These bonds are often so strong that the imido moiety acts as an unreactive spectator ligand. For example, the Mo-imido functionality in Schrock's olefin metathesis catalyst (Mo-N bond length: 1.75 Å)[93] is so unreactive that it acts as spectator ligand during the catalytic cycle.[94-96] In late transition metals (groups 8-11), on the other hand, the metal-nitrogen π-interactions are usually destabilized because d orbitals of the metal are filled and the π-interaction electrons would occupy the antibonding π* orbitals. This is particularly the case in the octahedral geometry, which is a common geometry for late transition metals. As a result, late transition metals typically form weak bonds with imido fragments, and structurally characterized imido complexes of them are uncommon.[88] Late transition metals, instead, form metal-nitrenoid species, which are very reactive intermediates, having a strongly electrophilic nitrene coordinated to the metal. Although these complexes have not been isolated due to their very reactive nature, indirect evidence proposes their involvement in metal-catalyzed nitrene transfer reactions as the reactive reagent (See 1.4).[77,91,92]

Metal-imido and metal-nitrenoid complexes are also differentiated based on the formal oxidation state of the metal atom. An imido species suggests the combination of (M^{2+}) with (NR^{2-}) whereas a metal-nitrenoid complex represents neutral nitrene (NR) coordinated to M.[88] Only recently has the intermediate case where an $(NR)^{-\cdot}$ radical is coordinated to M^{2+} been postulated by Wieghardt.[97] A similar argument can be used to explain why terminal oxo ligands are ubiquitous in the chemistry of the higher oxidation states of transition metals from group 3 up to group 8 (the so called oxo wall), whereas there are rarely any examples of stable terminal oxo complexes with transition metals d^6 or higher. The oxo ligand in the stable oxides and oxo complexes of the late transition metals often bridges two or more metal centers to avoid π antibonding.[92] Generally, between the two sides of the periodic table the most stable metal-oxo complexes are found along a diagonal from V to Os, the most common ones being the Mo family.

Recently, however, several research groups have been successful in stabilizing late transition metal -imido and -oxo complexes by adjusting factors such as lower coordination numbers and/or use of crowded highly electron donor ligands. These cases are highlighted in the following section 1.5.4.

1.5.4 Reactivity: Influence of the Metal and Ancillary Ligands

The charge polarization in the metal-oxygen and metal-nitrogen bonds results in the substantial accumulation of negative charge density at the heteroatom and therefore basicity of the oxo or imido ligands. Factors such as the number of metals bonded to the imido/oxo ligand, the nature of the ancillary ligands, and the metal center oxidation state can greatly affect this basic character of oxo and imido ligands. These factors are rationalized in terms of the acceptor properties of the metal center and ligands. The more metal centers bonded to the oxo or imido ligand, the more charge transfer from the ligand and hence less basicity. Similarly, the more acidic the ancillary ligands or the higher the metal oxidation state, the better the metal center at charge acceptance.[98]

The nature of the metal center, therefore, has a great influence not only on the preference for or against multiple bonding, but also affects the preference for a particular type of ligand. For instance, V and Ta -imido complexes are so oxophilic that they hydrolyze in the presence of even trace amounts of water to give the corresponding oxo species and the free amine, whereas Os-imido complexes are so water-stable that they can be prepared by addition of *t*-butylamine to an aqueous solution of OsO_4. This can be explained according to the fact that early transition metals are more electrophilic and “harder” and therefore have more preference for more electronegative “harder” ligands (O rather than NR).[91]

Generally, more electrophilic early transition metals form triply bonded metal-imido species, resulting in the electrophilic behavior of the imido ligand. As one moves up and to the right in the periodic table for transition metals, the nucleophilic nature of the metal increases and therefore results in a very reactive nucleophilic metal-nitrenoid species.[89] The same argument applies for the increase in the basicity of late transition metal-oxo complexes which leads to more favoured μ-oxo bridged complexes.[91]

Ancillary ligands and the geometry of the complex also significantly affect the reactivity of the imido/nitrenoid/oxo ligands. π-donor ancillary ligands can rival with imido/oxo ligands for the formation of π bonding with the central metal in coordinatively saturated complexes. Recently, a few isolable late transition metal-imido complexes have been prepared by use of bulky donor ligands (e.g β-diketiminates or phosphines) that enforce a coordinatively unsaturated metal center (Figure 30).[78,99-106] A low coordination number at the metal was confirmed as an important feature, as tetrahedral and trigonal metal centers have empty and appropriate π-symmetry orbitals to stabilize the metal-imido bond and hence, make it less reactive.[107]

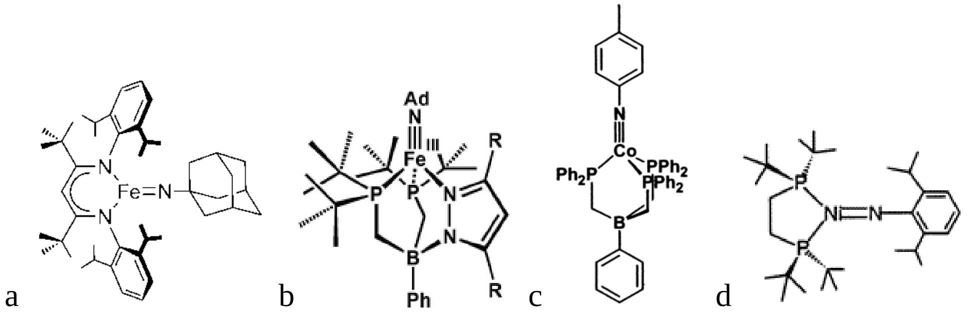

Figure 30. Late transition metal-imido complexes prepared by use of bulky donor ligands and in low coordination numbers, pictures adapted from a [77], b [103], c [102], d [105]

In addition, some late transition metal-imido complexes were stabilized by bridging the imido group in bimetallic complexes (Figure 31).[77,108-113]

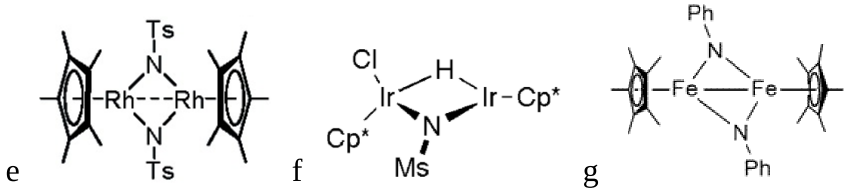

Figure 31. Late transition metal-bridging imido complexes, pictures adapted from e [111], f [109], g [112]

The same trend is observed with late metal-oxo complexes. Only recently were such complexes stabilized by both good σ-donor and π-acceptor ligands such as polyoxometallates[111] (Figure 32a) that lower the electron density on the metal-oxygen unit and/or in complexes with low coordination numbers (Figure 32b).[112] In a recent work, low-valent vanadium and chromium -oxo complexes were stabilized by the support of a tripodal *t*-Bu$_2$(Me)CO$^-$ alkoxide frame work in a pseudotetrahedral coordination (Figure 32c).[114] The Borovik group reported the isolation of a Fe(III)-oxo complex with a single Fe-O bond. This terminal oxo group was stabilized by distal hydrogen bond donors in the ligand backbone (Figure 32d).[115] The Warren group reported the synthesis of stable

Co, Ni, Cu β-diketiminate-complexes with bridging and terminal imido ligands.[106,116,117] These examples show that the structure and reactivity of metal-imido/nitrenoid or -oxo species can be tuned by appropriately manipulating the complex geometry and by using the proper supporting ligands.

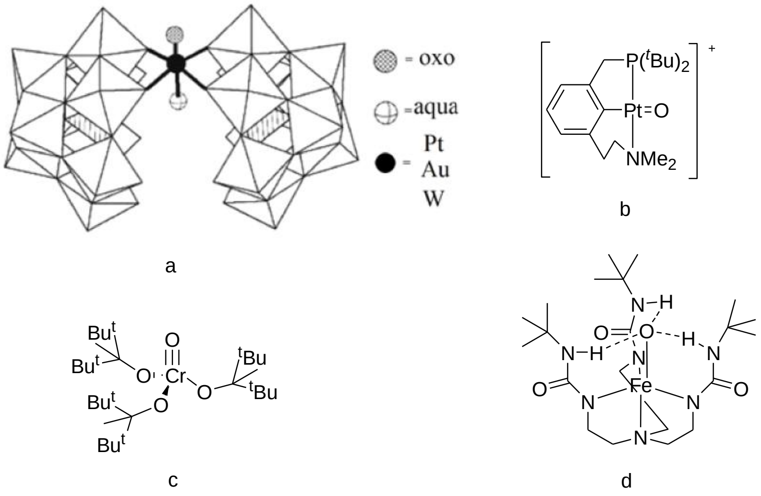

a b c d

Figure 32. Late transition metal-oxo complexes prepared by use of bulky donor ligands and in low coordination number [112,115,116], picture a adapted from [114,115,118,119]

1.5.5 Synthesis of the M=X Bond (X = O or NR)

Preparative methods for imido and oxo complexes are outlined in Figure 33. Early transition metal-oxo complexes are mostly obtained by facile reaction of the oxophilic metal precursors located along the vanadium-osmium diagonal with air or water.[90] Early syntheses of late transition metal-oxo complexes were generally serendipitous and with low yields. In planned syntheses, deprotonation of hydroxo complexes is a favoured route to oxo complexes and has produced Rh(I), Ir(I), Ir(III), and Pt(II) oxo complexes (Figure 33c).[120]

Transition metal-imido complexes are, however, less likely to be prepared serendipitously, as the result of there being fewer common sources of the NR group, the greater basicity of the imido ligand, and the reactivity of imido complexes with protic compounds including water.[120] Analogous to metal-oxo complexes, metal-imido complexes can be prepared by deprotonation of amido complexes by strong bases such as lithium amide reagents (LiNHR) (Figure 33d, e). The bulk of the R-group (aryl or alkyl) can play a significant role in the stabilization of late transition metal-imido complexes. For example, chromium[121] and ruthenium[122] -imido complexes can be isolated by this method.

Oxygen atom and nitrene transfer to metals is another widely used method in the synthesis of early transition metal-imido/oxo complexes. However, it is not an effective route for the synthesis of late transition metal terminal oxo complexes. The only reactions that have yielded late transition metal oxo complexes where OAT may be operative involve the donors ozone, dioxygen, PhIO, and Me_3NO, although these reactions have low yields (Figure 33a, b, f, g).[91]

Different sources of nitrenes have been utilized in the synthesis of imido species. Thermal or photochemical decomposition of organic azides is one of the most widely used methods in the synthesis of metal imido complexes. It also has been the most successful method in the recent synthesis of imido complexes with late transition metals such as Fe(II), Fe(III), Fe(IV), Fe(V), Co(III), Ni(II) and, Ni(III) (Figure 33h, i).[78,99-106,123]

Interconversion of oxo and imido complexes with isocyanates or by water or amine addition are also known (Figure 33j, k). The favoured direction varies: in some cases the oxo complex is stable in the presence of amine and in others the imido complex is stable in the presence of water.[88] A complication of this method is the potential reaction of the formed oxo or imido complex with excess water or amine. If the oxo or imido complexes are unstable in the presence of excess water or amine, hydroxo or amido complexes are obtained.[89,91,120]

Alkylation or acylation of the nitrido ligand has provided another synthetic route to imido complexes. Nucleophilic metal-nitrido complexes can be alkylated or acylated with electrophiles such as methyltriflate, anhydrides and trityl tetrafluoroborate to give metal-imido complexes (Figure 33l).[89] There are other more sophisticated methods for the synthesis of metal-imido/oxo complexes which may be employed in specific cases as needed. Some are outlined below (Figure 33m, n, o, p, q).[98]

Finally, a problem with the synthesis of oxo and imido complexes is the difficulty in their characterization. Characteristic NMR signatures are either absent or weak and the broad nature of OH and NH ^{1}H-NMR signals makes it difficult to conclusively prove the formation of metal-oxo or -imido bonds. Similarly, X-ray crystal structure analysis can be inconclusive as hydrogen atoms are difficult to detect. Therefore, identification of oxo and imido complexes must be viewed with some scepticism unless supported by other methods such as chemical reactivity and derivatization.[98]

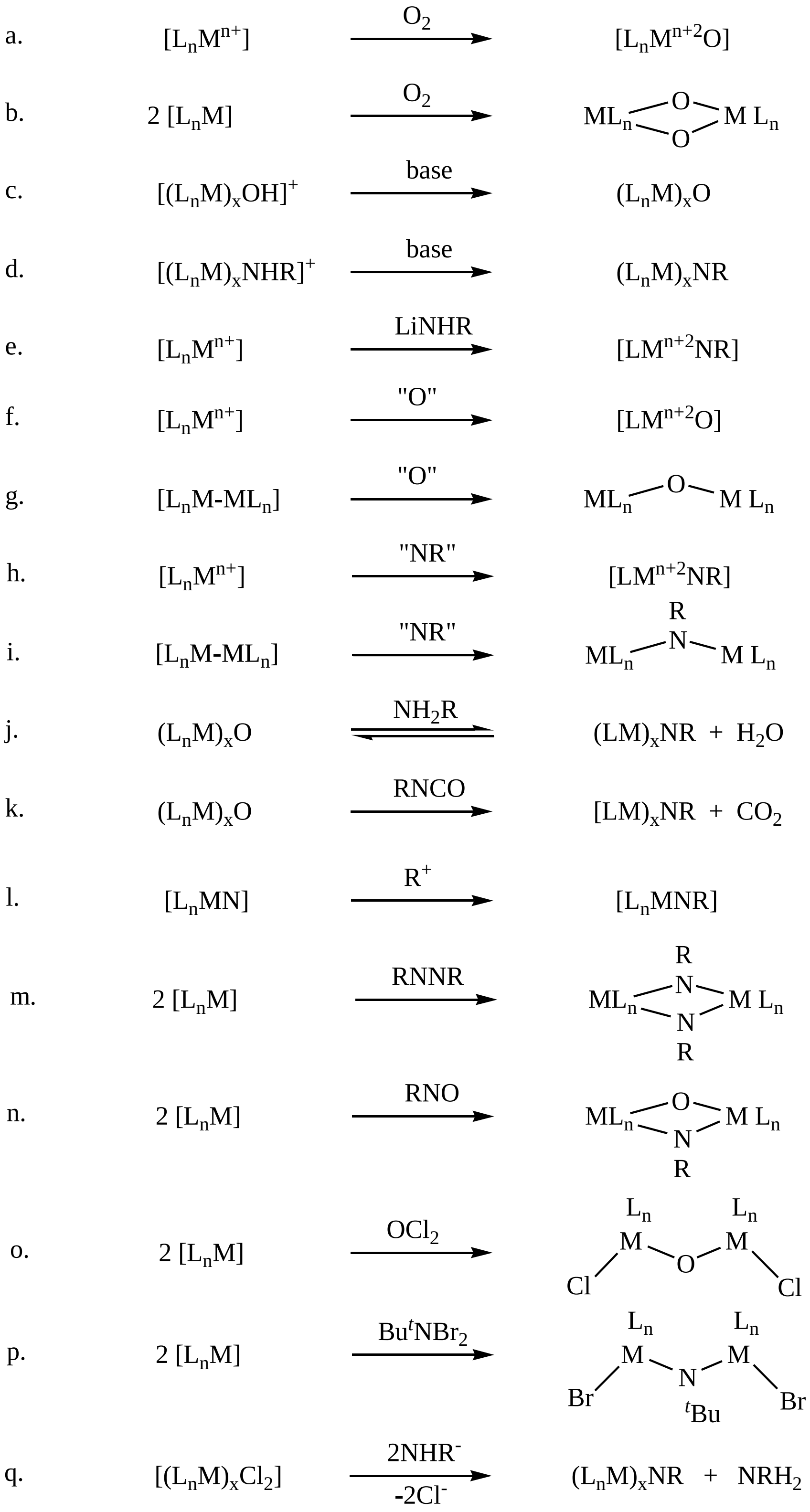

Figure 33. Preparative methods for -oxo and -imido complexes

2. Research Goals and Design

2.1 Importance of Iron as a Mid- to Late- Transition Metal

Iron, located in the middle of the first row transition metal series, represents exceptional catalytic features in oxygen atom and nitrogen group transfer reactions. Fifty years after the isolation and characterization of the iron-containing oxidation enzymes, cytochrome P450 and non-heme monoxygenases, the exact nature of the active species responsible for the OAT reaction is still a matter of debate. Numerous mimicking complexes have therefore been made both to unveil the mechanism of these enzymes and develop synthetic analogues for industrial purposes. Based on the same systems, synthetic iron-imido/nitrenoid complexes received intense scrutiny due to their postulated role in catalysis as the active reagents in nitrene transfer reactions. To date, only a few cases have been isolated due to the high reactivity of these species. The low toxicity and high abundance of iron make such complexes appealing for industrial purposes.

Formation of iron-imido bonding is highly dependent on the energy and availability of d orbitals. Iron's filled d orbitals are accountable for the formation of destabilizing π antibonding molecular orbitals and hence for weaker bonds in iron oxo and imido complexes in most common geometries in lower oxidation states. Therefore, iron-oxo/imido complexes have only been isolated with the aid of special stabilizing ligands such as heme-type ligands (porphyrins) in octahedral geometry or with non-heme bulky donor ligands in low coordination number geometries. With other non-stabilizing ligands, iron forms very reactive, non-isolable nitrenoid intermediates that readily react with organic compounds in the reaction media or form bridging -oxo/imido bonds in a multinuclear complex. Whether isolated or not, understanding these iron-oxo and

-imido/nitrenoid and -oxo species is potentially beneficial because the weak and electrophilic Fe-O and Fe-N bonds can enable thermodynamically favourable oxygen and nitrene transfer to organic compounds, and can also lower the activation barriers to stoichiometric and catalytic reactions.

We are interested in iron-catalyzed oxygen-atom and nitrene-transfer reactions. Important examples of iron complexes in charge of such reactions were discussed in the previous chapter. This chapter includes a detailed explanation of the objective of this research and the approach taken towards it.

2.2. Research Goal: Iron-Imido/Nitrenoid Synthesis via OAT from Iron-Nitroso Compounds

While OAT reactions in synthetic and biological systems proceed through oxo or peroxo species directly coordinated to metal centers in a high oxidation state, we propose to investigate the formation of iron-imido/nitrenoid species via OAT from iron(II)-nitroso complexes as substrates in a concerted mechanism (Figure 34).

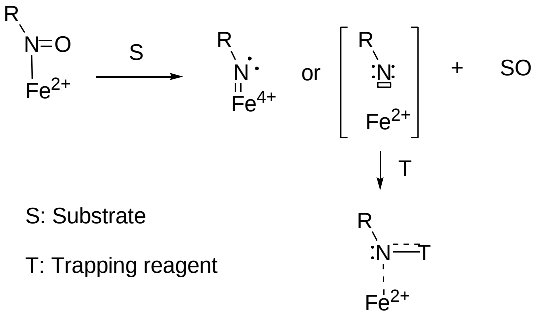

Figure 34. Proposed method for iron-mido/nitrenoid synthesis via OAT from an iron-nitroso complex

To achieve this goal, the ligand system surrounding the metal (first-coordination-sphere) is designed based on the active sites of OAT metalloenzymes such as non-heme oxygenases. Including the nitroso functionality into the polydentate ligand scaffold affords control over the second coordination sphere features and reactivity (Figure 35). The structure of the ligand is designed in a way to stabilize the formed iron-imido/nitrenoid intermediates by keeping the nitrene functionality in the vicinity of the metal and preventing unwanted polymerizations that are seen in organic systems. The ability of the synthesized iron-nitroso system to perform OAT to different substrates is then studied with various techniques to achieve mechanistic insight into this process. Isolation, tracing or trapping of iron-nitrenoid/imido intermediates as a proof of the mechanism is intended (Figure 34).

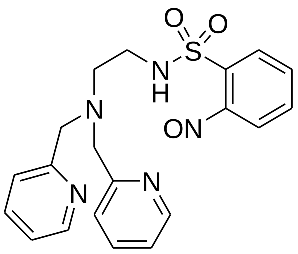

Figure 35. The proposed pentadentate ligand system with a built-in nitroso functionality

2.3 Literature Review

2.3.1 Iron-Nitroso Complexes

Several preparative methods exist for the synthesis of carbon-bonded (C-NO)-transition metal-nitroso complexes, such as: coordination of organic nitroso or hydroxylamines compounds, deoxygenation of organic nitro compounds, oxygenation of imido complexes, reaction of coordinated nitrosyls with carbanions, and NO insertion into a metal-carbon bond.[124] The first two methods are the most frequent techniques used to prepare iron-nitroso compounds. These preparation methods can result in diverse types of bonding between iron and the organic nitroso group (Figure 36), in which the monometallic *N*-binding (η^1-NO) is of interest to us and will be discussed in this thesis.

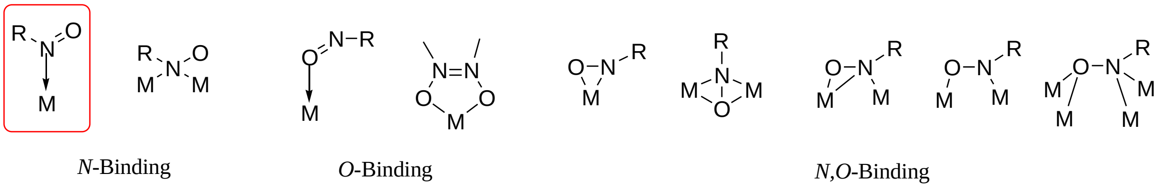

N-Binding *O*-Binding *N,O*-Binding

Figure 36. Binding modes in metal-RNO complexes established by single-crystal X-ray crystallography.[124] The first model represents monometallic *N*-bonding (η^1-NO).

Extensive study of iron-nitroso complexes with heme and heme-model ligands[125-133] was motivated by the observation that, as metabolites derived from amine oxidation or nitroaromatic reduction, such heme-RNO compounds are involved in possible inhibition of enzymatic activity of P450 or cyclooxygenase.[124] Almost all these compounds were synthesized by addition of organic nitroso or hydroxylamines to Fe(II)-heme complexes and resulted in the formation of *N*-bound nitroso structures (Figure 37). The exact mechanism underlying the formation of nitroso compounds from their hydroxylamine analogues is still a matter of debate. However, since hydroxylamines are known to be reducible to amines via the transfer of two electrons, it has been proposed that this electron is initially provided by oxidation of Fe(II) to Fe(III) in a disproportionation reaction (Figure 38).[134] Recent ESR (Electron Spin Resonance) studies[135] proved the involvement of RNHO radicals, suggesting a probable more complex radical mechanism that needs to be studied in more depth (see 4.3.2).

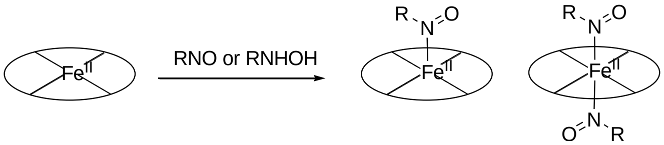

Figure 37. Synthesis of mono and di-substituted *N*-bound iron-nitroso heme complexes via addition of organic nitroso or hydroxylamine reagents

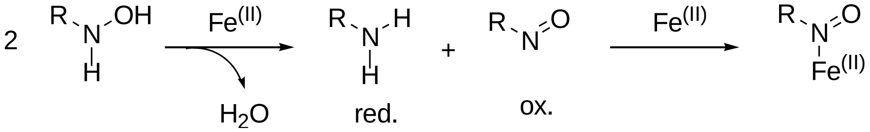

Figure 38. Disproportionation of organic hydroxylamines in presence of Fe(II) followed by formation of the iron nitroso complex[134]

In contrast to heme-type iron-nitroso compounds, very few examples of the synthesis of non-heme iron-nitroso complexes exist. Probably the first example of a non-heme iron-nitroso compound dates back to 1907, when it was prepared accidentally from light exposure to a solution of iron pentacarbonyl in nitrobenzene.[136] Years after, the most famous complex in this family was prepared by reaction of nitrosobenzene (PhNO) and hexacyanoferrate(II) to yield $[(PhNO)Fe(CN)_5]^{3-}$, Baudisch iron-nitroso complex.[134,137] Addition of organic nitroso or hydroxylamines has resulted in a small number of characterized iron-nitroso examples (Figure 39a).[134,138,139] Finally, other iron-nitroso complexes were prepared by migratory insertion of NO into metal carbon bonds (Figure 39b).[124,140] As there have been only a few non-heme iron-nitroso complexes synthesized previously, our ligand is considered to be one of the few designed systems in this field.

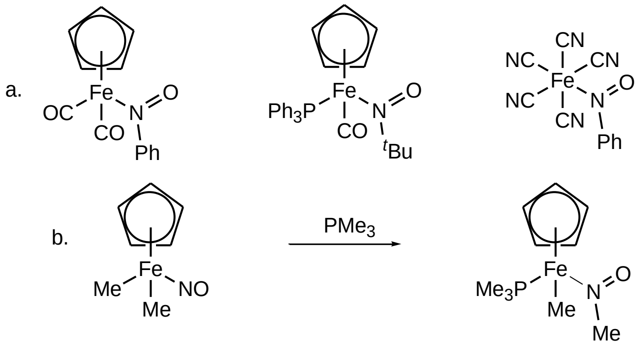

Figure 39. Iron-nitroso complexes prepared by a. Direct addition of organic nitroso or hydroxylamines to the iron precursor[134,138,139] b. Migratory insertion of nitro into Fe-C bond by addition of PMe_3 [140]

2.3.2 Oxygen Abstraction from Nitroso Compounds

Trivalent organophosphorous compounds such as trialkyl or triaryl phosphines (R_3P) are good oxophiles that have been found to react with electrophilic organic nitroso compounds to yield the corresponding tetravalent derivatives (R_3PO) with the driving force being the strong P=O bond (544 kJ/mol). Formed azoxyaryls (**I**) (Figure 40) as well as iminophosphorane compounds (**II**) (moderate yields) together with unknown polymeric mixtures have been obtained via deoxygenation of aromatic organic nitroso compounds.[141] Deoxygenation of aliphatic nitroso compounds is more complex and different rationalizations have been proposed for various types of obtained products. Altogether, these observations lead to the suggestion that these reactions proceed through formation of nitrene intermediates that further react with other reagents in the reaction medium to result in the mentioned products. This also explains the formation of the unknown polymeric mixtures, as the formed highly reactive nitrene could react uncontrollably in the reaction medium.[141]

$$\text{a.} \quad R_3P + ZO \longrightarrow R_3PO + Z$$

$$\text{b.} \quad R_3P + ArNO \longrightarrow R_3PO + \underset{\textbf{(I)}}{ArN{=}N(O)Ar} + \underset{\textbf{(II)}}{R_3P{=}NAr}$$

Figure 40. a. General formula of deoxygenation of oxygen-containing organic compounds with trivalent phosphines b. Isolated products from deoxygenation of organic aryl-nitroso compounds, (I) azoxyaryls and (II) iminophosphoranes

Deoxygenation of coordinated η^1-*C*-nitroso complexes by triphenylphosphine was first reported for Fe(III), Ni(II), Cu(II), and Zn(II) complexes of *o*-nitrosophenol, yielding phenazines or complexes of triphenyl(*o*-hydroxyphenylimino)phosphoranes depending on the metal (Figure 41).[142] These reactions were interpreted to proceed through transient nitrene/nitrenoid intermediates.

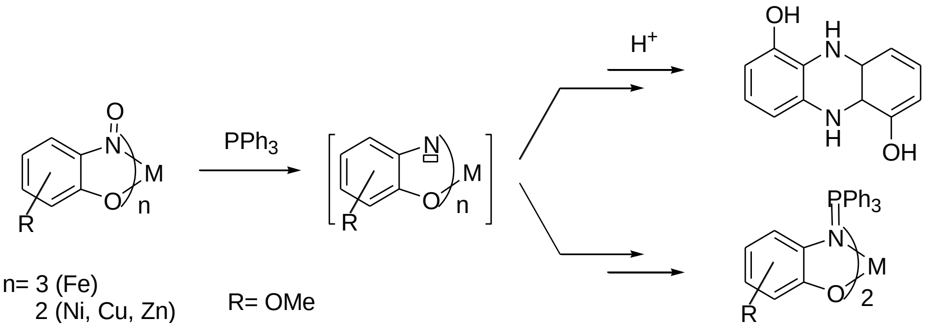

Figure 41. Deoxygenation of o-nitrosophenol by triphenylphosphine reagent, proposed nitrene intermediate and isolated products, Upper product: Phenazine, bottom product: triphenyl(*o* hydroxyphenylimino)phosphorane complex

Few other examples of coordinated nitroso deoxygenation with oxophilic reagents such as trialkyl/aryl-phosphines[143,144], alkyl/aryl-isocyanide[143,144], carbon monoxide[145], and organic arylnitroso compounds[143,146,147] have been reported to produce the oxygenated reagents as well as nitrene-related organic products (e.g. azo, azoxy, or iminophosphorane compounds). However, in all these examples the coordinated nitroso is either bridged between multiple metal centers or coordinated via N and O (side-on nitroso coordination). While none of these cases offer a consistent proof of mechanism based on the isolation of proposed nitrene/imido intermediates, a Re-imido complex has been isolated as the product of Re-nitroso deoxygenation by triphenylphosphine.[144] Formation of this structurally-proven stable complex is attributed to the high stability of Re-imido bonds, favoring a clean deoxygenation reaction. This finding confirms the possibility of nitrene/imido intermediate formation during deoxygenation of metal-nitroso compounds, although more in-depth studies are needed to reveal the exact mechanism in each particular case. Indeed, isolation of stable imido complexes with late transition metals on the upper rows is more challenging and in most cases highly reactive nitrenoids are expected. In such cases, formation of these intermediates, and hence the mechanism, is proposed based on the structure of “trapped” nitrene products. Another possible method to prove the formation of nitrenoid intermediates is to track their formation by time-resolved UV-visible stopped-flow techniques. However, this requires that formation of the nitrene intermediate is faster than its consumption so that its UV-visible absorption features can be observed.

2.4 Approach

The approach taken towards this project is divided into three steps: (1) Synthesis of Iron-Nitroso Complexes (2) Reactivity Study of the Iron-Nitroso Complexes with Oxygen Abstracting Agents (3) Mechanistic Study.

2.4.1 Synthesis of Iron-Nitroso Complexes

A pentadentate pre-ligand system with a built-in hydroxylamine functionality is designed that will form the iron-nitroso complex upon disproportionation of the hydroxylamine group. The ligand structure (Figure 35) is designed to form a relatively crowded coordination sphere around the metal, leaving only the nitroso function accessible for attack by oxophilic reagents. The sulfonamide group can be deprotonated to form a negatively charged ligand. The ligand structure should be stable and non reactive towards the oxophilic reagents used later for deoxygenation of the nitroso group. Iron(II) precursors are chosen as the starting materials to form the iron(II)-nitroso complexes since they could be further oxidized to iron(IV)-imido/iron(II)-nitrenoid species. Finally, π-acceptor groups would stabilize the high oxidation state iron(IV)-imido intermediates and are therefore incorporated in the ligand structure.

2.4.2 Reactivity Study of the Iron-Nitroso Complexes with Oxygen Abstracting Agents

The reactivity of the synthesized iron-nitroso complexes is studied with alkene and phosphine reagents. Reactions are followed by ESI-MS, ^{31}P-NMR, UV-visible, and GC techniques to trace the consumption of the starting iron-nitroso complex, as well as production of oxygenated substrate and trapped nitrene products.

2.4.3 Mechanistic Study

Structural elucidation of trapped nitrene products can suggest a possible mechanism for the deoxygenation of the iron-nitroso complex. This idea is supported by the information retrieved from kinetic studies of the deoxygenation reaction carried out with UV-visible techniques as well as control experiments.

3. Experimental

3.1 Synthetic Considerations

Due to the sensitivity of inorganic complexes to moisture and oxygen, all the synthesis and manipulation of these compounds were carried out under nitrogen atmosphere in an MBraun glovebox maintained at or below 1 ppm of O_2 and H_2O or by using standard Schlenk techniques. Unless noted otherwise, all the solvents were deoxygenated and dried by thorough sparging with N_2 gas followed by passage through a column of activated alumina or molecular sieves and were kept in the glovebox on activated molecular sieves prior to use. Deuterated NMR solvents were purchased from Cambridge Isotope Laboratories, Inc. and, except for $CDCl_3$ that was degassed and dried over activated 3Å molecular sieves in the glovebox, they were used as received (single-use breakseal ampoules). ^1H chemical shifts were referenced to internal tetramethylsilane (TMS). Bis(2-pycolyl)amine (BPA) was purchased from Richman Chemicals. All other reagents and solvents were purchased from Sigma-Aldrich or Alfa Aesar and used as received, unless otherwise stated. Except for PMe_3 that was purchased as a 1 molar solution in toluene, all other phosphine reagents were purchased as pure compounds and were used for the preparation of diluted stock solutions in different solvents. NMR tubes as well as other glassware were dried in the oven overnight and were then handled in dry atmosphere prior to use.

3.2 Instrumentation

^1H and ^{31}P-NMR spectra were recorded at ambient temperature on a Varian Innova 300 MHz or 500 MHz instrument. Magnetic susceptibility measurement was carried out at room temperature (26 °C) on the 500 MHz NMR instrument based on Evans method[148,149] (see Appendix II). Mass spectrometry data for samples were obtained by direct injection of their acetonitrile or dichloromethane/methanol (70:30) solutions into a Micromass Quattro LC triple-quad instrument equipped with an electrospray ionization (ESI) chamber. UV-visible measurements were done on an Agilent 8453 spectrophotometer using a 1 cm path length quartz cell with a septum cap. IR spectra were recorded on a Nicolet 6700 FT-IR spectrophotometer with a KBr solution cell. Gas Chromatography (GC) was performed on an Agilent 6850 instrument on an HP-5 column using anthracene as internal standard. A Parr 3911 hydrogenator was used for reduction of nitro ligands in the presence of a palladium catalyst and hydrogen gas. X-ray crystallography was performed on a Bruker Smart 6000 with a copper source and on a Bruker APEX-II DUO with a molybdenum or copper micro-focus source.

3.3 Preparation of the Ligands

3.3.1 Synthesis of *N*-[2-(Bis(2-pyridylmethyl)amino)ethyl]-2-hydroxylaminobenzenesulfonamide (BPAEB$_{NHOH}$)

Preparation of the ligand BPAEB$_{NHOH}$ is schematically shown in Figure 42. Synthetic details of each step are given below. All synthetic steps and manipulations were performed in air, using commercial reagents.

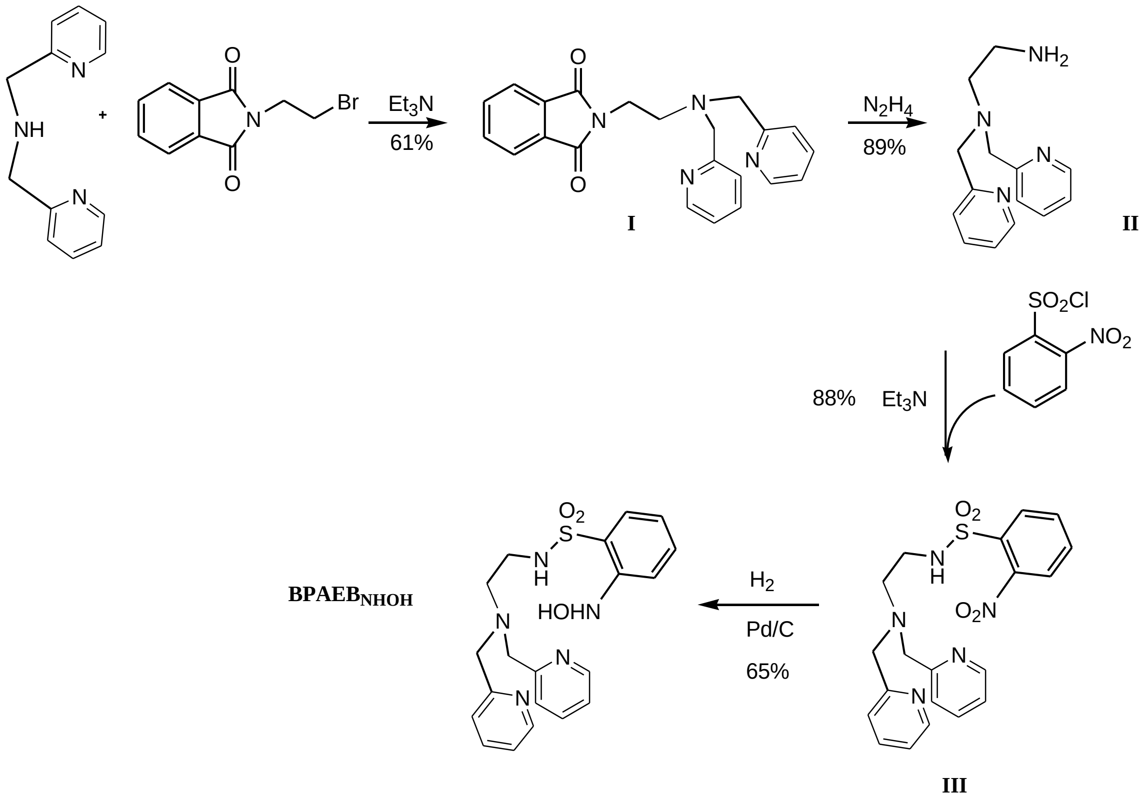

Figure 42. Synthetic steps of ligand BPAEB$_{\mathrm{NHOH}}$

2-[2-(Bis(2-pyridylmethyl)amino)ethyl]phthalimide (I): This compound was prepared using a modified literature procedure.[150] To a solution of bis(2-pyridylmethyl)amine (BPA) (8.0 g, 0.04 mol), in toluene (50 ml) was added triethylamine (5.6 mL, 0.04 mol) followed by a solution of *N*-(2-bromoethyl)phthalimide (10.2 g, 0.04 mol) in toluene (20 mL). The mixture was heated at reflux under nitrogen for 16 hours and was then concentrated under reduced pressure. The obtained red-brown solid residue was washed with 150 mL of ice-cold water followed by 50 mL of ether to give a cream (the colour can vary from gray-cream to violet) solid. The remaining of the product was recovered by recrystallization from filtrate at 4 °C and was added to the initially obtained solids to give 9.224 g (61%) of (I). ^{1}H-NMR (300 MHz, CDCl$_3$): δ 8.43 (d, 2H, aromatic H), 7.78 (m, 4H, aromatic H), 7.38 (m, 4H, aromatic H), 7.06 (t, 2H, aromatic H), 3.84 (t+s, 6H, CH_2), 2.89-2.81 (t, 2H, CH_2).

***N,N*-Bis(2-pyridylmethyl)ethane-1,2-diamine (II):** This compound was prepared based on a literature procedure.[151] A solution of the protected amine (I) (9.224 g, 0.024 mol) in absolute ethanol (50 mL) was added to a solution of hydrazine monohydrate (1.2 mL, 0.024 mol) in ethanol (50 mL). The solution was heated at reflux for 3 hours, resulting in the formation of a white precipitate after the first hour of reflux. The mixture was then concentrated under vacuum, and 1 M HCl (100 mL), followed by 12 M HCl (3 mL) was added to it while stirring in an ice bath. A white solid precipitated immediately. The suspension was stirred for 2 hours at 50 °C, followed by 24 hours at 25 °C. The white solid was then filtered off and the filtrate was evaporated to dryness under vacuum to yield a yellow oil which was re-dissolved in water (50 mL). To this aqueous solution was added aqueous NaOH solution (2M, 150 mL). The aqueous phase was extracted with CH_2Cl_2 (3 × 50 mL), and the combined organic phase was dried over Na_2SO_4 and evaporated to yield 5.34 g (89%) of pure (II) as a yellow oil. ^{1}H-NMR (500 MHz, $CDCl_3$): δ 8.52 (d, 2H, aromatic H), 7.65 (t, 2H, aromatic H), 7.49 (d, 2H, aromatic H), 7.15 (t, 2H, aromatic H), 3.85 (s, 4H, CH_2), 2.80 (t, 2H, CH_2), 2.65 (t, 2H, CH_2) , 1.50 (s, 2H, NH_2).

***N*-[2-(Bis(2-pyridylmethyl)amino)ethyl]-2-nitrobenzenesulfonamide (BPAEB$_{NO2}$) (III):**

Triethylamine (0.87 mL, 6.0 mmol) was added to the solution of amine (II) (1.39 g, 5 mmol) in CH_2Cl_2 (50 mL). The mixture was placed in an ice bath and was stirred until it reached 0 °C. The flask was then equipped with an addition funnel through which a solution of 2-nitrobenzenesulfonyl chloride (1.271 g, 0.006 mol, 1.1 eq) in CH_2Cl_2 (20 mL) was added dropwise to the stirring mixture at 0 °C over 3 minutes. When the addition was complete, the ice bath was removed and the reaction mixture was allowed to warm up to 25 °C and was stirred for 4 more hours at this temperature. The mixture was then quenched with saturated aqueous solution of $NaHCO_3$ (50 mL) and the solution was stirred at 25 °C overnight. The organic phase was separated and further washed with a saturated $NaHCO_3$ solution (2×50 mL) and then with water (1×50 mL). Combined organics were dried on Na_2SO_4 and evaporated to give 2.15 g of III as a pure light yellow-brown oil (88%). ^{1}H-NMR (500 MHz, CDCl3): δ 8.56 (d, 2H, aromatic Hs), 8.09 (m, 1H, aromatic H), 7.98 (bs, 1H, NH), 7.75 (m, 1H, aromatic H), 7.64 (m, 2H, aromatic H), 7.57 (t, 2H, aromatic H), 7.30 (d, 2H, aromatic H), 7.14 (t, 2H, aromatic H), 7.75 (m, 1H, aromatic H), 3.82 (s, 4H, CH_2), 3.19 (t, 2H, CH_2), 2.86 (t, 2H, CH_2).

_N_-[2-(Bis(2-pyridylmethyl)amino)ethyl]-2-hydroxylaminobenzenesulfonamide ($BPAEB_{NHOH}$)

A 250 mL Parr shaker flask was charged with 10% palladium on activated carbon catalyst (0.053 g, 1mol%) followed by 20 mL of methanol. A solution of $BPAEB_{NO2}$ (2.153 g, 0.005 mol) in methanol (50 mL) was added to the catalyst suspension and the flask was installed in the Parr apparatus followed by being degassed and purged 3 times with hydrogen. The pressure of the flask was adjusted to 40 psi and the connector valve between the flask and the 4 L tank was closed. The reaction mixture was shaken for 4 hours as the pressure in the flask went down to 25 psi. The set-up was depressurized and the light yellow suspension was passed through a packed celite pad to filter the catalyst off. The celite pad and the filtered palladium catalyst were allowed to stir in methanol for 4 hours to extract the remaining of product coordinated to the catalyst and were filtered over celite. The combined organics were evaporated under vacuum to yield a yellow oil. Pure yellow crystals of $BPAEB_{NHOH}$ (1.36 g, 65%) were obtained by recrystallization from ethanol/ether at -20 °C. ^{1}H-NMR (500 MHz, $CDCl_3$): δ 10.00 (br s, 1H, OH), 8.48 (dq, 2H, aromatic Hs), 7.78 (dd, 1H, aromatic Hs), 7,69 (br s, 1H, sulfonamide NH), 7.62 (d, 1H, aromatic Hs), 7.55 (t of d, 2H, aromatic Hs), 7.50 (t of d, 1H, aromatic Hs), 7.16 (d, 2H, aromatic Hs), 7.13 (q of d, 2H, aromatic Hs), 6.98 (t of d, 1H, aromatic Hs), 6.87 (br t, 1H, NH), 3.61 (s, 4H, CH_2), 2.90 (q, 2H, CH_2), 2.39 (t, 2H, CH_2). ^{13}C-NMR (500 MHz, $CDCl_3$): δ 159.35, 150.14, 149.35, 149.00, 148.15, 136.52, 134.58, 129.64, 128.42, 123.79, 123.20, 121.92, 122.52, 119.44, 115.08, 113.89, 60.51, 59.92, 59.19, 53.38. ESI mass spectrum: found m/z: 414.2, (calculated m/z: 414.2) $[BPAEB_{NHOH}]^{H+}$.

3.4 Preparation of the complexes

3.4.1 Synthesis of $[Fe^{(II)}BPAEB_{NO}(OAc)]$. MeCN

In the glovebox, a solution of ligand $BPAEB_{NHOH}$ (206.74 mg, 0.5 mmol) in MeCN (5 mL) was added dropwise to a stirring suspension of anhydrous $Fe(OAc)_2$ (86.74 mg, 0.5 mmol) in MeCN (3 mL). The reaction was stirred for 30 minutes, resulting in solubilizing the $Fe(OAc)_2$ and precipitation of a dark reddish-brown solid. The solid was filtered off and washed thoroughly with MeCN, then ether, and was dried under vacuum. This procedure afforded 132.6 mg of pure $[Fe^{(II)}BPAEB_{NO}(OAc)]$.MeCN (50%). Single crystals were grown by slow diffusion of a concentrated solution of the ligand in MeCN over a suspension of $Fe(OAc)_2$ in MeCN at -40 °C over 24 hours and were used for structural determination by X-ray crystallography (see 4.1). Crystals of this product were found to be stable in air (more than 6 months of shelf-life) and stayed intact in protic solvents. ESI mass spectrum: m/z: 466.1 (calculated m/z: 466.1)$[Fe^{(II)}BPAEB_{NO}]^+$. ^{1}H-NMR data were inconclusive due to paramagnetism of the complex. Magnetic moment of the complex (based on Evans method): 2.568 B.M.

3.4.2 Synthesis of $[Fe^{(II)}BPAEB_{NH_2}(OAc)]$

The yellow-brown solution obtained after the filtration of the reaction between $BPAEB_{NHOH}$ and $Fe(OAc)_2$ in MeCN was concentrated to 2 mL under vacuum and was layered with ether. 89.5 mg (40%) of light yellow rhombic crystals of $[Fe^{(II)}BPAEB_{NH_2}(OAc)]$ were obtained after a few days at -40 °C, and used to determine the structure by X-ray crystallography (see 4.1) Crystals of this product were air-stable but mildly hygroscopic. ESI mass spectrum: Found m/z: 452.2 (calculated m/z: 452.1) $[Fe^{(II)}BPAEB_{NH_2}]^+$. ^{1}H-NMR data were inconclusive due to paramagnetism of the complex.

3.4.3 Synthesis of $[Fe^{(II)}BPAEB_{NO}(MeCN)](OTf)\ .Et_2O$

$Fe(OTf)_2.2MeCN$[152] (109.02 mg, 0.25 mmol) was dissolved in MeCN (5 mL) and added dropwise to a stirring solution of ligand $BPAEB_{NHOH}$ (103.37 mg, 0.25 mmol) in MeCN (5 mL) in the glovebox. The mixture immediately changed color to deep purple. The solution was stirred for 30 additional minutes after which it was concentrated (3 mL) under vacuum, layered with ether, and kept at -40 °C for 2 days. Deep purple-black needle crystals (64.77 mg, 43%) were collected and washed with ether and used for structural studies by X-ray crystallography (see 4.1). Crystals of this product were stable enough to be manipulated in air for crystallographic purposes. ESI mass spectrum: Found m/z: 466.2 (calculated m/z: 466.1) $[Fe^{(II)}BPAEB_{NO}]^+$. ^{1}H-NMR data were inconclusive due to paramagnetism of the complex.

3.5 Reactivity Studies

Reactions of the synthesized $[Fe^{(II)}BPAEB_{NO}(OAc)]$ complexes with alkenes (1-hexene, α-methylstyrene) and different phosphine reagents (PPh_3, $PEtPh_2$, PMe_2Ph, PMe_3) were carried out in CH_2Cl_2 or MeCN at 25 °C in the glovebox. Choices of solvents were limited due to the poor solubility of $[Fe^{(II)}BPAEB_{NO}(OAc)]$ in aprotic solvents. Stock solutions of $[Fe^{(II)}BPAEB_{NO}(OAc)]$ (3.286 mM) and phosphine reagents (7.238 mM) were prepared prior to use, although they were found to be stable for days when stored at -40 °C. Alkenes were dried on molecular sieves and stored under dry nitrogen, and were used as neat chemicals. Twenty equivalents of alkene reagent or 2 equivalents of phosphine reagent were reacted with 1 equivalent of $[Fe^{(II)}BPAEB_{NO}(OAc)]$ and the total concentrations were constant between experiments to compare the reaction times in different conditions (alkene/phosphine, solvent). Control experiments with equimolar, 5 equivalents, 10 equivalents and 100 equivalents of phosphine were also performed. Reactions were monitored by mass spectrometry, UV-visible and GC up to consumption of all the $Fe^{(II)}BPAEB_{NO}$ complex. In reactions with phosphines the completion of the reaction was visibly noticeable by decay of the reaction mixture's color from deep red ($[Fe^{(II)}BPAEB_{NO}(OAc)]$) to light green and then yellow over time. No color change was noticed in reactions with alkene reagents. Preliminary reactivity studies with $[Fe^{(II)}BPAEB_{NO}(MeCN)](OTf)$ complex and 2 equivalents of PMe_3 was performed in CH_2Cl_2 or MeCN and the reaction was followed by mass spectrometry. Completion of this reaction was visibly noticeable by decay of the color from deep purple to light yellow.

3.6 Characterization

The reaction of [Fe$^{(II)}$BPAEB$_{NO}$(OAc)] with 2.16 equivalents of PMe$_2$Ph was followed by proton-decoupled ^{31}P-NMR (300 MHz) at 40 °C. After recording the ^{31}P-NMR of 2.763 mg (0.02 mmol) of PMe$_2$Ph solution in CDCl$_3$ in an NMR tube with a screw septum cap, a solution of 5.5 mg (0.01 mmol) [Fe$^{(II)}$BPAEB$_{NO}$(OAc)] in CDCl$_3$ was added to it via syringe and ^{31}P-NMR spectrum of the reaction mixture was recorded every 8 minutes (allowing enough relaxation delays between each acquisition) for 5 hours.

To the reactions of [Fe$^{(II)}$BPAEB$_{NO}$(OAc)] with 2 equivalents of PPh$_3$, PMe$_2$Ph, and PEtPh$_2$ in dichloromethane, after completion, were added 2 equivalents of anthracene and the mixtures were diluted and directly injected into the GC. The oven temperature was fixed at 250 °C and the running method was set for 15 minutes. Retention times of the phosphines and their corresponding phosphine oxides were assigned by control experiments with pure samples (phosphine oxides were prepared by oxidation of their corresponding phosphines with hydrogen peroxide). Peaks in the GC chromatograms were integrated and referenced to the anthracene concentration. The yield of phosphine oxide is based on the starting [Fe$^{(II)}$BPAEB$_{NO}$(OAc)] concentration.

To study the effect of the reaction of [Fe$^{(II)}$BPAEB$_{NO}$(OAc)] with PMe$_3$ on the ligand backbone, the product of this reaction was demetallated with ammonium hydroxide. Before demetallation, the solvent was evaporated under vacuum and ^{31}P and ^{1}H-NMR of the solid yellow product was obtained in CDCl$_3$. This solution was then treated with pure ammonium hydroxide and extracted into CH_2Cl_2 (3×20 mL). Combined organics were dried on Na_2SO_4 and evaporated under vacuum to yield a pale greenish-yellow oil. Proton-decoupled ^{31}P-NMR of the product before demetallation: (500 MHz, CDCl3): δ 40.7 (s, $OPMe_3$), peaks of unknown identity appear at 15.65 and 30.33 ppm. ^{1}H-NMR of the product before demetallation was inconclusive due to paramagnetism of the product complex. ^{1}H-NMR of the product after demetallation was inconclusive due to presence of intractable mixture of organics.

3.7 Kinetic studies

Kinetic studies via UV-visible spectroscopy were performed in a 1 mL UV-Visible cuvette with 1 cm path length, sealed with a septum cap. The cuvette was loaded with 1 mL of CH_2Cl_2 and 100 μL of a [$Fe^{(II)}BPAEB_{NO}(OAc)$] stock solution (3.709 mM). 102 μL of a PMe_2Ph stock solution (7.238 mM) was loaded and sealed under nitrogen in a gastight syringe and was then injected at once in to the stirred [$Fe^{(II)}BPAEB_{NO}(OAc)$] solution through the septa. UV-visible absorbance was then read every 2 minutes until the intense red color of the solution decayed to light green. Kinetic studies were performed at 14, 17, and 21 °C and the obtained data were fitted to calculate the rate constants and rate laws. SPECFIT32 software was used for data fitting purposes.

3.8 Structural Studies by X-ray Crystallography

Crystallographic details of data collection, refinement, and list of atomic coordinates for complexes [$Fe^{(II)}BPAEB_{NO}(OAc)$], [$Fe^{(II)}BPAEB_{NH_2}(OAc)$] and [$Fe^{(II)}BPAEB_{NO}(MeCN)$](OTf) are provided in Appendix I. All crystallographic plots were made with Ortep3v2 and tables were generated by publCIF.

4. Results and Discussion

4.1 Synthetic Results

4.1.1 Synthesis and Characterization of [Fe$^{(II)}$BPAEB$_{NO}$(OAc)].MeCN

[Fe$^{(II)}$BPAEB$_{NO}$(OAc)] was synthesized in 50% yield from disproportionation of the hydroxylamine (BPAEB$_{NHOH}$) ligand, in presence of equimolar amounts of Fe(OAc)$_2$. Structure of this complex in the solid state was verified by X-ray crystallography of its brown-red crystals (Figure 43). Complex [Fe$^{(II)}$BPAEB$_{NO}$(OAc)] crystallizes in a monoclinic system with P 2_1/c space group and its unit cell contains four independent molecules co-crystallizing with 4 molecules of acetonitrile (Table 1) (see Appendix I). This structure confirms the formation of a nitroso function, coordinated to the Fe center in a η^1 fashion through nitrogen. It also verifies the deprotonation of the sulfonamide group upon coordination to iron and coordination of an acetate anion, all in agreement with the oxidation state of iron as +2. The coordination around the iron atom is a slightly distorted octahedron (equatorial plane is shifted upwards) with five positions being occupied by the ligand and an acetate anion occupying the sixth position. The nitroso group is located *trans* to the tertiary amine and the acetate anion is positioned *trans* to one of the pyridines, placing the pyridyl arms *cis* to each other.

Distances and angles pertaining to the inner coordination sphere of the iron are listed in Table 2. Comparison of the bond lengths in coordinated N-O (1.266(2) Å) with free ArNO ligands (1.25 Å)[124] shows a small elongation in the typical NO double bond[124], hence suggesting the presence of a small degree of Fe-to-π*(NO) backbonding. The high dihedral angle between O1-N1-C1-C6 (41.13 degrees) and the Fe1-N1 bond length

(1.8046(18) Å), which is typical of Fe(II)-N single bond, are also in agreement with a very modest backbonding interaction between the filled iron d orbitals and the π* system of the NO moiety.[138]

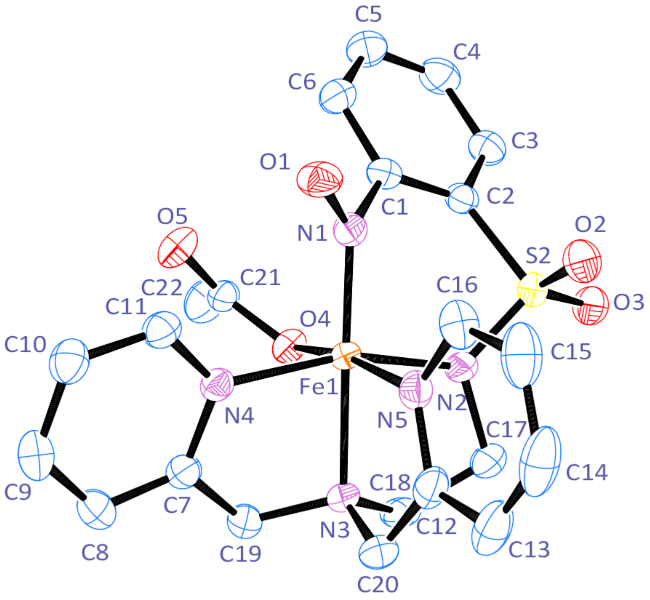

Figure 43. ORTEP representation (50% thermal ellipsoid) of the solid-state molecular structure of [Fe$^{(II)}$BPAEB$_{NO}$(OAc)]. Hydrogen atoms and an acetonitrile molecule have been omitted for clarity.

Table 1. Crystallographic data for [Fe$^{(II)}$BPAEB$_{NO}$(OAc)]

	Space Group	***Z***	***R$_1$***	***wR$_2$***	**S**
[Fe$^{(II)}$BPAEB$_{NO}$(OAc)]	$P2_1/c$	4	4.27%	8.31%	1.06

Table 2. Selected bond lengths (Å) and angles (°) for [$Fe^{(II)}BPAEB_{NO}(OAc)$]

Selected Bonds	**Bond Length [Å]**	**Selected Angles**	**[Deg]**
Fe1-N1	1.8046(18)	N1-Fe1-O4	92.99(7)
Fe1-N2	1.9846(17)	N1-Fe1-N2	96.56(7)
Fe1-N3	2.0561(17)	N1-Fe1-N5	96.44(8)
Fe1-N4	2.0205(17)	N1-Fe1-N4	100.36(7)
Fe1-N5	1.9939(18)	N3-Fe1-N1	178.77(8)
Fe1-O4	1.9546(15)	O4-Fe1-N2	85.41(7)
N1-O1	1.266(2)	O4-Fe1-N4	90.61(7)
		N4-Fe1-N5	91.05(7)
		N5-Fe1-N2	90.11(7)
		O1-N1-Fe1	125.86(14)
		O1-N1-C1-C6	41.13

[$Fe^{(II)}BPAEB_{NO}(OAc)$] complex was also characterized by spectroscopic means. The UV-visible absorbance spectrum of this complex (Figure 44) was measured in CH_2Cl_2, from which the absorption coefficient was calculated for each absorption maximum (Table 3). In infrared spectroscopy, the ν_{NO} vibration for N-bound metal-nitroso complexes is typically in the 1300-1450 cm^{-1} region; however, due to overlapping vibrations of the sulfonamide group in the same region, these bands for [$Fe^{(II)}BPAEB_{NO}(OAc)$] complex could not be confidently identified.

Table 3. Absorption coefficients for each absorption maximum of [$Fe^{(II)}BPAEB_{NO}(OAc)$] complex in UV-visible region, $1.426*10^{-4}$ M in CH_2Cl_2

Wavelength (nm) (λ)	**Absorption coefficient (ε) (M^{-1} cm^{-1})**
295	8100
415	3640
525	2350

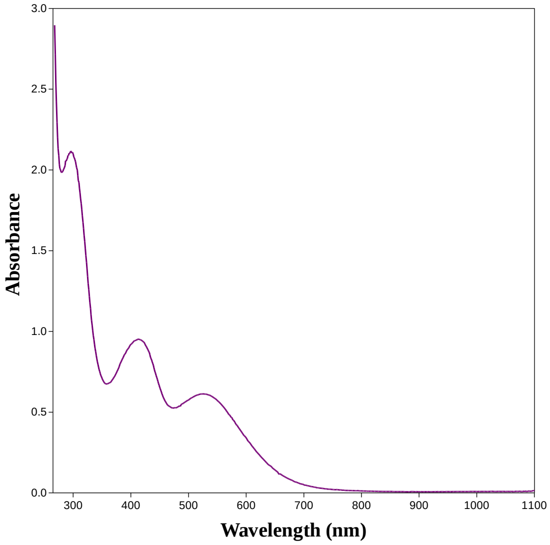

Figure 44. UV-visible absorption spectrum of $[Fe^{(II)}BPAEB_{NO}(OAc)]$ complex in CH_2Cl_2

The magnetic susceptibility of $[Fe^{(II)}BPAEB_{NO}(OAc)]$ complex, measured based on the Evans method, is 2.56 BM, which is close to the value reported for species with spin state of 1. This finding explains the paramagnetic behaviour of this complex in solution during NMR studies. However, Fe(II) high-spin complexes in octahedral geometry could only adopt 4 unpaired electrons and presence of only 2 unpaired electrons is not in accordance with the octahedral ligand field of this complex in solid-state. A possible reason for this discrepancy is that spin-crossover happens in this complex and hence, the presence of spin equilibrium lowers the measured magnetic moment. Spin-orbit coupling could also lower the magnetic susceptibility in such complexes. However, not much decrease in the paramagnetic susceptibility value is expected to happen for this case and therefore, spin-orbit coupling would not likely be responsible for the observed low magnetic susceptibility. This phenomenon should be studied by accurate measurements of the magnetic susceptibility of the complex at variable temperatures with a SQUID magnetometer. A more likely justification for this phenomenon is that the structure of this complex in solution is different than the octahedral geometry seen in its solid-state structure and therefore, the measured magnetic moment corresponds to a different ligand field at the coordination center. If the acetate anion dissociates in solution, then the complex in solution would adopt trigonal-bipyramidal geometry. This geometry matches well with the arrangement of electrons to give 2 unpaired electrons in the d orbitals of iron and hence, its spin-state of 1.

4.1.2 Synthesis and Characterization of $[\mathrm{Fe}^{(II)}\mathrm{BPAEB}_{NO}(\mathrm{MeCN})](\mathrm{OTf})$

Like its acetate analogue, the $[\mathrm{Fe}^{(II)}\mathrm{BPAEB}_{NO}(\mathrm{MeCN})](\mathrm{OTf})$ complex was prepared by disproportionation of the hydroxylamine (BPAEB_{NHOH}) ligand with an equimolar amount of $[\mathrm{Fe(OTf)_2}]\cdot 2\,\mathrm{MeCN}$ in acetonitrile, in 43% yield. This complex crystallizes in a monoclinic system with P 2_1/c space group and its unit cell contains four independent molecules and two molecules of ether (Table 4) (see Appendix I). X-ray crystallography of the isolated deep purple crystals confirmed that, similar to $[\mathrm{Fe}^{(II)}\mathrm{BPAEB}_{NO}(\mathrm{OAc})]$, $[\mathrm{Fe}^{(II)}\mathrm{BPAEB}_{NO}(\mathrm{MeCN})](\mathrm{OTf})$ has a η^1-nitroso group that is coordinated to iron through nitrogen as well as a deprotonated sulfonamide. However, $[\mathrm{Fe}^{(II)}\mathrm{BPAEB}_{NO}(\mathrm{MeCN})](\mathrm{OTf})$ has an acetonitrile molecule coordinated to iron and there is one non-coordinated triflate anion to neutralize the $[\mathrm{Fe}^{(II)}\mathrm{BPAEB}_{NO}(\mathrm{MeCN})]^+$ moiety, again confirming the oxidation state of iron as +2.

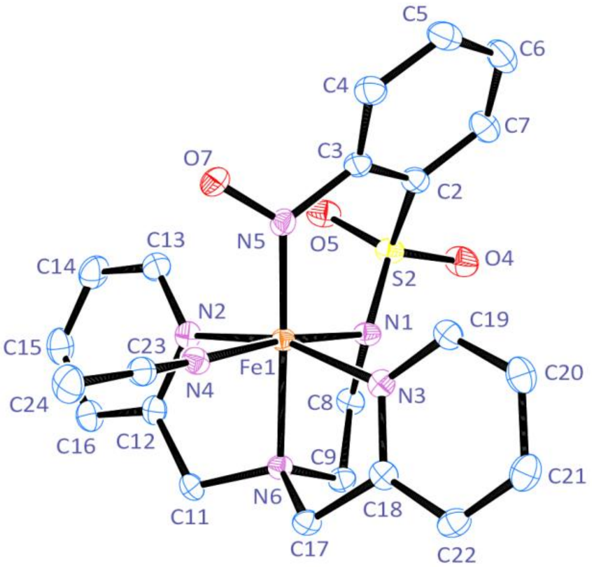

Figure 45. ORTEP representation (50% thermal ellipsoid) of the solid-state molecular structure of [Fe$^{(II)}$BPAEB$_{NO}$(MeCN)](OTf). Hydrogen atoms, an ether molecule and a triflate anion have been omitted for clarity.

Table 4. Crystallographic data for [Fe$^{(II)}$BPAEB$_{NO}$(MeCN)](OTf)

	Space Group	***Z***	***R_1***	***wR_2***	**S**
[Fe$^{(II)}$BPAEB$_{NO}$(MeCN)](OTf)	$P2_1/c$	4	6.05%	10.93%	1.00

Table 5. Selected bond lengths (Å) and angles (°) in [Fe$^{(II)}$BPAEB$_{NO}$(MeCN)](OTf)

Selected Bonds	Bond Length [Å]	Selected Angles	[Deg]
Fe1-N5	1.818(2)	N5-Fe1-N4	90.16(9)
Fe1-N1	1.983(2)	N5-Fe1-N1	96.06(9)
Fe1-N6	2.037(2)	N5-Fe1-N3	101.15(9)
Fe1-N3	2.014(2)	N5-Fe1-N2	95.21(9)
Fe1-N2	1.975(2)	N5-Fe1-N6	177.49(9)
Fe1-N4	1.954(2)	N4-Fe1-N2	88.25(9)
N5-O7	1.259(3)	N4-Fe1-N3	88.26(8)
		N1-Fe1-N3	88.97(8)
		N1-Fe1-N2	92.76(9)
		O7-N5-Fe1	122.10(17)
		O7-N5-C3-C4	33.91

The coordination around the iron atom is a distorted octahedron with a different configuration compared with the [Fe$^{(II)}$BPAEB$_{NO}$(OAc)] complex. It is structured with two coplanar pyridines *trans* to each other, resulting in the sulfonamide group being *trans* to the acetonitrile molecule (Figure 45). The position of nitroso group is *trans* to the tertiary amine, similar to the [Fe$^{(II)}$BPAEB$_{NO}$(OAc)] complex. Distances and angles pertaining to the inner coordination sphere of the iron are listed in (Table 5). Compared with [Fe$^{(II)}$BPAEB$_{NO}$(OAc)], the nitroso (N5-O7) bond in [Fe$^{(II)}$BPAEB$_{NO}$(MeCN)](OTf) is shorter (1.259(3) vs. 1.266(2)) and closer to the NO bond length in free aryl nitroso ligands (1.25 Å), whereas the Fe1-N5 bond is longer (1.818(2) vs. 1.8046(18)), suggesting that there is not any significant backbonding between Fe and the NO unit. However, the smaller O7-N5-C3-C4 dihedral angle between the nitroso group and the phenyl ring in [Fe$^{(II)}$BPAEB$_{NO}$(MeCN)](OTf) (33.91 vs. 41.13 degrees), which suggests a stabilizing backbonding from iron d orbitals to the nitroso π* orbitals, seems unlikely according to the discussed bond length data. The origin of this observed conformational preference in the solid state structure of [Fe$^{(II)}$BPAEB$_{NO}$(MeCN)](OTf) remains uncertain and could be due to crystal packing effects. Other bonds in the coordination sphere of this complex are similar to their corresponding bonds in [Fe$^{(II)}$BPAEB$_{NO}$(OAc)] and hence their lengths are rationalized based on the same arguments.

UV-visible absorbance measurements of this complex (Figure 46) led to the absorption coefficients for each absorption maximum reported in Table 6. Compared to the UV-visible spectra of [Fe$^{(II)}$BPAEB$_{NO}$(OAc)], the absorption maxima appear at the same wavelength, except for the absorption at 295 nm which is not well defined since MeCN absorbs in that region. Different intensities of the absorbance of these two complexes, however, can be due to the difference in the electron-richness of iron center when bonded to acetate (better electron donor) or acetonitrile ligands.

Table 6. Absorption coefficients for each absorption maximum of [Fe$^{(II)}$BPAEB$_{NO}$(MeCN)](OTf) complex in UV-visible region, $1.426*10^{-4}$ M in CH_2Cl_2

Wavelength (λ) (nm)	**Absorption coefficient (ε) (M^{-1} cm^{-1})**
415	11000
525	7700

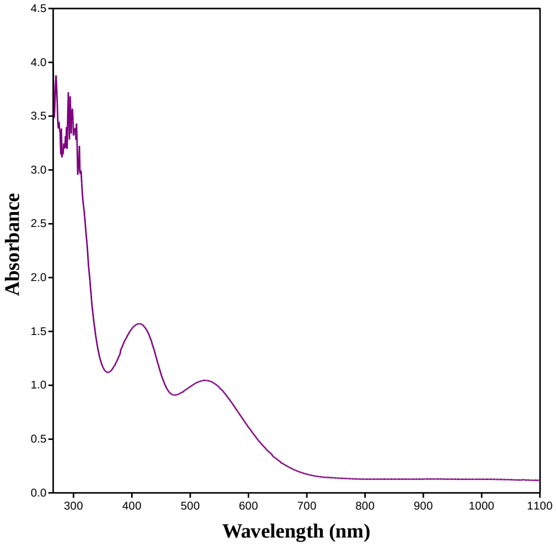

Figure 46. UV-visible absorption spectrum of [Fe$^{(II)}$BPAEB$_{NO}$(MeCN)](OTf) complex in CH_2Cl_2

4.1.3 Synthesis and Characterization of [Fe$^{(II)}$BPAEB$_{NH2}$(OAc)]

Complex [Fe$^{(II)}$BPAEB$_{NH2}$(OAc)] was formed as the reduced product of disproportionation during the synthesis of [Fe$^{(II)}$BPAEB$_{NO}$(OAc)] and was isolated as block yellow crystals in 35% yield. X-ray crystallography was performed on the obtained crystals and they were solved in triclinic system with P −1 space group, containing two independent molecules in each unit cell (Table 7). The structure of this complex in solid state was established as a distorted trigonal bipyramidal complex of Fe(II) with the BPAEB$_{NH2}$ ligand having two pyridines and the deprotonated sulfonamide in equatorial positions and the tertiary amine and acetate anion in axial positions (Figure 47). Table 8 lists a selection of important bond lengths and angles. The significant tilt of the acetate ligand from a strict axial position, as well as the spatial orientation of the aniline arm, are due to formation of inter- and intra-molecular hydrogen bonds in the crystal lattice between the acetate oxygens, the hanging aniline group, and the sulfonamide oxygens.

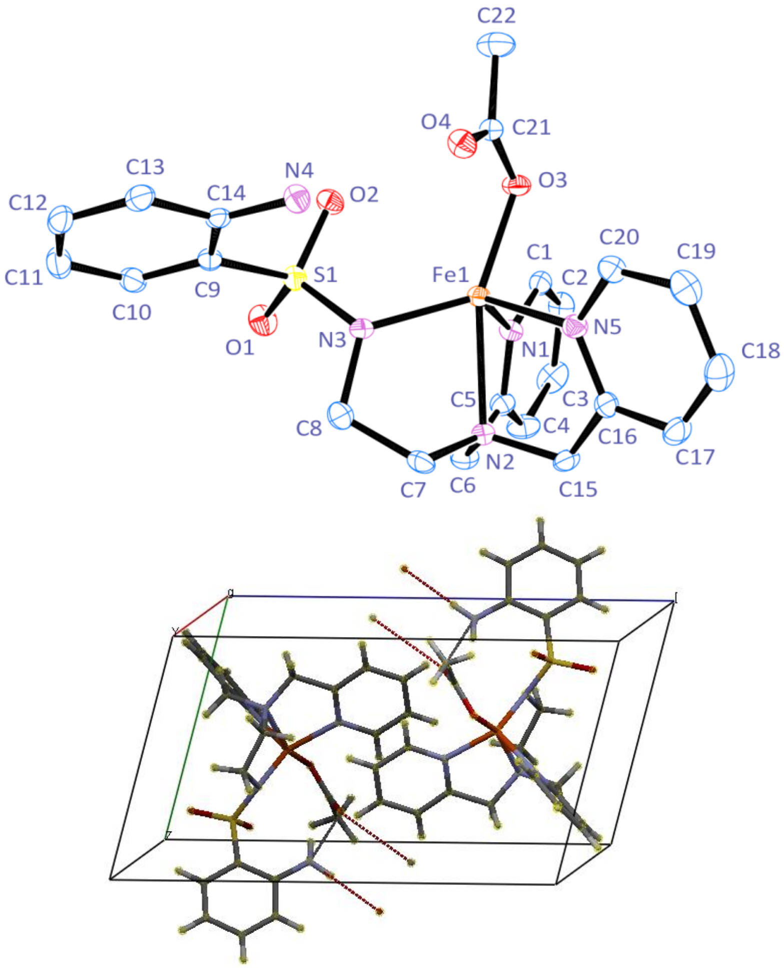

Figure 47. Top: ORTEP (50% thermal ellipsoid) representation of the solid-state molecular structure of [Fe$^{(II)}$BPAEB$_{NH2}$(OAc)]. Hydrogen atoms have been omitted for clarity. Bottom: Crystal packing of [Fe$^{(II)}$BPAEB$_{NH2}$(OAc)] showing the hydrogen bondings as dashed lines

Table 7. Crystallographic data for [Fe$^{(II)}$BPAEB$_{NH2}$(OAc)]

	Space Group	***Z***	***R$_1$***	***wR$_2$***	**S**
[Fe$^{(II)}$BPAEB$_{NH2}$(OAc)]	*P-1*	2	5.73%	10.48%	0.99

Table 8. Selected bond lengths (Å) and angles (°) in [Fe$^{(II)}$BPAEB$_{NH2}$(OAc)]

Selected Bonds	**Bond Length [Å]**	**Selected Angles**	**[Deg]**
Fe1-N1	2.159(3)	O3-Fe1-N1	89.34(10)
Fe1-N2	2.284(3)	O3-Fe1-N3	125.73(10)
Fe1-N3	2.050(3)	O3-Fe1-N5	96.75(10)
Fe1-N5	2.161(3)	N1-Fe1-N5	111.86(10)
Fe1-O3	2.004(2)	N5-Fe1-N3	116.11(10)
		N3-Fe1-N1	113.55(10)
		O3-Fe1-N3-S1	34.04
		C9-S1-N3-Fe1	-140.15

4.2 Reactivity and Kinetic Studies

Reactivity of the iron-nitroso complex [Fe$^{(II)}$BPAEB$_{NO}$(OAc)] as an OAT agent was studied with two types of nucleophilic substrates: alkenes and phosphines. Neither of the used alkenes (α-methylstyrene and *n*-hexene) were capable of deoxygenating the nitroso group under the reaction conditions mentioned in the experimental chapter (large excess of alkene, 25 °C, 7 days of reaction time). Phosphines were, therefore, chosen as substrates, since they are great oxophiles and are known to react with electrophilic organic C-nitroso compounds (see 2.3.2). Also, since they are good nucleophiles, they can trap the electrophilic nitrene intermediate as well.

4.2.1 Characterization of Reaction Products

Reactivity studies with different phosphines (PR_3 = PPh_3, $PEtPh_2$, PMe_2Ph, PMe_3) showed that the iron-nitroso complex [Fe$^{(II)}$BPAEB$_{NO}$(OAc)] could transfer the oxygen atom at the nitroso functionality to these phosphine reagents in yields varying from 47 to 100% with respect to the initial concentration of complex (Table 9).

Table 9. Yields of formation of phosphine oxides from phosphines based on GC experiments. Retention time (RT) for each compound is noted in parentheses (HP-5 column, 250 ˚C)

PR_3 (RT-min)	**OPR_3 (RT-min)**	**Yield %**	**Reaction Time**
PPh_3 (10.5)	$OPPh_3$ (14)	47	48 h
$PEtPh_2$ (7.7)	$OPEtPh_2$ (9.8)	100	10 h
PMe_2Ph (3.3)	$OPMe_2Ph$ (6)	52	4 h
PMe_3 (-)	$OPMe_3$ (-)	-	2 h

Reaction times of the [$Fe^{(II)}BPAEB_{NO}(OAc)$] complex with different phosphine reagents (PPh_3, $PEtPh_2$, PMe_2Ph, and PMe_3) were greatly affected by the oxophilicity of the used phosphine, in a way that more nucleophilic phosphines (more alkyl groups attached to phosphorus, e.g. PMe_3), were able to deoxygenate the iron-nitroso complexes faster than less nucleophilic phosphines (more aryl groups attached to phosphorus, e.g. PPh_3). This could also be attributed to the steric effects and the fact that phosphines with less steric hindrance were able to react faster with the iron-nitroso complex. Reaction times (the time needed for the reaction mixture’s color to decay to yellow) for these phosphines are shown in Table 9. OAT from [$Fe^{(II)}BPAEB_{NO}(OAc)$] to phosphine reagents was confirmed by GC of reacted mixtures, showing the consumption of the phosphine reagent and formation of the phosphine oxides as one of the products (Table 9). However, due to the high sensitivity of trialkyl phosphines to oxygen, only the yields of PPh_3, $PEtPh_2$, and PMe_2Ph could be estimated by this method. The discrepancy in these yields could be due to the sensitive nature of these reagents which makes the presence of small amounts of free phosphine oxides inevitable. These experiments need to be repeated more carefully to obtain more accurate results proper for comparison purposes.

The nature of other products (metal-containing products) was determined by ESI-MS of the completed reaction mixtures of [Fe$^{(II)}$BPAEB$_{NO}$(OAc)] with different phosphines (PR$_3$ = PPh$_3$, PMe$_2$Ph, PMe$_3$). Data obtained from these experiments proved the formation of a new species with an m/z ratio consistent with a (Fe$^{(II)}$BPAEB$_N$ + PR$_3$) formulation, where [Fe$^{(II)}$BPAEB$_N$] is the deoxygenated iron-nitroso complex. Interestingly, ESI-MS of the same reaction with PEtPh$_2$ showed a peak with m/z: 610 which was assigned to the deoxygenated ligand and the phosphine (BPAEB$_N$ + PEtPh$_2$). This finding eliminates the alternative of coordination of the phosphine to the metal in a potential iron-imido species ([FeBPAEB$_N$(PR$_3$)] vs. [FeBPAEB$_{NPR_3}$]), suggesting that the phosphine group should be bonded to the ligand backbone so that it is not removed by demetallation (Table 10). Isotopic patterns of all these products were also in agreement with the calculated isotopic patterns (Figure 48).

Table 10. m/z ratios of the products of the reaction of phosphine reagents with [Fe$^{(II)}$BPAEB$_{NO}$(OAc)] (P)

PR$_3$	**Products**	**m/z of Products**	**Calculated m/z**
PPh$_3$	[FeBPAEB$_{NPPh_3}$]	712.925	712.156
PMe$_2$Ph	[FeBPAEB$_{NPMe_2Ph}$]	588.609	588.125
PMe$_3$	[FeBPAEB$_{NPMe_3}$]	526.518	526.109
PEtPh$_2$	[BPAEB$_{NPEtPh_2}$]	610.107	610.240

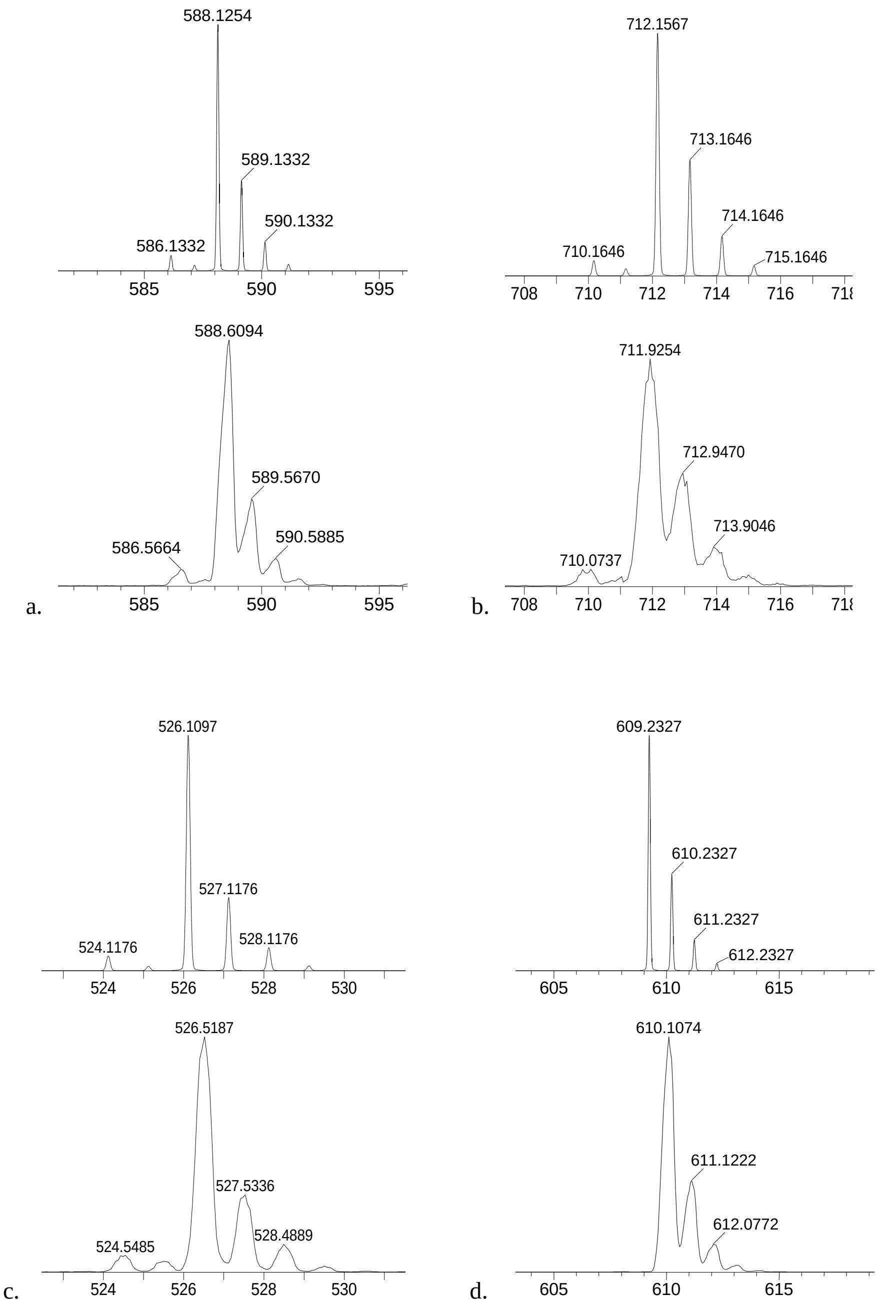

Figure 48. Mass spectra of products of the reactions of [Fe$^{(II)}$BPAEB$_{NO}$(OAc)] with phosphine reagents, a. PMe$_2$Ph b.PPh$_3$ c. PMe$_3$ d. PEtPh$_2$, In each case the calculated isotopic patterns are on top and experimental isotopic patterns are on the bottom. In d. the experimental state is one unit higher than the calculated due to the protonation of the moiety.

Unfortunately, all our efforts to isolate and crystallize these phosphine-containing species were unsuccessful and when crystals were obtained, because of weak diffraction at high angles no proper X-ray structural data could be gained. However, although not isolated, based on the data obtained from ESI-MS of the products, we propose that these species have iminophosphorane-type structures which are analogous to the known examples[141,142] of phosphine-mediated deoxygenation of both coordinated and non-coordinated C-nitroso compounds (Figure 49) (see 2.3.2 and 4.3.3). Iminophosphoranes are known to be prone to hydrolysis into their respective amines, especially when they are activated by coordination to a metal, which could explain the difficulty in isolating a crystalline sample.

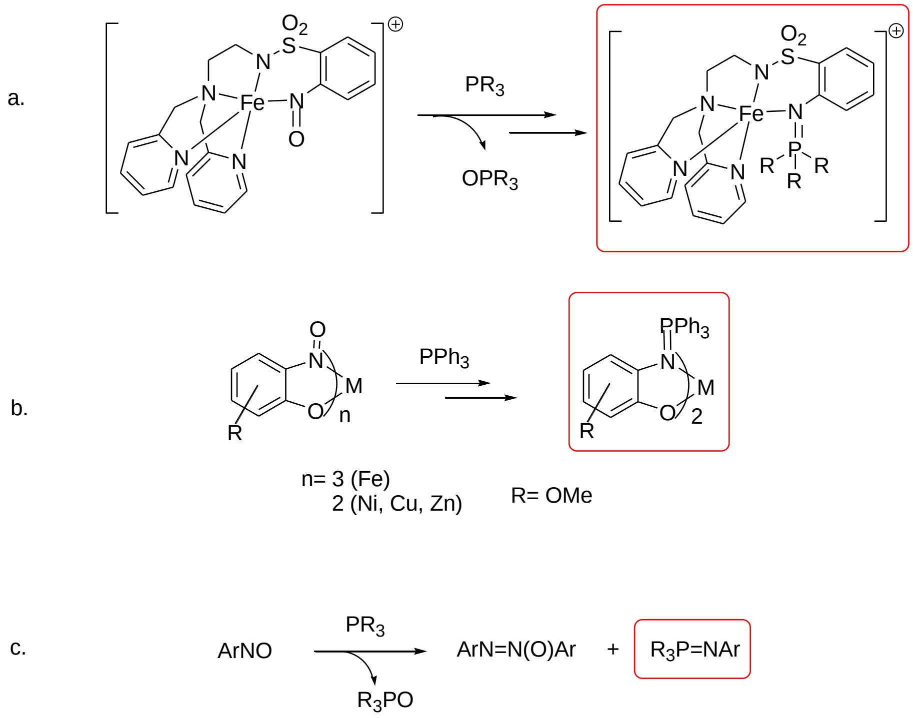

Figure 49. a. Phosphine-mediated formation of iminophosphrane-iron complex and its comparison with reported examples of iminophosphorane formation from b. metal-coordinated nitroso complex[142] and c. organic C-nitroso compounds[141]

The reactivity of the [$Fe^{(II)}BPAEB_{NO}(MeCN)$](OTf) complex was studied with PMe_3 and analyzed by mass spectrometry. ESI-MS results show that this complex was also capable of performing OAT to PMe_3 in one hour when the reaction was performed in CH_2Cl_2 (in the same concentration conditions as [$Fe^{(II)}BPAEB_{NO}(OAc)$] complex). However, although formation of the iminophosphorane complex was seen by ESI-MS, these compounds could not be isolated either. Interestingly, when the same reaction was performed in MeCN, there was no sign of reaction proceeding and the starting [$Fe^{(II)}BPAEB_{NO}(MeCN)$](OTf) complex was not consumed after 2 days of reaction. This solvent effect suggests that the dissociation of the coordinated MeCN may be of key importance in triggering the reaction. When the reaction is done in MeCN medium, the de-coordination of the acetonitrile molecule is not favoured, hence no reaction would occur (see 4.3.3). This effect is more explained in the discussion chapter (see 4.3.3).

4.2.2 Kinetic Studies

Kinetics of the reaction of the [$Fe^{(II)}BPAEB_{NO}(OAc)$] complex with phosphine reagents was studied by means of ^{31}P-NMR and UV-visible spectroscopic techniques. The ^{31}P-NMR measured during the reaction of [$Fe^{(II)}BPAEB_{NO}(OAc)$] with 2.16 equivalents of PMe_2Ph over 4 hours shows the formation and increase of the $OPMe_2Ph$ peak at 35 ppm, while the PMe_2Ph peak at -42 ppm is decreasing (Figure 50). It also shows a third phosphorous-containing species at 15 ppm and its concentration increased along with the formation of the $OPMe_2Ph$, which could tentatively be assigned to the iminophosphorane complex. Unfortunately, no example of well-studied Fe-iminophosphorane complexes has been reported in literature for comparison purposes, but the position of this peak, compared with that of the free PMe_2Ph and $OPMe_2Ph$, indicates that the phosphorous is attached to an electronegative group and it’s resonance is hence moved downfield. The only available ^{31}P NMR examples of aryliminophosphorane complexes (Ni[153], Pd[154]) have δ values between 14 to 20 ppm, in comparison with free iminophosphorane ligands[155] which appear around 3 to 7 ppm. Clearly the only way to confidently assign this peak to the corresponding free or coordinated iminophosphorane is when it is isolated and studied separately.

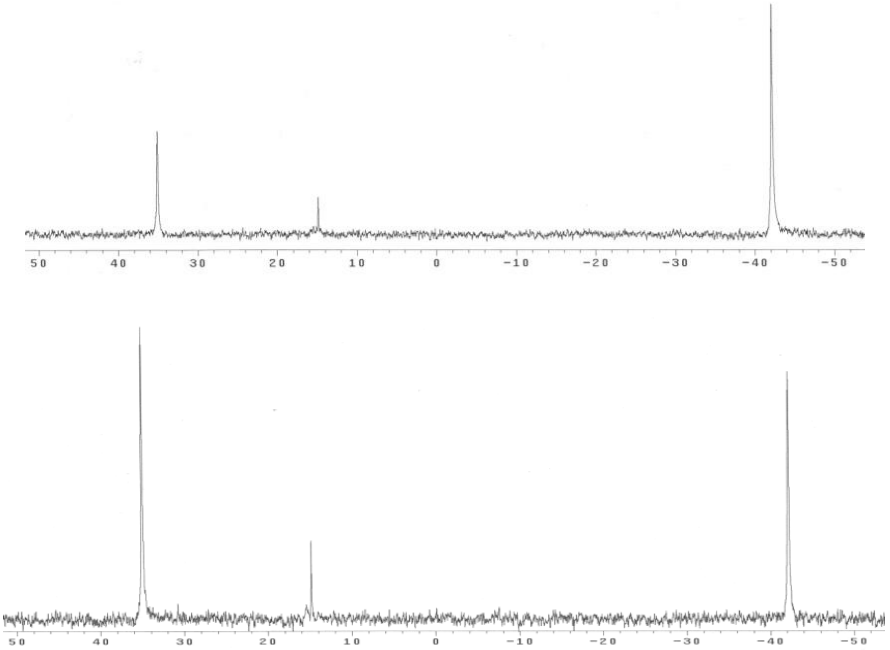

Figure 50. ^{31}P-NMR spectra of the reaction of [Fe$^{(II)}$BPAEB$_{NO}$(OAc)] with PMe$_2$Ph showing the decrease of PMe$_2$Ph at -42 ppm and increase of OPMe$_2$Ph at 35 ppm, middle peak at 15 ppm is proposed to be the iminophosphorane product, top: spectrum after 15 minutes, bottom: spectrum after 2 hours

The ^{31}P-NMR spectrum of the solution obtained after complete reaction of [Fe$^{(II)}$BPAEB$_{NO}$(OAc)] with 2 equivalents of PMe$_3$ (all solvents and unreacted PMe$_3$ evaporated) show a single peak at 40 ppm which corresponds to OPMe$_3$. The two other peaks (at 15.6 and 30.3 ppm) cannot be confidently assigned but, according to the same argument mentioned before, could belong to an iminophosphorane species (free and coordinated). ^{1}H-NMR of this mixture before demetallation was inconclusive due to paramagnetic effects of the products. Demetallation through an ammonium hydroxide workup was also not helpful in identifying the nature of the organic products because the ^{1}H-NMR spectrum indicated the presence of an inseparable mixture of compounds.

UV-visible monitoring of the reaction of [$Fe^{(II)}$$BPAEB_{NO}$(OAc)] and PMe_2Ph shows that the bands at 295, 415, and 525 nm decay over time and a new band at 625 nm is formed (Figure 51). There may be two isosbestic points present: one at around 295 nm (appearing at a high absorbance), and the other one which is positioned vertically at around 330 nm. Although these isosbestic points are not very well defined, they suggest that either the reaction has no intermediates, or if there are any, the consumption of intermediates is so fast that they could not be accumulated and traced on the timescale of the performed kinetics. Obtained data from kinetic studies of this reaction at different temperatures (14, 17, and 21 °C) were fitted to obtain the corresponding rate law and constant (Figure 51). Although individual datasets could be fitted each into a rate law, to the best of our efforts, we were not able to fit the three sets of data to a single model. Accordingly, there is no doubt that the mechanism of this reaction is more complicated than what has been proposed by earlier studies[142] (see 2.3.2); more in-depth studies are required (see 4.3.3).

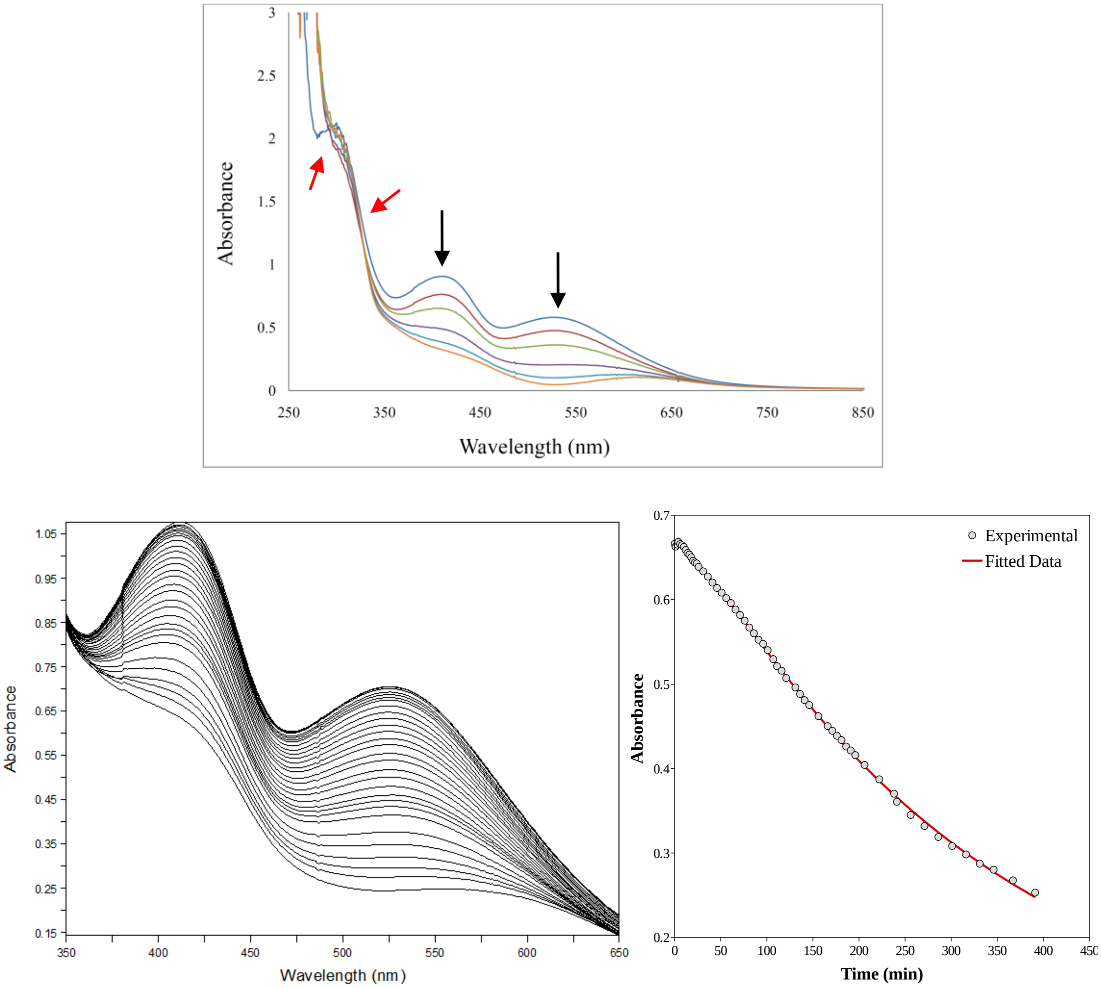

Figure 51. Kinetic studies of the reaction between [Fe$^{(II)}$BPAEB$_{NO}$(OAc)] and PMe$_2$Ph, top: decayed and formed bands (black arrows), isosbestic points (red arrows) bottom: spectra obtained from kinetic studies at 14 °C and second order fit of the data to A+B -> C / C+B -> D

4.3 Discussion

4.3.1 Mechanism of the Synthesis of Iron-Nitroso Complexes from Hydroxylamine Ligands

The mechanism of the formation of iron-nitroso compounds from their corresponding hydroxylamine ligands has only been discussed for the formation of $[(RNO)Fe(CN)_5]^{3-}$, Baudisch iron-nitroso complexes, from hexacyanoferrate(II).[134] Although this method has been utilized in the synthesis of a few iron-nitroso porphyrin complexes,[125-133] its mechanism with other sources of iron is still vague and entails more studies. Reaction of $Fe(OAc)_2$ with the hydroxylamine ($BPAEB_{NHOH}$) ligand in equimolar fashion, which produces $[Fe^{(II)}BPAEB_{NO}(OAc)]$ and $[Fe^{(II)}BPAEB_{NH_2}(OAc)]$, at first glance suggested a straightforward disproportionation reaction (see 2.3.1). Yet, control experiments showed that the reaction does not proceed with Fe(III) salts or with catalytic amounts of Fe(II) salts. Recently, detailed mechanistic studies on formation of Baudisch iron-nitroso complex from hexacyanoferrate(II) and alkylhydroxylamines in aqueous medium have shown that, during the course of reaction, free RNHO radicals and Fe(III) species could be detected by ESR and UV-Visible spectroscopy (Figure 52).[135] These findings propose that there might be other alternatives for the mechanism of iron-nitroso formation in our case and the initial assumption of a disproportionation mechanism could be an over-simplification of a more complex radical mechanism. Accordingly, an alternate mechanism for the formation of $[Fe^{(II)}BPAEB_{NO}(OAc)]$ and $[Fe^{(II)}BPAEB_{NH_2}(OAc)]$, involving radical intermediates is proposed (Figure 53).[134] However, these mechanistic studies on Baudisch complexes were performed in protic solvents and it is yet to be discovered if such a mechanism could occur in acetonitrile as well.

$$\mathrm{Fe^{II}} + \mathrm{ArNHOH} \longrightarrow \mathrm{Fe^{III}} + \mathrm{ArNH^{\bullet}} + \mathrm{OH^{-}}$$

$$\mathrm{Fe^{III}} + \mathrm{ArNHOH} \longrightarrow \mathrm{Fe^{II}} + \mathrm{ArNHO^{\bullet}} + \mathrm{H^{+}}$$

$$\mathrm{Fe^{III}} + \mathrm{ArNHO^{\bullet}} \longrightarrow \mathrm{Fe^{II}} + \mathrm{ArNOH}$$

$$\mathrm{Fe^{II}} + \mathrm{ArNH^{\bullet}} + \mathrm{H_2O} \longrightarrow \mathrm{Fe^{III}} + \mathrm{ArNH_2} + \mathrm{OH^{-}}$$

$$\mathrm{ArNH^{\bullet}} + \mathrm{ArNHOH} \longrightarrow \mathrm{ArNH_2} + \mathrm{RNHO^{\bullet}}$$

$$2\ \mathrm{ArNHO^{\bullet}} \longrightarrow \mathrm{Ar(N_2O)Ar} + \mathrm{H_2O}$$

Figure 52. Possible radical mechanism for the synthesis of [$\mathrm{Fe^{(II)}BPAEB_{NO}(OAc)}$] and [$\mathrm{Fe^{(II)}BPAEB_{NH2}(OAc)}$] based on the proposed mechanism for the synthesis of Baudisch complexes,[134] $\mathrm{Fe^{II}}$ source: $\mathrm{Fe(OAc)_2}$, ArNHOH: $\mathrm{BPAEB_{NHOH}}$

This mechanism is based on the facile exchange between Fe(II) and Fe(III), producing radical intermediates that end up as arylamine and arylnitroso compounds that undergo complexation with the present Fe(II) ions. The degree to which the amine or nitroso compounds are formed depends on various factors, such as the Fe(II) source and its redox potential, pH, and the nature and reactivity of the ArNH radicals. Validation of this radical mechanism requires in-depth ESR studies and, at this point, no final decision can be made on the exact nature of the reaction mechanism in our case. When [$\mathrm{Fe(OTf)_2}$]·2 MeCN was used as the source of Fe(II), the formed $\mathrm{BPAEB_{NO}}$ was complexed to Fe(II) to make the [$\mathrm{Fe^{(II)}BPAEB_{NO}(MeCN)}$](OTf) complex, whereas the formed $\mathrm{BPAEB_{NH_2}}$ stayed in solution without further complexation. This is in contrary to the formation of the [$\mathrm{Fe^{(II)}BPAEB_{NH2}(OAc)}$] complex upon disproportionation of $\mathrm{BPAEB_{NHOH}}$ with $\mathrm{Fe(OAc)_2}$. It is important to note that $\mathrm{Fe(OAc)_2}$ has a polymeric nature and was initially not soluble in the reaction solvent ($\mathrm{CH_3CN}$), whereas [$\mathrm{Fe(OTf)_2}$] ·2 MeCN was perfectly soluble in the same solvent and is known to have a monomeric structure in solution. Accordingly, the difference seen in results could be due to the different reactivity of these reagents in solution, resulting in different reaction mechanisms. Preliminary results show that, other than $Fe(OAc)_2$ and $[Fe(OTf)_2]\cdot 2$ MeCN, $FeCl_2$, and $Co(OAc)_2$ are also able to perform this reaction and therefore, it seems viable that this method could be developed for the synthesis of other alkyl or aryl nitroso transition metal complexes.

4.3.2 Comparison of Iron-Nitroso Complexes

The preceding sections have presented structural and spectroscopic characterization for two iron-nitroso complexes $[Fe^{(II)}BPAEB_{NO}(OAc)]$ and $[Fe^{(II)}BPAEB_{NO}(MeCN)](OTf)$ and an iron-amine complex $[Fe^{(II)}BPAEB_{NH2}(OAc)]$, as well as reactivity studies of the iron-nitroso complexes as OAT reagents. All of the discussed complexes have broadened ^{1}H-NMR spectra, which is characteristic of paramagnetic species. Magnetic susceptibility measurement performed for $[Fe^{(II)}BPAEB_{NO}(OAc)]$ showed the presence of 2 unpaired electrons in this complex in solution at room temperature. Iron(II) has a d^6 electronic configuration and is capable of forming complexes in either low-spin or high-spin electronic configurations depending primarily on their coordination geometry and ligand field. Based on the value of the magnetic moment, it is likely that $[Fe^{(II)}BPAEB_{NO}(OAc)]$ adopts a trigonal-bipyramidal geometry in solution, wih the acetate anion possibly de-ccordinated (see 4.1.1).

The nitroso group is also able to accept π bonding from the metal. Comparison of the NO bond lengths in η^1 N-bound metal-nitroso complexes (1.19-1.32 A) and especially in iron-nitroso complexes (1.25-1.265 A)[124] with NO bond length in free nitroso ligand (1.25 A)[124,156] shows that this bond in $[Fe^{(II)}BPAEB_{NO}(OAc)]$ falls in the upper range of a nitroso double bond. This elongation may be due to the presence of minor backbonding from filled d orbitals of iron to the π^* orbitals of NO; this also results in shorter Fe-N(O) bond compared to normal Fe-N bond lengths (Table 11). Moreover, a large twist from coplanarity is observed between the phenyl ring and the nitroso moiety (O1-N1-C1-C6 torsion angle: 41.13°). This shows that the conjugation between the phenyl ring and the nitroso group is reduced and indicates the presence of π coordination with this ligand.[124]. It is important to note that these comparisons are done with non-restricted PhNO systems and the observed effects in our complexes could partly be due to the chelating effect of the ligand as well.

A comparison of these structural parameters between $[Fe^{(II)}BPAEB_{NO}(OAc)]$, $[Fe^{(II)}BPAEB_{NO}(MeCN)](OTf)$ and the only reported iron-aryl nitroso monomeric complex, $[CpFe(CO)_2(\eta^1\text{-}PhNO)]SbF_6$[138] is given in Table 11 and Figure 54. The NO bond lengths are longer in the first two complexes, indicating the presence of significant π backbonding interactions. These longer bonds are likely weaker and hence should be more reactive. Indeed, the two $BPAEB_{NO}$ complexes are more reactive than $[CpFe(CO)_2(\eta^1\text{-}PhNO)]SbF_6$ with phosphines: the latter complex is unreactive with PPh_3 even at elevated temperatures. Of course, a more precise analysis requires more in-depth reactivity studies of $[Fe^{(II)}BPAEB_{NO}(MeCN)](OTf)$ with different phosphine reagents as well as DFT calculations to understand the exact electronic nature of their nitroso bonds.

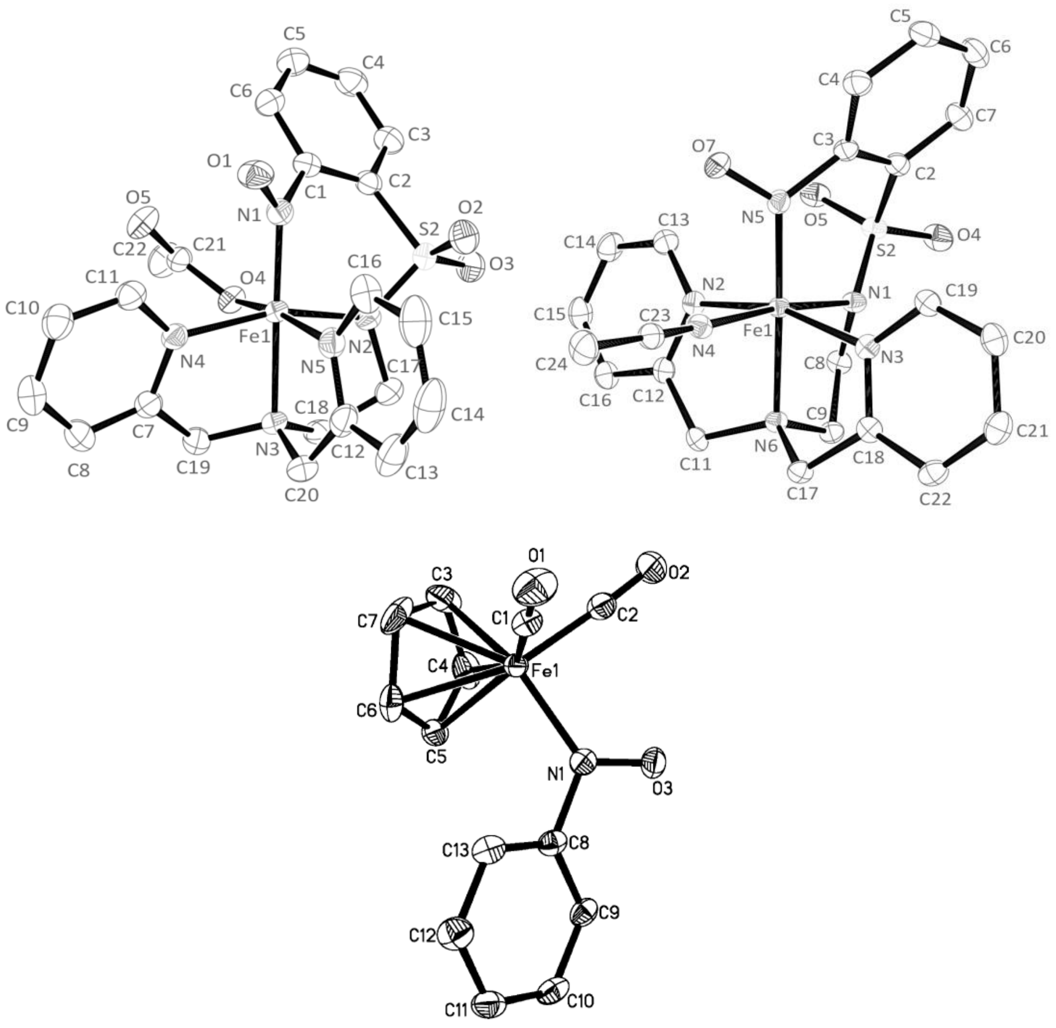

Figure 53. Top left: [Fe$^{(II)}$BPAEB$_{NO}$(OAc)], top right: [Fe$^{(II)}$BPAEB$_{NO}$(MeCN)](OTf), bottom: [CpFe(CO)$_2$(η^1-PhNO)]SbF$_6$**,** picture adapted from**[138]**, all ellipsoids are drawn with 50% probability.

Table 11. Comparison of the selected bond lengths and angles between [Fe$^{(II)}$BPAEB$_{NO}$(OAc)], middle: [Fe$^{(II)}$BPAEB$_{NO}$(MeCN)](OTf), Right: [CpFe(CO)$_2$(η^1-PhNO)]SbF$_6$, TA: O1-N1-C1-C6 torsion angle

	[Fe$^{(II)}$BPAEB$_{NO}$(OAc)]	[Fe$^{(II)}$BPAEB$_{NO}$ (MeCN)](OTf)	([CpFe(CO)$_2$(η^1-PhNO)]SbF$_6$ [138]
N-O (Å)	1.266 (2)	1.259 (3)	1.226(3)
Fe-N(O) (Å)	1.8046 (18)	1.818 (2)	1.916(2)
TA (°)	41.13	33.91	9.00
O-N-C (°)	125.86 (14)	122.10 (17)	114.4(2)

It is important to note that all these comparisons are based on solid-state structures. However, reactivity of these complexes in solution is highly dependent on their structures in solution. In mass spectrometry (in CH_2Cl_2 with 10%MeOH), both $BPAEB_{NO}$ complexes show the same $[Fe^{(II)}BPAEB_{NO}]^+$ ionized species with dissociated acetate anion and MeCN, respectively. Obtained data from UV-visible in CH_2Cl_2 show that both complexes absorb at the same wavelengths, although with different molar absorptivities. They also represent different colours in CH_2Cl_2 solution, which suggests small differences in their solution structures. In total, when comparing the reactivity and mechanism of reaction in these complexes, all these uncertainties about the solution structures of these two complexes should be taken into account.

4.3.3 Mechanism of the OAT from Iron-Nitroso Complexes

The mechanism proposed in the literature for OAT from metal-nitroso complexes or organic C-nitroso compounds generally involves two phosphine equivalents, as one equivalent is needed for deoxygenation of the nitroso group (OAT) and the other is used to trap the nitrenoid/nitrene intermediate. Our mechanistic studies, however, show that the mechanism of this reaction is more complex and the above assumption is too simplistic for the exact mechanism of OAT from $[Fe^{(II)}BPAEB_{NO}(OAc)]$ and $[Fe^{(II)}BPAEB_{NO}(MeCN)](OTf)$ complexes to different phosphines. The reaction indeed requires more than 1 equivalent of phosphine to proceed, but two equivalents were found to be excess (not all the phosphine is consumed, as seen by ^{31}P-NMR and GC). Also, kinetic studies showed that the reaction could not be fitted to regular rate laws, which could be due to the involvement of some sort of equilibrium. Therefore, the mechanism of reaction could not be retrieved only based on these studies. One possible complication could be due to the extreme reactivity of the metal-nitrenoid species. Once it is formed, it could react with the solvent (or an impurity or another molecule of complex…) before finding the second phosphine and perform a hydrogen abstraction reaction to yield a more stable amido (C-NH$^-$) complex.

During experiments with [Fe$^{(II)}$BPAEB$_{NO}$(MeCN)](OTf) and PMe$_2$Ph it was found that the reaction was inhibited in MeCN. This finding suggests that dissociation of the coordinated MeCN is a key step in starting the OAT reaction. Unfortunately, none of the available literature on deoxygenation of metal-nitroso complexes reported detailed mechanistic studies. The only research proposing a different mechanism was reported for a [W(CO)$_5$(N(O)^{t}Bu)] complex.[157] When this complex was reacted with PPh$_3$ in the absence of CO atmosphere, the complex decayed to form the amine complex, perhaps through a transient imido species formed by deoxygenation of the nitroso group. But this reaction was inhibited in the presence of CO atmosphere (Figure 55). The authors suggests that CO dissociation is a key step in the reaction mechanism and is necessary to enable reactions with the phosphine. Comparison of the [Fe$^{(II)}$BPAEB$_{NO}$(MeCN)](OTf) and [W(CO)$_5$(N(O)^{t}Bu)] complexes show that both these complexes have saturated coordination spheres and therefore it is concluded that availability of one empty coordination site in a dissociative mechanism might be necessary in order for a reactant (PPh$_3$ or CO) to coordinate to the metal. This idea also explains why [Fe$^{(II)}$BPAEB$_{NO}$(MeCN)](OTf) has higher reaction rates than [Fe$^{(II)}$BPAEB$_{NO}$(OAc)] (in CH$_2$Cl$_2$). [Fe$^{(II)}$BPAEB$_{NO}$(MeCN)](OTf) complex has a more labile MeCN ligand that can dissociate much more easily than the acetate ligand in [Fe$^{(II)}$BPAEB$_{NO}$(OAc)].

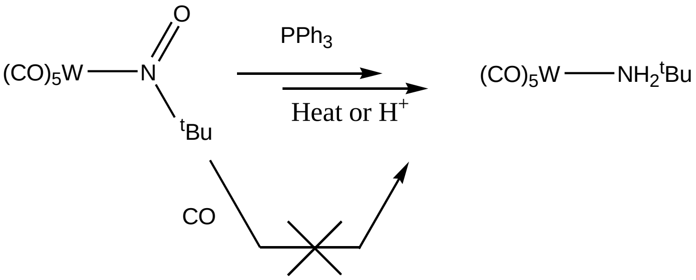

Figure 54. OAT reaction inhibition in presence of CO atmosphere, suggesting the CO dissociation as a key step in the mechanism

Based on these data, we propose that the mechanism of OAT from [Fe$^{(II)}$BPAEB$_{NO}$(OAc)] and [Fe$^{(II)}$BPAEB$_{NO}$(MeCN)](OTf) could proceed through dissociation of the acetate/MeCN ligand followed by coordination of a phosphine to the iron (Figure 56). This phosphine-bound intermediate is well-suited for an intramolecular OAT reaction from the nitroso group by the coordinated phosphine, although the the exact mechanism involved in these steps is not known and an intermolecular deoxygenation by non-coordinated phosphines is also possible. The nitrenoid-type intermediate formed after this step is readily trapped by phosphine reagents to form the iminophosphorane products. Consumption of this nitrenoid intermediate is so fast that accumulation of it cannot be detected with UV-visible experiments (pseudo-isosbestic points). However, confirmation of this mechanism requires more control and kinetic studies that are proposed as perspective of this project.

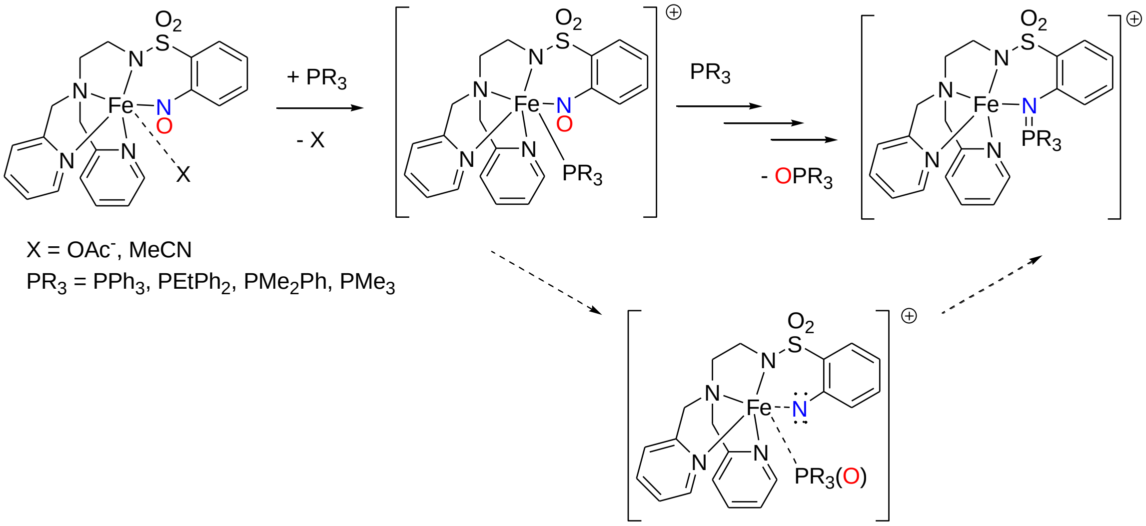

X = OAc^-, MeCN
PR_3 = PPh_3, $PEtPh_2$, PMe_2Ph, PMe_3

Figure 55. Proposed mechanism of OAT from [$Fe^{(II)}$$BPAEB_{NO}$(OAc)] and [$Fe^{(II)}$$BPAEB_{NO}$(MeCN)](OTf) in presence of phosphine reagents

5. Conclusion and Perspective

[Fe$^{(II)}$BPAEB$_{NO}$(OAc)] and [Fe$^{(II)}$BPAEB$_{NO}$(MeCN)](OTf) complexes proved to be capable of OAT to phosphine reagents in moderate to very good yields and in mild conditions. Based on mass spectrometry evidence, the metal-containing products of these reactions are iminophosphorane complexes that are believed to be formed by nitrene-transfer from iron-nitrenoid intermediates to phosphine reagents. The mechanism of this reaction is not fully known and requires more in-depth control and kinetic studies; however, indirect evidence from preliminary control experiments suggest that it proceeds through dissociation of the acetate or MeCN ligands followed by coordination of the phosphine. These complexes could be modified by altering the ligand environment with more electron donor ligands (e.g: phenolate ligands in place of pyridines) in order to stabilize the highly reactive nitrenoid intermediates and trace their formation. Also reducing the number of coordinating ligands (by use of tetradentate or tridentate ligands) to the metal would facilitate the approach of oxygen abstractor reagents to the nitroso group, as well as stabilize the Fe-imido/nitrenoid intermediates. Stabilization of intermediates can also be obtained by choosing a different metal of a lower row (e.g. Ru, Os) or earlier (e.g. Cr, V) in the transition metal series. The synthetic method that was used to produce [Fe$^{(II)}$BPAEB$_{NO}$(OAc)] and [Fe$^{(II)}$BPAEB$_{NO}$(MeCN)](OTf) complexes is applicable to produce other versatile metal-nitroso complexes and may not be limited to iron only. The mechanism of this disproportionation reaction could be revealed by electrochemical techniques and ESR study of the reaction intermediates.

References

(1) E. T. Denisov, I. B. Afanas'ev, *Oxidation and Antioxidants in Organic Chemistry and Biology*; Taylor and Francis Group, 2005.

(2) Donohoe, T. J. *Oxidation and reduction in organic synthesis*; Oxford University Press, 2000.

(3) Kahlich, D.; Wiechern, U.; Lindner, J. *Propylene Oxide*; Wiley-VCH Verlag GmbH & Co. KGaA, 2000.

(4) Joergensen, K. A. *Chemical Reviews* **1989**, *89*, 431.

(5) Godula, K. *Science* **2006**, *312*, 67.

(6) Punniyamurthy, T.; Velusamy, S.; Iqbal, J. *Chemical Reviews* **2005**, *105*, 2329.

(7) Shilov, A. E.; Shul'pin, G. B. *Chemical Reviews* **1997**, *97*, 2879.

(8) Periana, R. A.; Mironov, O.; Taube, D.; Bhalla, G.; Jones, C. *Science* **2003**, *301*, 814.

(9) Periana, R. A.; Taube, D. J.; Gamble, S.; Taube, H.; Satoh, T.; Fujii, H. *Science* **1998**, *280*, 560.

(10) Lersch, M.; Tilset, M. *Chemical Reviews* **2005**, *105*, 2471.

(11) Desai, L. V.; Hull, K. L.; Sanford, M. S. *Journal of the American Chemical Society* **2004**, *126*, 9542.

(12) Dick, A. R.; Sanford, M. S. *Tetrahedron* **2006**, *62*, 2439.

(13) Chianese, A.; Lee, S.; Gagné, M. *Angewandte Chemie International Edition* **2007**, *46*, 4042.

(14) Sawyer, D. T. *Coordination Chemistry Reviews* **1997**, *165*, 297.

(15) Wong, O. A.; Shi, Y. *Chemical Reviews* **2008**, *108*, 3958.

(16) Brodsky, B. H.; Du Bois, J. *Journal of the American Chemical Society* **2005**, *127*, 15391.

(17) Adam, W.; Saha-Möller, C. R.; Ganeshpure, P. A. *Chemical Reviews* **2001**, *101*, 3499.

(18) Ortiz de Montellano, P. R. *Chemical Reviews* **2009**, *110*, 932.

(19) Shaik, S.; Cohen, S.; Wang, Y.; Chen, H.; Kumar, D.; Thiel, W. *Chemical Reviews* **2009**, *110*, 949.

(20) Meunier, B.; de Visser, S. P.; Shaik, S. *Chem. Rev.* **2004**, *104*, 3947.

(21) Costas, M.; Mehn, M. P.; Jensen, M. P.; Que, L. *Chemical Reviews* **2004**, *104*, 939.

(22) Meunier, B.; de Visser, S. P.; Shaik, S. *Chemical Reviews* **2004**, *104*, 3947.

(23) Yin, G. *Coordination Chemistry Reviews* **2010**, *254*, 1826.

(24) de Oliveira, F. T.; Chanda, A.; Banerjee, D.; Shan, X.; Mondal, S.; Que, L., Jr.; Bominaar, E. L.; Munck, E.; Collins, T. J. *Science* **2007**, *315*, 835.

(25) Merkx, M.; Kopp, D. A.; Sazinsky, M. H.; Blazyk, J. L.; Müller, J.; Lippard, S. J. *Angewandte Chemie International Edition* **2001**, *40*, 2782.

(26) Tinberg, C. E.; Lippard, S. J. *Biochemistry* **2009**, *48*, 12145.

(27) Liu, K. E.; Wang, D.; Huynh, B. H.; Edmondson, D. E.; Salifoglou, A.; Lippard, S. J. *Journal of the American Chemical Society* **1994**, *116*, 7465.

(28) Valentine, A. M.; Stahl, S. S.; Lippard, S. J. *Journal of the American Chemical Society* **1999**, *121*, 3876.

(29) Beauvais, L. G.; Lippard, S. J. *Journal of the American Chemical Society* **2005**, *127*, 7370.

(30) Shu, L.; Nesheim, J. C.; Kauffmann, K.; Munck, E.; Lipscomb, J. D.; Que, L., Jr. *Science* **1997**, *275*, 515.
(31) Liu, K. E.; Valentine, A. M.; Wang, D.; Huynh, B. H.; Edmondson, D. E.; Salifoglou, A.; Lippard, S. J. *Journal of the American Chemical Society* **1995**, *117*, 10174.
(32) Ambundo, E. A.; Friesner, R. A.; Lippard, S. J. *Journal of the American Chemical Society* **2002**, *124*, 8770.
(33) Baik, M.-H.; Gherman, B. F.; Friesner, R. A.; Lippard, S. J. *Journal of the American Chemical Society* **2002**, *124*, 14608.
(34) Tinberg, C. E.; Lippard, S. J. *Biochemistry* **2010**, *49*, 7902.
(35) Solomon, E. I.; Brunold, T. C.; Davis, M. I.; Kemsley, J. N.; Lee, S.-K.; Lehnert, N.; Neese, F.; Skulan, A. J.; Yang, Y.-S.; Zhou, J. *Chemical Reviews* **1999**, *100*, 235.
(36) Solomon, E. I.; Wong, S. D.; Liu, L. V.; Decker, A.; Chow, M. S. *Current Opinion in Chemical Biology* **2009**, *13*, 99.
(37) Que, L.; Tolman, W. B. *Nature* **2008**, *455*, 333.
(38) Meunier, B. *Biomimetic oxidations catalyzed by transition metal complexes*; Imperial College Press, 2000
(39) Breslow, R.; Nemo, T. E.; Myers, R. S. *J. Am. Chem. Soc.* **1979**, *101*, 1032.
(40) Jacobsen, E. N.; Zhang, W.; Muci, A. R.; Ecker, J. R.; Deng, L. *J. Am. Chem. Soc.* **1991**, *113*, 7063.
(41) Hili, R.; Yudin, A. K. *Nature Chemical Biology* **2006**, *2*, 284.
(42) Linker, T. *Angewandte Chemie International Edition in English* **1997**, *36*, 2060.
(43) Jacobsen, E. N., Pfaltz, A., Yamamoto, H., Eds. *Comprehensive Asymmetric Catalysis*; Springer-Verlag: Berlin, 1999; Vol. 2.
(44) Costas, M.; Chen, K.; Que, L. *Coordination Chemistry Reviews* **2000**, *200-202*, 517.
(45) Kojima, T.; Leising, R. A.; Yan, S.; Que, L. *Journal of the American Chemical Society* **1993**, *115*, 11328.
(46) Leising, R. A.; Norman, R. E.; Que, L. *Inorganic Chemistry* **1990**, *29*, 2553.
(47) Tetard, D.; Verlhac, J.-B. *Journal of Molecular Catalysis A: Chemical* **1996**, *113*, 223.
(48) Nguyen, C.; Guajardo, R. J.; Mascharak, P. K. *Inorganic Chemistry* **1996**, *35*, 6273.
(49) Fantauzzi, S.; Caselli, A.; Gallo, E. *Dalton Transactions* **2009**, 5434.
(50) Watson, I. D. G.; Yu, L.; Yudin, A. K. *Accounts of Chemical Research* **2006**, *39*, 194.
(51) Díaz-Requejo, M. M.; Pérez, P. J. *Chemical Reviews* **2008**, *108*, 3379.
(52) Davies, H. M. L.; Manning, J. R. *Nature* **2008**, *451*, 417.
(53) Halfen, J. A. *Current Organic Chemistry* **2005**, *9*, 657.
(54) Dauban, P.; Dodd, R. H. *Synlett* **2003**, *2003*, 1571.
(55) Muller, P.; Fruit, C. *Chemical Reviews* **2003**, *103*, 2905.
(56) Sandra Fürmeier, J. O. M. *European Journal of Organic Chemistry* **2003**, 649.
(57) Regueiro-Ren, A.; Borzilleri, R. M.; Zheng, X.; Kim, S.-H.; Johnson, J. A.; Fairchild, C. R.; Lee, F. Y. F.; Long, B. H.; Vite, G. D. *Organic Letters* **2001**, *3*, 2693.
(58) Dauban, P.; Dodd, R. H. *Synlett* **2003**, 1571.
(59) Müller, P.; Fruit, C. *Chemical Reviews* **2003**, *103*, 2905.
(60) Arndtsen, B. A.; Sleiman, H. F.; McElwee-White, L.; Rheingold, A. L. *Organometallics* **1993**, *12*, 2440.

(61) Mindiola, D. J.; Hillhouse, G. L. *Chemical Communications* **2002**, 1840.
(62) Hamilton, C. W., Massachusetts Institute of Technology, 2007.
(63) Sharpless, K. B.; Patrick, D. W.; Truesdale, L. K.; Biller, S. A. *Journal of the American Chemical Society* **1975**, *97*, 2305.
(64) Sharpless, K. B.; Chong, A. O.; Oshima, K. *The Journal of Organic Chemistry* **1976**, *41*, 177.
(65) Breslow, R.; Gellman, S. H. *Journal of the Chemical Society, Chemical Communications* **1982**, 1400.
(66) Breslow, R.; Gellman, S. *Journal of the American Chemical Society* **1983**, *105*, 6729.
(67) Yang, J.; Weinberg, R.; Breslow, R. *Chemical Communications* **2000**, 531.
(68) Groves, J. T.; Nemo, T. E. *Journal of the American Chemical Society* **1983**, *105*, 5786.
(69) Mansuy, D.; Mahy, J. P.; Dureault, A.; Bedi, G.; Battioni, G. *Journal of the Chemical Society, Chemical Communications* **1984**, 1161.
(70) Mahy, J. P.; Bedi, G.; Battioni, P.; Mansuy, D. *Journal of the Chemical Society, Perkin Transactions 2* **1988**, 1517.
(71) Mahy, J. P.; Bedi, G.; Battioni, P.; Mansuy, D. *Tetrahedron Letters* **1988**, *29*, 1927.
(72) O'Connor, K. J.; Wey, S. J.; Burrows, C. *Tetrahedron Letters* **1992**, *33*, 1001.
(73) Mahy, J. P.; Bedi, G.; Battioni, P.; Mansuy, D. *New Journal of Chemistry* **1989**, *13*, 651.
(74) Simkhovich, L.; Gross, Z. *Tetrahedron Letters* **2001**, *42*, 8089.
(75) Jensen, M. P.; Mehn, M. P.; Que, L. *Angewandte Chemie International Edition* **2003**, *42*, 4357.
(76) Cowley, R. E.; Eckert, N. A.; Elhaik, J.; Holland, P. L. *Chemical Communications* **2009**, 1760.
(77) Cowley, R. E.; DeYonker, N. J.; Eckert, N. A.; Cundari, T. R.; DeBeer, S.; Bill, E.; Ottenwaelder, X.; Flaschenriem, C.; Holland, P. L. *Inorganic Chemistry* **2010**, *49*, 6172.
(78) Brown, S. D.; Betley, T. A.; Peters, J. C. *Journal of the American Chemical Society* **2002**, *125*, 322.
(79) Au, S. M.; Zhang, S. B.; Fung, W. H.; Yu, X. Q.; Che, C. M.; Cheung, K. K. *Chemical Communications* **1998**, 2677.
(80) Au, S. M.; Huang, J. S.; Che, C. M.; Yu, W. Y. *Journal of Organic Chemistry* **2000**, *65*, 7858.
(81) Leung, S. K.-Y.; Tsui, W.-M.; Huang, J.-S.; Che, C.-M.; Liang, J.-L.; Zhu, N. *Journal of the American Chemical Society* **2005**, *127*, 16629.
(82) Müller, P.; Baud, C.; Jacquier, Y.; Moran, M.; Nägeli, I. *Journal of Physical Organic Chemistry* **1996**, *9*, 341.
(83) Müller, P.; Baud, C.; Jacquier, Y. *Tetrahedron* **1996**, *52*, 1543.
(84) Nägeli, I.; Baud, G.; Bernadinelli, Y.; Jacquier, M.; Moran, M.; Müller, P. *Helvetica Chimica Acta* **1997**, *80*, 1087.
(85) Müller, P.; Baud, C.; Jacquier, Y. *Canadian Journal of Chemistry* **1998**, *76*, 738.
(86) Fruit, C.; Müller, P. *Tetrahedron: Asymmetry* **2004**, *15*, 1019.
(87) Espino, C. G.; DuBois, J. A. *Angewandte Chemie International Edition* **2001**, *40*, 598.
(88) Berry, J. *Comments on Inorganic Chemistry* **2009**, *30*, 28.

(89) Eikey, R. A.; Abu-Omar, M. M. *Coordination Chemistry Reviews* **2003**, *243,* 83.
(90) Astruc, D. *Organometallic Chemistry and Catalysis*; Springer, 2007.
(91) James M. Mayer, W. A. N. *Metal-Ligand Multiple Bond*; Wiley, 1988.
(92) Mayer, J. M. *Comments on Inorganic Chemistry: A Journal of Critical Discussion of the Current Literature* **1988**, *8*, 125
(93) Oskam, J. H.; Fox, H. H.; Yap, K. B.; McConville, D. H.; O`Dell, R.; Lichtenstein, B. J.; Schrock, R. R. *Journal of Organometallic Chemistry* **1993**, *459*, 185.
(94) Schrock, R. R. *Chemical Reviews* **2009**, *109*, 3211.
(95) Schrock, R. R. *Angewandte Chemie International Edition* **2006**, *45,* 3748.
(96) Schrock, R. R. *Journal of Molecular Catalysis A: Chemical* **2004**, *213*, 21.
(97) Lu, C.; DeBeer George, S.; Weyhermüller, T.; Bill, E.; Bothe, E.; Wieghardt, K. *Angewandte Chemie International Edition* **2008**, *47*, 6384.
(98) Sharp, P. R. *Comments on Inorganic Chemistry: A Journal of Critical Discussion of the Current Literature* **1999**, *21*, 85
(99) Brown, S. D.; Peters, J. C. *Journal of the American Chemical Society* **2005**, *127*, 1913.
(100) Lu, C. C.; Saouma, C. T.; Day, M. W.; Peters, J. C. *Journal of the American Chemical Society* **2006**, *129*, 4.
(101) Betley, T. A.; Peters, J. C. *Journal of the American Chemical Society* **2003**, *125*, 10782.
(102) Jenkins, D. M.; Betley, T. A.; Peters, J. C. *Journal of the American Chemical Society* **2002**, *124*, 11238.
(103) Thomas, C. M.; Mankad, N. P.; Peters, J. C. *Journal of the American Chemical Society* **2006**, *128*, 4956.
(104) Hu, X.; Meyer, K. *Journal of the American Chemical Society* **2004**, *126*, 16322.
(105) Mindiola, D. J.; Hillhouse, G. L. *Journal of the American Chemical Society* **2001**, *123*, 4623.
(106) Kogut, E.; Wiencko, H. L.; Zhang, L.; Cordeau, D. E.; Warren, T. H. *Journal of the American Chemical Society* **2005**, *127*, 11248.
(107) Holland, P. L. *Accounts of Chemical Research* **2008**, *41*, 905.
(108) Ge, Y.-W.; Ye, Y.; Sharp, P. R. *Journal of the American Chemical Society* **1994**, *116*, 8384.
(109) Arita, H.; Ishiwata, K.; Kuwata, S.; Ikariya, T. *Organometallics* **2008**, *27*, 493.
(110) Oro, L. A.; Ciriano, M. A.; Tejel, C.; Bordonaba, M.; Graiff, C.; Tiripicchio, A. *Chemistry – A European Journal* **2004**, *10*, 708.
(111) Ishiwata, K.; Kuwata, S.; Ikariya, T. *Journal of the American Chemical Society* **2009**, *131*, 5001.
(112) Takemoto, S.; Ogura, S.-i.; Yo, H.; Hosokoshi, Y.; Kamikawa, K.; Matsuzaka, H. *Inorganic Chemistry* **2006**, *45*, 4871.
(113) Anandhi, U.; Holbert, T.; Lueng, D.; Sharp, P. R. *Inorganic Chemistry* **2003**, *42*, 1282.
(114) Groysman, S.; Villagrán, D.; Nocera, D. G. *Inorganic Chemistry* **2010**, 10759.
(115) MacBeth, C. E.; Golombek, A. P.; Young, V. G., Jr.; Yang, C.; Kuczera, K.; Hendrich, M. P.; Borovik, A. S. *Science* **2000**, *289*, 938.
(116) Dai, X.; Kapoor, P.; Warren, T. H. *Journal of the American Chemical Society* **2004**, *126*, 4798.

(117) Badiei, Y. M.; Krishnaswamy, A.; Melzer, M. M.; Warren, T. H. *Journal of the American Chemical Society* **2006**, *128*, 15056.
(118) Hill, C. L. *Nature* **2008**, *455*, 1045.
(119) Anderson, T. M.; Neiwert, W. A.; Kirk, M. L.; Piccoli, P. M. B.; Schultz, A. J.; Koetzle, T. F.; Musaev, D. G.; Morokuma, K.; Cao, R.; Hill, C. L. *Science* **2004**, *306*, 2074.
(120) Sharp, P. *Comments on Inorganic Chemistry* **1999**, *21*, 85.
(121) Hankin, D. M.; Danopoulos, A. A.; Wilkinson, G.; Sweet, T. K. N.; Hursthouse, M. B. *Journal of the Chemical Society, Dalton Transactions* **1996**, 4063.
(122) Burrell, A. K.; Steedman, A. J. *Organometallics* **1997**, *16*, 1203.
(123) Ryabov, A. D.; Collins, T. J. In *Advances in Inorganic Chemistry*; Rudi van, E., Colin, D. H., Eds.; Academic Press: 2009; Vol. Volume 61, p 471.
(124) Lee, J.; Chen, L.; West, A. H.; Richter-Addo, G. B. *Chemical Reviews* **2002**, *102*, 1019.
(125) Mansuy, D.; Battioni, P.; Chottard, J. C.; Riche, C.; Chiaroni, A. *Journal of the American Chemical Society* **1983**, *105*, 455.
(126) Wang, L. S.; Chen, L.; Khan, M. A.; Richter-Addo, G. B. *Chemical Communications* **1996**, 323.
(127) Ozaki, H.; Kinuta, M.; Matteson, J. L.; Itano, H. A. *Biochimica et Biophysica Acta* **1988**, *955*, 220.
(128) Fukuto, J. M.; Brady, J. F.; Burstyn, J. N.; VanAtta, R. B.; Valentine, J. S.; Cho, A. K. *Biochemistry* **1986**, *25*, 2714.
(129) Gibson, Q. H. *Biochemical Journal* **1960**, *77*, 519.
(130) Chottard, G.; Mansuy, D. *Biochemical and Biophysical Research Communications* **1977**, *77*, 1333.
(131) Mansuy, D.; Chottard, J. C.; Chottard, G. *European Journal of Biochemistry* **1977**, *76*, 617.
(132) Mansuy, D.; Beaune, P.; Chottard, J. C.; Bartoli, J. F.; Gans, P. *Biochemical Pharmacology* **1976**, *25*, 609.
(133) James, R. C.; Franklin, M. R. *Biochemical Pharmacology* **1975**, *24*, 835.
(134) Waters, W. A. *Journal of the Chemical Society, Perkin Transactions 2* **1976**, 732.
(135) Gutierrez, M. M.; Alluisetti, G. B.; Olabe, J. A.; Amorebieta, V. T. *Dalton Transactions* **2009**, 1187.
(136) Dewar, J.; Jones, H. O. *Proceedings of the Royal Society of London. Series A* **1905**, *76*, 558.
(137) Baudisch, O. *Berichte der deutschen chemischen Gesellschaft (A and B Series)* **1921**, *54*, 413.
(138) Stephens, J. C.; Khan, M. A.; Nicholas, K. M. *Journal of Organometallic Chemistry* **2005**, *690*, 4727.
(139) Pilato, R. S.; McGettigan, C.; Geoffroy, G. L.; Rheingold, A. L.; Geib, S. *J. Oranometallics* **1990**, *9*, 312.
(140) Seidler, M. D.; Bergman, R. G. *Organometallics* **1983**, *2*, 1897.
(141) Cadogan, J. I. G. *Quarterly Reviews, Chemical Society* **1968**, *22*, 222.
(142) Charalambous, J.; Kensett, M. J.; Jenkins, J. M. *Journal of the Chemical Society, Chemical Communications* **1977**, 400.

(143) Otsuka, S.; Aotani, Y.; Tatsuno, Y.; Yoshida, T. *Inorganic Chemistry* **1976**, *15*, 656.

(144) La Monica, G.; Cenini, S. *Journal of the Chemical Society, Dalton Transactions* **1980**, 1145.

(145) Collman, J. P. *Accounts of Chemical Research* **1968**, *1*, 136.

(146) Fochi, G.; Floriani, C. *Journal of the Chemical Society, Dalton Transactions* **1984**, 2577.

(147) Vasapollo, G.; Nobile, C. F.; Giannoccaro, P.; Allegretta, F. *Journal of Organometallic Chemistry* **1984**, *277*, 417.

(148) Evans, D. F.; Fazakerley, G. V.; Phillips, R. F. *Journal of the Chemical Society A: Inorganic, Physical, Theoretical* **1971**, 1931.

(149) Piguet, C. *Journal of Chemical Education* **1997**, *74*, 815.

(150) Matouzenko, G. S.; Bousseksou, A.; Lecocq, S.; van Koningsbruggen, P. J.; Perrin, M.; Kahn, O.; Collet, A. *Inorganic Chemistry* **1997**, *36*, 2975.

(151) Incarvito, C.; Lam, M.; Rhatigan, B.; Rheingold, A. L.; Qin, C. J.; Gavrilova, A. L.; Bosnich, B. *Journal of the Chemical Society, Dalton Transactions* **2001**, 3478.

(152) Hagen, K. S. *Inorganic Chemistry* **2000**, *39*, 5867.

(153) Al-Benna, S.; Sarsfield, M. J.; Thornton-Pett, M.; Ormsby, D. L.; Maddox, P. J.; Bres, P.; Bochmann, M. *Journal of the Chemical Society, Dalton Transactions* **2000**, 4247.

(154) Avis, M. W.; Vrieze, K.; Ernsting, J. M.; Elsevier, C. J.; Veldman, N.; Spek, A. L.; Katti, K. V.; Barnes, C. L. *Organometallics* **1996**, *15*, 2376.

(155) Spencer, L. P.; Altwer, R.; Wei, P.; Gelmini, L.; Gauld, J.; Stephan, D. W. *Organometallics* **2003**, *22*, 3841.

(156) Cameron, M.; Gowenlock, B. G.; Vasapollo, G. *Chemical Society Reviews* **1990**, *19*, 355.

(157) Pilato, R. S.; McGettigan, C.; Geoffroy, G. L.; Rheingold, A. L.; Geib, S. J. *Organometallics* **1990**, *9*, 312.

Appendix I: Crystal Structure Data

[Fe$^{(II)}$BPAEB$_{NO}$(OAc)].MeCN

Computing details

Data collection: *APEX2* (Bruker AXS, 2009); cell refinement: *SAINT* V7.68A(Bruker AXS, 2009); data reduction: *SAINT* V7.68A(Bruker AXS, 2009); program(s) used to solve structure: *SHELXS97* (Sheldrick, 2008); program(s) used to refine structure: *SHELXL97* (Sheldrick, 2008); molecular graphics: *SHELXTL* v6.12 (Bruker AXS, 2001); software used to prepare material for publication: UdMX (Maris, 2004).

Geometry. All esds (except the esd in the dihedral angle between two l.s. planes) are estimated using the full covariance matrix. The cell esds are taken into account individually in the estimation of esds in distances, angles and torsion angles; correlations between esds in cell parameters are only used when they are defined by crystal symmetry. An approximate (isotropic) treatment of cell esds is used for estimating esds involving l.s. planes.

Refinement. Refinement of F^2 against ALL reflections. The weighted R-factor wR and goodness of fit S are based on F^2, conventional R-factors R are based on F, with F set to zero for negative F^2. The threshold expression of $F^2 > 2\text{sigma}(F^2)$ is used only for calculating R-factors(gt) etc. and is not relevant to the choice of reflections for refinement. R-factors based on F^2 are statistically about twice as large as those based on F, and R- factors based on ALL data will be even larger.

Crystal data, data collection and refinement details for [Fe$^{(II)}$BPAEB$_{NO}$(OAc)].MeCN

Empirical formula	$C_{22}H_{23}FeN_5O_5S\cdot C_2H_3N$
Formula mass (g mol^{-1})	566.42
Colour, habit	dark red, needle
Crystal dimensions (mm)	0.10 × 0.08 × 0.04 mm
Crystal system	Monoclinic
Space group	$P2_1/c$
Z	4
a (Å)	8.8210 (4)
b (Å)	17.7100 (8)
c (Å)	16.2410 (7)
α (°)	90.0°
β (°)	105.614 (2)°
γ (°)	90.0°
Unit cell volume (Å^3)	2443.54 (19)
D$_{calc}$ (Mg m^{-3})	1.540
Radiation	Cu $K\alpha$ radiation, $\lambda = 1.54178$ Å
Temperature	200 K
θ range for data collection (º)	3.8–71.5°
Collection ranges	$-10 \le h \le 10$
	$-21 \le k \le 21$
	$-19 \le l \le 19$
Absorption coeff. (μ) (mm^{-1})	6.17
Absorption correction	multi-scan
F(000)	1428
Observed reflections	31746
Independent reflections	3880 ($R_{int} = 0.049$)
Data/restraints / parameters	4781 / 0 / 336
Goodness of fit on F^2	1.06
Final R indices ($I > 2\sigma$ (I))	$R_1 = 0.033$; $wR_2 = 0.080$
R indices (all data)	$R_1 = 0.0427$; $wR_2 = 0.0831$
Largest diff. peak and hole (e Å^{-3})	0.353 and -0.307

Fractional atomic coordinates and isotropic or equivalent isotropic displacement parameters (Å^2)

	x	*y*	*z*		*x*	*y*	*z*
Fe1	0.35858 (4)	0.180601 (17)	0.62411 (2)	C9	0.5257 (3)	-0.05873 (13)	0.75622 (16)
S2	0.24159 (6)	0.32956 (3)	0.52492 (3)	H9	0.5523	-0.1062	0.7835
O1	0.4872 (2)	0.13674 (8)	0.49540 (10)	C10	0.5536 (3)	-0.04375 (13)	0.67812 (15)
O2	0.15260 (19)	0.29653 (9)	0.44486 (10)	H10	0.6027	-0.0806	0.6514
O3	0.19964 (19)	0.40718 (9)	0.53723 (11)	C11	0.5095 (2)	0.02537 (12)	0.63889 (14)
O4	0.52605 (16)	0.23223 (8)	0.70891 (9)	H11	0.5287	0.0347	0.5850
O5	0.73656 (18)	0.16958 (9)	0.69050 (11)	C12	0.0518 (3)	0.11770 (12)	0.59051 (16)
N1	0.4592 (2)	0.18978 (10)	0.54148 (11)	C13	-0.0961 (3)	0.09144 (13)	0.54560 (19)
N2	0.2536 (2)	0.28067 (10)	0.60620 (12)	H13	-0.1749	0.0821	0.5744
N3	0.2417 (2)	0.17237 (10)	0.71751 (11)	C14	-0.1269 (3)	0.07913 (14)	0.4590 (2)
N4	0.44128 (19)	0.07934 (10)	0.67378 (11)	H14	-0.2270	0.0611	0.4272
N5	0.1643 (2)	0.13249 (10)	0.55106 (12)	C15	-0.0105 (3)	0.09337 (13)	0.41913 (18)
C1	0.5256 (3)	0.26144 (12)	0.52463 (14)	H15	-0.0288	0.0845	0.3596
C2	0.4408 (3)	0.32855 (12)	0.52085 (13)	C16	0.1325 (3)	0.12060 (13)	0.46621 (15)
C3	0.5087 (3)	0.39625 (13)	0.50657 (14)	H16	0.2115	0.1314	0.4380
H3	0.4510	0.4420	0.5036	C17	0.1416 (3)	0.29354 (14)	0.65779 (15)
C4	0.6599 (3)	0.39775 (14)	0.49666 (15)	H17A	0.0359	0.2741	0.6278
H4	0.7072	0.4445	0.4889	H17B	0.1331	0.3481	0.6692
C5	0.7417 (3)	0.33094 (15)	0.49819 (17)	C18	0.2090 (3)	0.25052 (13)	0.74077 (15)
H5	0.8442	0.3316	0.4897	H18A	0.3072	0.2749	0.7745
C6	0.6747 (3)	0.26299 (14)	0.51201 (16)	H18B	0.1325	0.2500	0.7756
H6	0.7313	0.2172	0.5128	C19	0.3494 (3)	0.13098 (13)	0.78944 (14)
C7	0.4188 (2)	0.06620 (13)	0.75206 (14)	H19A	0.2907	0.1119	0.8292
C8	0.4577 (3)	-0.00226 (13)	0.79363 (15)	H19B	0.4340	0.1650	0.8215
H8	0.4378	-0.0105	0.8476	C20	0.0942 (3)	0.12736 (14)	0.68529 (16)
C9	0.5257 (3)	-0.05873 (13)	0.75622 (16)	H20A	0.1085	0.0770	0.7128
H9	0.5523	-0.1062	0.7835	H20B	0.0067	0.1531	0.7014
C10	0.5536 (3)	-0.04375 (13)	0.67812 (15)	C21	0.6762 (2)	0.22004 (13)	0.72423 (14)
H10	0.6027	-0.0806	0.6514	C22	0.7760 (3)	0.27238 (15)	0.78898 (17)
C11	0.5095 (2)	0.02537 (12)	0.63889 (14)	H22A	0.8703	0.2456	0.8216
H11	0.5287	0.0347	0.5850	H22B	0.7159	0.2900	0.8280
C12	0.0518 (3)	0.11770 (12)	0.59051 (16)	H22C	0.8070	0.3158	0.7598
C13	-0.0961 (3)	0.09144 (13)	0.54560 (19)	N6	-0.0756 (4)	0.45437 (16)	0.7013 (2)
H13	-0.1749	0.0821	0.5744	C23	-0.0003 (4)	0.49484 (16)	0.67531 (18)
C14	-0.1269 (3)	0.07913 (14)	0.4590 (2)	C24	0.0945 (3)	0.54782 (15)	0.64332 (18)
H14	-0.2270	0.0611	0.4272	H24A	0.0259	0.5843	0.6055
C15	-0.0105 (3)	0.09337 (13)	0.41913 (18)	H24B	0.1570	0.5205	0.6114
H15	-0.0288	0.0845	0.3596	H24C	0.1651	0.5746	0.6914
C16	0.1325 (3)	0.12060 (13)	0.46621 (15)				

Atomic displacement parameters (Å^2)

	U^{11}	U^{22}	U^{33}	U^{12}	U^{13}	U^{23}
Fe1	0.01851 (16)	0.02390 (16)	0.02149 (17)	0.00109 (13)	0.00758 (13)	0.00114 (14)
S2	0.0246 (3)	0.0272 (3)	0.0270 (3)	0.0039 (2)	0.0068 (2)	0.0030 (2)
O1	0.0443 (10)	0.0300 (8)	0.0319 (9)	0.0021 (7)	0.0201 (8)	-0.0048 (7)
O2	0.0327 (9)	0.0443 (10)	0.0277 (9)	-0.0001 (7)	0.0013 (7)	-0.0002 (7)
O3	0.0396 (9)	0.0275 (8)	0.0417 (10)	0.0098 (7)	0.0153 (8)	0.0045 (7)
O4	0.0230 (7)	0.0298 (8)	0.0288 (8)	0.0012 (6)	0.0070 (6)	-0.0036 (7)
O5	0.0249 (8)	0.0415 (10)	0.0466 (10)	0.0044 (7)	0.0112 (8)	-0.0063 (8)
N1	0.0271 (9)	0.0247 (9)	0.0245 (9)	0.0030 (7)	0.0080 (8)	-0.0003 (7)
N2	0.0273 (9)	0.0263 (9)	0.0291 (10)	0.0060 (7)	0.0136 (8)	0.0033 (8)
N3	0.0234 (9)	0.0325 (10)	0.0256 (10)	0.0051 (7)	0.0119 (8)	0.0037 (8)
N4	0.0192 (8)	0.0275 (9)	0.0247 (9)	0.0003 (7)	0.0059 (7)	0.0000 (8)
N5	0.0246 (9)	0.0242 (9)	0.0301 (10)	0.0019 (7)	0.0053 (8)	0.0032 (8)
C1	0.0287 (11)	0.0288 (11)	0.0255 (11)	-0.0004 (9)	0.0110 (9)	0.0030 (9)
C2	0.0265 (11)	0.0281 (11)	0.0209 (10)	-0.0007 (8)	0.0075 (9)	0.0011 (9)
C3	0.0368 (13)	0.0282 (11)	0.0295 (12)	-0.0015 (9)	0.0106 (10)	0.0008 (10)
C4	0.0379 (14)	0.0372 (13)	0.0374 (14)	-0.0092 (10)	0.0126 (11)	0.0047 (11)
C5	0.0299 (13)	0.0502 (15)	0.0476 (16)	-0.0023 (11)	0.0170 (12)	0.0108 (12)
C6	0.0335 (13)	0.0386 (13)	0.0442 (15)	0.0081 (10)	0.0195 (12)	0.0104 (11)
C7	0.0240 (11)	0.0342 (12)	0.0259 (12)	0.0024 (9)	0.0077 (9)	0.0018 (9)
C8	0.0388 (13)	0.0376 (13)	0.0272 (12)	0.0044 (10)	0.0091 (10)	0.0069 (10)
C9	0.0379 (14)	0.0289 (12)	0.0373 (14)	0.0062 (10)	0.0024 (11)	0.0039 (10)
C10	0.0352 (13)	0.0305 (12)	0.0354 (13)	0.0061 (10)	0.0088 (11)	-0.0037 (10)
C11	0.0280 (11)	0.0303 (11)	0.0283 (12)	0.0017 (9)	0.0099 (9)	-0.0023 (9)
C12	0.0232 (11)	0.0248 (11)	0.0439 (14)	0.0031 (8)	0.0081 (10)	0.0045 (10)
C13	0.0227 (12)	0.0333 (13)	0.0660 (19)	0.0004 (10)	0.0040 (12)	0.0024 (13)
C14	0.0282 (13)	0.0331 (13)	0.073 (2)	-0.0009 (10)	-0.0109 (14)	-0.0028 (14)
C15	0.0444 (15)	0.0325 (13)	0.0434 (15)	0.0045 (11)	-0.0100 (12)	-0.0062 (12)
C16	0.0383 (14)	0.0306 (12)	0.0332 (13)	0.0033 (10)	0.0032 (11)	0.0005 (10)
C17	0.0325 (12)	0.0353 (12)	0.0399 (14)	0.0105 (10)	0.0181 (11)	0.0044 (11)
C18	0.0397 (13)	0.0369 (13)	0.0370 (14)	0.0084 (10)	0.0251 (11)	0.0026 (11)
C19	0.0325 (12)	0.0379 (12)	0.0260 (12)	0.0078 (10)	0.0115 (10)	0.0053 (10)
C20	0.0247 (11)	0.0419 (13)	0.0441 (14)	0.0004 (10)	0.0150 (11)	0.0121 (12)
C21	0.0208 (10)	0.0350 (12)	0.0232 (11)	0.0020 (9)	0.0054 (9)	0.0018 (9)
C22	0.0286 (12)	0.0494 (15)	0.0480 (16)	-0.0055 (11)	0.0027 (12)	-0.0098 (13)
N6	0.106 (3)	0.0566 (17)	0.088 (2)	0.0001 (16)	0.063 (2)	-0.0041 (16)
C23	0.0609 (18)	0.0424 (15)	0.0450 (16)	0.0123 (13)	0.0265 (14)	-0.0053 (13)
C24	0.0470 (16)	0.0459 (15)	0.0486 (17)	0.0089 (12)	0.0159 (14)	0.0012 (13)

Geometric parameters (Å, º)

Fe1-N5	1.818 (2)	C11-C12	1.497 (3)	N5-Fe1-N4	90.16 (9)	N2-C12-C11	115.5 (2)
Fe1-N4	1.954 (2)	C11-H11A	0.99	N5-Fe1-N2	95.21 (9)	C16-C12-C11	122.2 (2)
Fe1-N2	1.975 (2)	C11-H11B	0.99	N4-Fe1-N2	88.25 (9)	N2-C13-C14	122.1 (3)
Fe1-N1	1.983 (2)	C12-C16	1.383 (4)	N5-Fe1-N1	96.06 (9)	N2-C13-H13A	119.0
Fe1-N3	2.014 (2)	C13-C14	1.376 (4)	N4-Fe1-N1	173.58 (9)	C14-C13-H13A	119.0
Fe1-N6	2.037 (2)	C13-H13A	0.95	N2-Fe1-N1	92.76 (9)	C13-C14-C15	119.7 (3)
S1-O1	1.438 (2)	C14-C15	1.382 (4)	N5-Fe1-N3	101.15 (9)	C13-C14-H14A	120.1
S1-O2	1.440 (2)	C14-H14A	0.95	N4-Fe1-N3	88.26 (8)	C15-C14-H14A	120.1
S1-O3	1.440 (2)	C15-C16	1.380 (4)	N2-Fe1-N3	163.28 (9)	C16-C15-C14	118.7 (3)
S1-C1	1.827 (3)	C15-H15A	0.95	N1-Fe1-N3	88.97 (8)	C16-C15-H15A	120.7
S2-O4	1.447 (19)	C16-H16A	0.95	N5-Fe1-N6	177.49 (9)	C14-C15-H15A	120.7
S2-O5	1.450 (2)	C17-C18	1.499 (3)	N4-Fe1-N6	90.21 (8)	C15-C16-C12	119.2 (3)
S2-N1	1.583 (2)	C17-H17A	0.99	N2-Fe1-N6	82.32 (8)	C15-C16-H16A	120.4
S2-C2	1.771 (3)	C17-H17B	0.99	N1-Fe1-N6	83.64 (8)	C12-C16-H16A	120.4
F1-C1	1.310 (4)	C18-C22	1.387 (4)	N3-Fe1-N6	81.35 (8)	N6-C17-C18	107.76 (19)
F2-C1	1.332 (4)	C19-C20	1.382 (4)	O1-S1-O2	114.49 (13)	N6-C17-H17A	110.2
F3-C1	1.337 (3)	C19-H19A	0.95	O1-S1-O3	114.89 (13)	C18-C17-H17A	110.2
N5-O7	1.259 (3)	C20-C21	1.378 (4)	O2-S1-O3	114.85 (14)	N6-C17-H17B	110.2
N5-C3	1.455 (3)	C20-H20A	0.95	O1-S1-C1	103.64 (14)	C18-C17-H17B	110.2
N1-C8	1.481 (3)	C21-C22	1.389 (4)	O2-S1-C1	103.38 (15)	H17A-C17-H17B	108.5
N2-C12	1.351 (3)	C21-H21A	0.95	O3-S1-C1	103.41 (14)	N3-C18-C22	122.3 (2)
N2-C13	1.352 (3)	C22-H22A	0.95	O4-S2-O5	113.92 (12)	N3-C18-C17	115.5 (2)
N3-C19	1.347 (3)	C23-C24	1.454 (4)	O4-S2-N1	110.94 (11)	C22-C18-C17	122.2 (2)
N3-C18	1.352 (3)	C24-H24A	0.98	O5-S2-N1	114.90 (12)	N3-C19-C20	122.8 (2)
N4-C23	1.142 (3)	C24-H24B	0.98	O4-S2-C2	108.27 (12)	N3-C19-H19A	118.6
C2-C7	1.388 (4)	C24-H24C	0.98	O5-S2-C2	105.63 (12)	C20-C19-H19A	118.6
C2-C3	1.393 (4)	O8-C26B^{i}	1.381 (6)	N1-S2-C2	102.14 (11)	C21-C20-C19	119.3 (2)
C3-C4	1.391 (4)	O8-C26B	1.381 (6)	O7-N5-C3	112.4 (2)	C21-C20-H20A	120.4
C4-C5	1.385 (4)	O8-C26A^{i}	1.539 (6)	O7-N5-Fe1	122.10 (17)	C19-C20-H20A	120.4

C4-H4B	0.95	O8-C26A	1.539 (6)	C3-N5-Fe1	125.45 (16)	C20-C21-C22	118.7 (2)
C5-C6	1.391 (4)	C25-C26A	1.394 (7)	C8-N1-S2	113.13 (16)	C20-C21-H21A	120.7
C5-H5B	0.95	C25-C26B	1.535 (7)	C8-N1-Fe1	109.57 (15)	C22-C21-H21A	120.7
C6-C7	1.379 (4)	C25-H25A	0.98	S2-N1-Fe1	122.57 (12)	C18-C22-C21	119.1 (2)
C6-H6A	0.95	C25-H25B	0.98	C12-N2-C13	118.1 (2)	C18-C22-H22A	120.4
C7-H7A	0.95	C25-H25C	0.98	C12-N2-Fe1	115.01 (17)	C21-C22-H22A	120.4
C8-C9	1.503 (3)	C25-H25D	0.98	C13-N2-Fe1	126.91 (19)	N4-C23-C24	178.9 (3)
C8-H8A	0.99	C25-H25E	0.98	C19-N3-C18	117.7 (2)	C23-C24-H24A	109.5
C8-H8B	0.99	C25-H25F	0.98	C19-N3-Fe1	128.43 (17)	C23-C24-H24B	109.5
C9-N6	1.496 (3)	C26A-H26A	0.99	C18-N3-Fe1	113.79 (16)	H24A-C24-H24B	109.5
C9-H9A	0.99	C26A-H26B	0.99	C23-N4-Fe1	177.9 (2)	C23-C24-H24C	109.5
C9-H9B	0.99	C26B-H26C	0.99	F1-C1-F2	107.7 (3)	H24A-C24-H24C	109.5
N6-C11	1.488 (3)	C26B-H26D	0.99	F1-C1-F3	108.3 (3)	H24B-C24-H24C	109.5
N6-C17	1.490 (3)	H25B-C25-H25E	178.3	F2-C1-F3	106.8 (3)	C26B^{i}-O8-C26B	179.9980 (10)
C9-C8-H8A	110.8	H25C-C25-H25E	72.0	F1-C1-S1	111.7 (2)	C26B^{i}-O8-C26A^{i}	72.1 (4)
N1-C8-H8B	110.8	H25D-C25-H25E	109.5	F2-C1-S1	111.0 (2)	C26B-O8-C26A^{i}	107.9 (4)
C9-C8-H8B	110.8	C26A-C25-H25F	70.6	F3-C1-S1	111.0 (2)	C26B^{i}-O8-C26A	107.9 (4)
H8A-C8-H8B	108.8	C26B-C25-H25F	109.5	C7-C2-C3	119.6 (2)	C26B-O8-C26A	72.1 (4)
N6-C9-C8	110.1 (2)	H25A-C25-H25F	71.9	C7-C2-S2	118.0 (2)	C26A^{i}-O8-C26A	179.9980 (10)
N6-C9-H9A	109.6	H25B-C25-H25F	69.1	C3-C2-S2	121.3 (2)	C26A-C25-C26B	71.9 (4)
C8-C9-H9A	109.6	H25C-C25-H25F	178.3	C4-C3-C2	120.2 (2)	C26A-C25-H25A	109.5
N6-C9-H9B	109.6	H25D-C25-H25F	109.5	C4-C3-N5	118.8 (2)	C26B-C25-H25A	178.4
C8-C9-H9B	109.6	H25E-C25-H25F	109.5	C2-C3-N5	121.0 (2)	C26A-C25-H25B	109.5
H9A-C9-H9B	108.2	C25-C26A-O8	107.5 (4)	C5-C4-C3	119.6 (3)	C26B-C25-H25B	70.6
C11-N6-C17	111.65 (19)	C25-C26A-H26A	110.2	C5-C4-H4B	120.2	H25A-C25-H25B	109.5
C11-N6-C9	112.02 (19)	O8-C26A-H26A	110.2	C3-C4-H4B	120.2	C26A-C25-H25C	109.5
C17-N6-C9	109.13 (19)	C25-C26A-H26B	110.2	C4-C5-C6	120.3 (3)	C26B-C25-H25C	69.1
C11-N6-Fe1	107.75 (15)	O8-C26A-H26B	110.2	C4-C5-H5B	119.9	H25A-C25-H25C	109.5
C17-N6-Fe1	107.28 (14)	H26A-C26A-H26B	108.5	C6-C5-H5B	119.9	H25B-C25-H25C	109.5
C9-N6-Fe1	108.85 (15)	O8-C26B-C25	108.4 (4)	C7-C6-C5	119.9 (3)	C26A-C25-H25D	178.3

N6-C11-C12	110.0 (2)	O8-C26B-H26C	110.0	C7-C6-H6A	120.0	C26B-C25-H25D	109.5
N6-C11-H11A	109.7	C25-C26B-H26C	110.0	C5-C6-H6A	120.0	H25A-C25-H25D	69.1
C12-C11-H11A	109.7	O8-C26B-H26D	110.0	C6-C7-C2	120.4 (3)	H25B-C25-H25D	72.0
N6-C11-H11B	109.7	C25-C26B-H26D	110.0	C6-C7-H7A	119.8	H25C-C25-H25D	70.5
C12-C11-H11B	109.7	H26C-C26B-H26D	108.4	C2-C7-H7A	119.8	C26A-C25-H25E	69.1
H11A-C11-H11B	108.2	N2-C12-C16	122.3 (2)	N1-C8-C9	104.97 (19)	C26B-C25-H25E	109.5
				N1-C8-H8A	110.8	H25A-C25-H25E	70.6

[Fe$^{(II)}$BPAEB$_{NO}$(MeCN)](OTf).Et$_2$O

Computing details

Data collection: Bruker Instrument Service v2010.9.0.0; cell refinement: *SAINT* V7.68A (Bruker AXS, 2009); data reduction: *SAINT* V7.68A (Bruker AXS, 2009); program(s) used to solve structure: *SHELXS97* (Sheldrick, 2008); program(s) used to refine structure: *SHELXL97* (Sheldrick, 2008).

Geometry. All esds (except the esd in the dihedral angle between two l.s. planes) are estimated using the full covariance matrix. The cell esds are taken into account individually in the estimation of esds in distances, angles and torsion angles; correlations between esds in cell parameters are only used when they are defined by crystal symmetry. An approximate (isotropic) treatment of cell esds is used for estimating esds involving l.s. planes.

Refinement. Refinement of F^2 against ALL reflections. The weighted R-factor wR and goodness of fit S are based on F^2, conventional R-factors R are based on F, with F set to zero for negative F^2. The threshold expression of $F^2 > 2\text{sigma}(F^2)$ is used only for calculating R-factors(gt) etc. and is not relevant to the choice of reflections for refinement. R-factors based on F^2 are statistically about twice as large as those based on F, and R- factors based on ALL data will be even larger.

Crystal data, data collection and refinement details for $[\mathrm{Fe^{(II)}BPAEB_{NO}(MeCN)}](\mathrm{OTf}).\mathrm{Et_2O}$

Empirical formula	$(\mathrm{C_{22}H_{23}FeN_6O_3S})\cdot0.5(\mathrm{C_4H_{10}O})\cdot(\mathrm{CF_3OS})$
Formula mass (g mol^{-1})	693.50
Colour, habit	metallic dark purple, prism
Crystal dimensions (mm)	0.22 × 0.19 × 0.15 mm
Crystal system	Monoclinic
Space group	$P2_1/c$
Z	4
a (Å)	14.0633 (14) Å
b (Å)	12.7557 (13) Å
c (Å)	16.5187 (17) Å
α (°)	90°
β (°)	107.076 (1)°
γ (°)	90°
Unit cell volume (Å^3)	2832.6 (5)
D_{calc} (Mg m^{-3})	1.626
Radiation	Mo $K\alpha$ radiation, $\lambda = 0.71073$ Å
Temperature	$T = 110$ K
θ range for data collection (º)	2.2–27.5°
Collection ranges	$-18 \leq h \leq 18$ $-16 \leq k \leq 16$ $-21 \leq l \leq 21$
Absorption coeff. (μ) (mm^{-1})	0.75
Absorption correction	multi-scan
F(000)	1428
Observed reflections	31600
Independent reflections	6481 ($R_{int} = 0.047$)
Data/restraints / parameters	6481/ 0 / 404
Goodness of fit on F^2	1.00
Final R indices ($I > 2\sigma(I)$)	$R_1 = 0.0402$; $wR_2 = 0.0994$
R indices (all data)	$R_1 = 0.0605$; $wR_2 = 0.1093$
Largest diff. peak and hole (e Å^{-3})	0.503 and -0.500

Fractional atomic coordinates and isotropic or equivalent isotropic displacement parameters (Å^2)

	x	*y*	*z*		*x*	*y*	*z*
Fe1	0.30032 (3)	0.24749 (3)	0.84632 (2)	C13	0.2190 (2)	0.1101 (2)	0.69520 (17)
S1	0.74803 (5)	0.19507 (6)	0.03661 (4)	H13A	0.1788	0.1679	0.6695
S2	0.35229 (5)	0.37228 (5)	0.70150 (4)	C14	0.2111 (2)	0.0176 (2)	0.65090 (18)
F1	0.87565 (16)	0.1484 (3)	0.18223 (14)	H14A	0.1669	0.0125	0.5952
F2	0.90528 (16)	0.2937 (2)	0.13036 (16)	C15	0.2678 (2)	-0.0678 (2)	0.68785 (18)
F3	0.93801 (12)	0.14901 (15)	0.07826 (12)	H15A	0.2622	-0.1326	0.6585
O1	0.75864 (15)	0.25510 (15)	-0.03394 (13)	C16	0.3327 (2)	-0.0571 (2)	0.76830 (17)
O2	0.72842 (15)	0.08527 (16)	0.01913 (15)	H16A	0.3725	-0.1146	0.7952
O3	0.68823 (16)	0.24386 (19)	0.08344 (14)	C17	0.44298 (19)	0.1959 (2)	1.00394 (15)
O4	0.42986 (14)	0.43635 (16)	0.68560 (12)	H17A	0.513	0.1813	1.0361
O5	0.30103 (14)	0.30607 (15)	0.63076 (11)	H17B	0.3993	0.1531	1.0282
N5	0.18813 (15)	0.31283 (17)	0.78326 (13)	C18	0.42052 (18)	0.3101 (2)	1.00947 (15)
O7	0.10359 (13)	0.27106 (15)	0.76783 (13)	C19	0.32239 (19)	0.4503 (2)	0.94680 (16)
N1	0.39125 (15)	0.31366 (17)	0.78952 (13)	H19A	0.2728	0.4792	0.9001
N2	0.28212 (16)	0.12132 (17)	0.77408 (13)	C20	0.3641 (2)	0.5135 (2)	1.01606 (17)
N3	0.34905 (15)	0.34950 (16)	0.94269 (13)	H20A	0.3416	0.5835	1.0175
N4	0.22408 (15)	0.17750 (16)	0.91226 (13)	C21	0.4388 (2)	0.4740 (2)	1.08298 (17)
C1	0.8730 (2)	0.1960 (3)	0.1113 (2)	H21A	0.4695	0.5165	1.1307
C2	0.26007 (19)	0.4565 (2)	0.71886 (15)	C22	0.46825 (19)	0.3706 (2)	1.07933 (16)
C3	0.18358 (19)	0.4181 (2)	0.74829 (15)	H22A	0.5204	0.3417	1.1241
C4	0.1016 (2)	0.4806 (2)	0.74534 (16)	C23	0.17747 (19)	0.1390 (2)	0.95013 (16)
H4B	0.0485	0.4538	0.7639	C24	0.1164 (2)	0.0903 (2)	0.99695 (18)
C5	0.0978 (2)	0.5823 (2)	0.71515 (17)	H24A	0.0491	0.0788	0.959
H5B	0.0424	0.6256	0.7138	H24B	0.1131	0.1363	1.0436
C6	0.1747 (2)	0.6213 (2)	0.68674 (18)	H24C	0.1456	0.0229	1.0198
H6A	0.1722	0.6914	0.6668	O8	0	0.5	0
C7	0.2546 (2)	0.5581 (2)	0.68764 (17)	C25	-0.0113 (3)	0.6559 (3)	0.0744 (3)
H7A	0.3061	0.5842	0.6668	H25A	-0.0034	0.7322	0.0783
C8	0.47588 (19)	0.2425 (2)	0.79409 (16)	H25B	0.0328	0.6233	0.1254
H8A	0.5294	0.2798	0.7781	H25C	-0.0804	0.6375	0.0692
H8B	0.4541	0.1817	0.7558	H25D	-0.0292	0.6831	0.1234
C9	0.51124 (18)	0.2075 (2)	0.88492 (15)	H25E	-0.0537	0.6883	0.0225
H9A	0.5605	0.1504	0.891	H25F	0.0585	0.6724	0.0804
H9B	0.5441	0.2667	0.9212	C26A	0.0134 (4)	0.6198 (5)	0.0034 (4)
N6	0.42523 (15)	0.16955 (16)	0.91284 (12)	H26A	0.0831	0.6382	0.0078
C11	0.40693 (19)	0.05548 (19)	0.89685 (16)	H26B	-0.0306	0.6523	-0.0486
H11A	0.3765	0.0259	0.9388	C26B	-0.0259 (4)	0.5365 (5)	0.0693 (4)
H11B	0.4709	0.019	0.9033	H26C	0.0163	0.5032	0.1217
C12	0.33906 (18)	0.0384 (2)	0.80930 (16)	H26D	-0.0962	0.5191	0.0634

Atomic displacement parameters (Å^2)

	U^{11}	U^{22}	U^{33}	U^{12}	U^{13}	U^{23}
Fe1	0.01390 (17)	0.01481 (18)	0.01235 (17)	0.00037 (14)	0.00377 (13)	0.00068 (14)
S1	0.0190 (3)	0.0279 (4)	0.0206 (3)	0.0044 (3)	0.0042 (3)	0.0032 (3)
S2	0.0201 (3)	0.0225 (3)	0.0142 (3)	0.0022 (2)	0.0073 (2)	0.0040 (2)
F1	0.0331 (12)	0.177 (3)	0.0336 (12)	0.0314 (15)	0.0079 (10)	0.0407 (15)
F2	0.0384 (12)	0.0760 (17)	0.0800 (17)	0.0053 (11)	-0.0101 (11)	-0.0525 (14)
F3	0.0227 (9)	0.0433 (11)	0.0453 (11)	0.0077 (8)	0.0121 (8)	-0.0048 (9)
O1	0.0309 (11)	0.0234 (10)	0.0268 (10)	-0.0016 (8)	0.0079 (9)	0.0051 (8)
O2	0.0302 (11)	0.0236 (11)	0.0490 (14)	0.0005 (9)	0.0135 (10)	0.0115 (10)
O3	0.0251 (11)	0.0574 (15)	0.0306 (12)	0.0146 (10)	0.0096 (9)	-0.0005 (10)
O4	0.0254 (10)	0.0322 (11)	0.0289 (11)	0.0005 (9)	0.0145 (9)	0.0122 (9)
O5	0.0277 (10)	0.0291 (11)	0.0155 (9)	0.0056 (8)	0.0058 (8)	-0.0002 (8)
N5	0.0155 (10)	0.0183 (11)	0.0178 (10)	-0.0022 (8)	0.0051 (8)	0.0001 (9)
O7	0.0140 (9)	0.0256 (11)	0.0316 (11)	-0.0029 (7)	0.0031 (8)	0.0041 (8)
N1	0.0163 (10)	0.0199 (11)	0.0141 (10)	0.0014 (8)	0.0054 (8)	0.0023 (8)
N2	0.0196 (10)	0.0185 (11)	0.0151 (10)	-0.0018 (8)	0.0069 (9)	-0.0016 (8)
N3	0.0148 (10)	0.0186 (11)	0.0147 (10)	-0.0009 (8)	0.0075 (8)	-0.0001 (8)
N4	0.0192 (10)	0.0149 (10)	0.0154 (10)	0.0016 (8)	0.0047 (9)	-0.0008 (8)
C1	0.0260 (15)	0.061 (2)	0.0286 (17)	0.0106 (15)	0.0076 (13)	0.0000 (16)
C2	0.0220 (13)	0.0187 (13)	0.0132 (12)	0.0013 (10)	0.0038 (10)	0.0004 (10)
C3	0.0193 (12)	0.0191 (13)	0.0124 (12)	0.0003 (10)	0.0013 (10)	0.0007 (10)
C4	0.0214 (13)	0.0238 (14)	0.0189 (13)	0.0011 (11)	0.0046 (11)	0.0023 (11)
C5	0.0277 (14)	0.0220 (14)	0.0215 (14)	0.0075 (11)	0.0045 (11)	0.0010 (11)
C6	0.0350 (16)	0.0178 (14)	0.0274 (15)	0.0019 (12)	0.0084 (13)	0.0045 (11)
C7	0.0298 (15)	0.0210 (14)	0.0230 (14)	0.0012 (11)	0.0095 (12)	0.0041 (11)
C8	0.0201 (12)	0.0211 (13)	0.0164 (12)	0.0010 (10)	0.0084 (10)	0.0014 (10)
C9	0.0177 (12)	0.0206 (13)	0.0150 (12)	0.0005 (10)	0.0043 (10)	0.0001 (10)
N6	0.0167 (10)	0.0160 (10)	0.0125 (10)	0.0010 (8)	0.0041 (8)	-0.0011 (8)
C11	0.0205 (12)	0.0126 (12)	0.0196 (12)	0.0014 (10)	0.0066 (10)	0.0003 (10)
C12	0.0183 (12)	0.0194 (13)	0.0180 (12)	-0.0026 (10)	0.0095 (10)	-0.0003 (10)
C13	0.0254 (14)	0.0237 (14)	0.0207 (14)	-0.0026 (11)	0.0015 (11)	0.0012 (11)
C14	0.0336 (16)	0.0327 (16)	0.0171 (13)	-0.0094 (13)	0.0019 (12)	-0.0042 (12)
C15	0.0356 (16)	0.0212 (14)	0.0269 (15)	-0.0060 (12)	0.0136 (13)	-0.0074 (12)
C16	0.0249 (13)	0.0190 (13)	0.0247 (14)	0.0002 (11)	0.0107 (11)	-0.0026 (11)
C17	0.0199 (12)	0.0183 (13)	0.0104 (11)	0.0014 (10)	0.0043 (10)	-0.0007 (9)
C18	0.0181 (12)	0.0187 (13)	0.0151 (12)	0.0004 (10)	0.0088 (10)	0.0004 (10)
C19	0.0186 (12)	0.0180 (13)	0.0197 (13)	0.0011 (10)	0.0081 (10)	0.0019 (10)
C20	0.0271 (14)	0.0167 (13)	0.0249 (14)	0.0011 (11)	0.0122 (11)	-0.0035 (11)
C21	0.0238 (13)	0.0254 (14)	0.0203 (13)	-0.0043 (11)	0.0086 (11)	-0.0062 (11)
C22	0.0187 (12)	0.0271 (14)	0.0140 (12)	-0.0010 (11)	0.0044 (10)	0.0007 (10)

C23	0.0193 (12)	0.0171 (13)	0.0180 (12)	0.0012 (10)	0.0042 (10)	-0.0012 (10)
C24	0.0250 (14)	0.0272 (15)	0.0245 (14)	-0.0048 (11)	0.0123 (12)	0.0025 (11)
O8	0.0238 (14)	0.0407 (18)	0.0285 (15)	-0.0049 (13)	0.0078 (12)	-0.0037 (13)
C25	0.042 (2)	0.037 (2)	0.059 (2)	0.0063 (16)	-0.0002 (18)	-0.0032 (17)
C26A	0.026 (3)	0.025 (3)	0.036 (3)	-0.002 (2)	0.003 (3)	0.005 (3)
C26B	0.025 (3)	0.042 (4)	0.029 (3)	0.006 (3)	0.009 (2)	-0.007 (3)

Geometric parameters (Å, º)

Fe1-N5	1.818 (2)	C11-C12	1.497 (3)	N2-C12-C11	115.5 (2)	O1-S1-O2	114.49 (13)
Fe1-N4	1.954 (2)	C11-H11A	0.99	C16-C12-C11	122.2 (2)	O1-S1-O3	114.89 (13)
Fe1-N2	1.975 (2)	C11-H11B	0.99	N2-C13-C14	122.1 (3)	O2-S1-O3	114.85 (14)
Fe1-N1	1.983 (2)	C12-C16	1.383 (4)	N2-C13-H13A	119.0	O1-S1-C1	103.64 (14)
Fe1-N3	2.014 (2)	C13-C14	1.376 (4)	C14-C13-H13A	119.0	O2-S1-C1	103.38 (15)
Fe1-N6	2.037 (2)	C13-H13A	0.95	C13-C14-C15	119.7 (3)	O3-S1-C1	103.41 (14)
S1-O1	1.438 (2)	C14-C15	1.382 (4)	C13-C14-H14A	120.1	O4-S2-O5	113.92 (12)
S1-O2	1.440 (2)	C14-H14A	0.95	C15-C14-H14A	120.1	O4-S2-N1	110.94 (11)
S1-O3	1.440 (2)	C15-C16	1.380 (4)	C16-C15-C14	118.7 (3)	O5-S2-N1	114.90 (12)
S1-C1	1.827 (3)	C15-H15A	0.95	C16-C15-H15A	120.7	O4-S2-C2	108.27 (12)
S2-O4	1.4474 (19)	C16-H16A	0.95	C14-C15-H15A	120.7	O5-S2-C2	105.63 (12)
S2-O5	1.450 (2)	C17-C18	1.499 (3)	C15-C16-C12	119.2 (3)	N1-S2-C2	102.14 (11)
S2-N1	1.583 (2)	C17-H17A	0.99	C15-C16-H16A	120.4	O7-N5-C3	112.4 (2)
S2-C2	1.771 (3)	C17-H17B	0.99	C12-C16-H16A	120.4	O7-N5-Fe1	122.10 (17)
F1-C1	1.310 (4)	C18-C22	1.387 (4)	N6-C17-C18	107.76 (19)	C3-N5-Fe1	125.45 (16)
F2-C1	1.332 (4)	C19-C20	1.382 (4)	N6-C17-H17A	110.2	C8-N1-S2	113.13 (16)
F3-C1	1.337 (3)	C19-H19A	0.95	C18-C17-H17A	110.2	C8-N1-Fe1	109.57 (15)
N5-O7	1.259 (3)	C20-C21	1.378 (4)	N6-C17-H17B	110.2	S2-N1-Fe1	122.57 (12)
N5-C3	1.455 (3)	C20-H20A	0.95	C18-C17-H17B	110.2	C12-N2-C13	118.1 (2)
N1-C8	1.481 (3)	C21-C22	1.389 (4)	H17A-C17-H17B	108.5	C12-N2-Fe1	115.01 (17)
N2-C12	1.351 (3)	C21-H21A	0.95	N3-C18-C22	122.3 (2)	C13-N2-Fe1	126.91 (19)
N2-C13	1.352 (3)	C22-H22A	0.95	N3-C18-C17	115.5 (2)	C19-N3-C18	117.7 (2)
N3-C19	1.347 (3)	C23-C24	1.454 (4)	C22-C18-C17	122.2 (2)	C19-N3-Fe1	128.43 (17)

N3-C18	1.352 (3)	C24-H24A	0.98	N3-C19-C20	122.8 (2)	C18-N3-Fe1	113.79 (16)
N4-C23	1.142 (3)	C24-H24B	0.98	N3-C19-H19A	118.6	C23-N4-Fe1	177.9 (2)
C2-C7	1.388 (4)	C24-H24C	0.98	C20-C19-H19A	118.6	F1-C1-F2	107.7 (3)
C2-C3	1.393 (4)	O8-C26B^{i}	1.381 (6)	C21-C20-C19	119.3 (2)	F1-C1-F3	108.3 (3)
C3-C4	1.391 (4)	O8-C26B	1.381 (6)	C21-C20-H20A	120.4	F2-C1-F3	106.8 (3)
C4-C5	1.385 (4)	O8-C26A^{i}	1.539 (6)	C19-C20-H20A	120.4	F1-C1-S1	111.7 (2)
C4-H4B	0.95	O8-C26A	1.539 (6)	C20-C21-C22	118.7 (2)	C5-C6-H6A	120.0
C5-C6	1.391 (4)	C25-C26A	1.394 (7)	C20-C21-H21A	120.7	C6-C7-C2	120.4 (3)
C5-H5B	0.95	C25-C26B	1.535 (7)	C22-C21-H21A	120.7	C6-C7-H7A	119.8
C6-C7	1.379 (4)	C25-H25A	0.98	C18-C22-C21	119.1 (2)	C2-C7-H7A	119.8
C6-H6A	0.95	C25-H25B	0.98	C18-C22-H22A	120.4	N1-C8-C9	104.97 (19)
C7-H7A	0.95	C25-H25C	0.98	C21-C22-H22A	120.4	N1-C8-H8A	110.8
C8-C9	1.503 (3)	C25-H25D	0.98	N4-C23-C24	178.9 (3)	C9-C8-H8A	110.8
C8-H8A	0.99	C25-H25E	0.98	C23-C24-H24A	109.5	N1-C8-H8B	110.8
C8-H8B	0.99	C25-H25F	0.98	C23-C24-H24B	109.5	C9-C8-H8B	110.8
C9-N6	1.496 (3)	C26A-H26A	0.99	H24A-C24-H24B	109.5	H8A-C8-H8B	108.8
C9-H9A	0.99	C26A-H26B	0.99	C23-C24-H24C	109.5	N6-C9-C8	110.1 (2)
C9-H9B	0.99	C26B-H26C	0.99	H24A-C24-H24C	109.5	N6-C9-H9A	109.6
N6-C11	1.488 (3)	C26B-H26D	0.99	H24B-C24-H24C	109.5	C8-C9-H9A	109.6
N6-C17	1.490 (3)	F2-C1-S1	111.0 (2)	C26B^{i}-O8-C26B	179.9980 (10)	N6-C9-H9B	109.6
N5-Fe1-N4	90.16 (9)	F3-C1-S1	111.0 (2)	C26B-O8-C26A^{i}	107.9 (4)	C8-C9-H9B	109.6
N5-Fe1-N2	95.21 (9)	C7-C2-C3	119.6 (2)	C26B^{i}-O8-C26A	107.9 (4)	H9A-C9-H9B	108.2
N4-Fe1-N2	88.25 (9)	C7-C2-S2	118.0 (2)	C26B-O8-C26A	72.1 (4)	C11-N6-C17	111.65 (19)
N5-Fe1-N1	96.06 (9)	C3-C2-S2	121.3 (2)	C26A^{i}-O8-C26A	179.9980 (10)	C11-N6-C9	112.02 (19)
N4-Fe1-N1	173.58 (9)	C4-C3-C2	120.2 (2)	C26A-C25-C26B	71.9 (4)	C17-N6-C9	109.13 (19)
N2-Fe1-N1	92.76 (9)	C4-C3-N5	118.8 (2)	C26A-C25-H25A	109.5	C11-N6-Fe1	107.75 (15)
N5-Fe1-N3	101.15 (9)	C2-C3-N5	121.0 (2)	C26B-C25-H25A	178.4	C17-N6-Fe1	107.28 (14)
N4-Fe1-N3	88.26 (8)	C5-C4-C3	119.6 (3)	C26A-C25-H25B	109.5	C9-N6-Fe1	108.85 (15)
N2-Fe1-N3	163.28 (9)	C5-C4-H4B	120.2	C26B-C25-H25B	70.6	N6-C11-C12	110.0 (2)
N1-Fe1-N3	88.97 (8)	C3-C4-H4B	120.2	H25A-C25-H25B	109.5	N6-C11-H11A	109.7

N5-Fe1-N6	177.49 (9)	C4-C5-C6	120.3 (3)	C26A-C25-H25C	109.5	C12-C11-H11A	109.7
N4-Fe1-N6	90.21 (8)	C4-C5-H5B	119.9	C26B-C25-H25C	69.1	N6-C11-H11B	109.7
N2-Fe1-N6	82.32 (8)	C6-C5-H5B	119.9	H25A-C25-H25C	109.5	C12-C11-H11B	109.7
N1-Fe1-N6	83.64 (8)	C7-C6-C5	119.9 (3)	H25B-C25-H25C	109.5	H11A-C11-H11B	108.2
N3-Fe1-N6	81.35 (8)	C7-C6-H6A	120.0	C26A-C25-H25D	178.3	N2-C12-C16	122.3 (2)
C26A-C25-H25E	69.1	H25C-C25-H25E	72.0	C26B-C25-H25D	109.5	H25A-C25-H25F	71.9
C26B-C25-H25E	109.5	H25D-C25-H25E	109.5	H25A-C25-H25D	69.1	H25B-C25-H25F	69.1
H25A-C25-H25E	70.6	C26A-C25-H25F	70.6	H25B-C25-H25D	72.0	H25C-C25-H25F	178.3
H25B-C25-H25E	178.3	C26B-C25-H25F	109.5	H25C-C25-H25D	70.5	H25D-C25-H25F	109.5
H25E-C25-H25F	109.5	O8-C26A-H26A	110.2	H26A-C26A-H26B	108.5	C25-C26B-H26C	110.0
C25-C26A-O8	107.5 (4)	C25-C26A-H26B	110.2	O8-C26B-C25	108.4 (4)	O8-C26B-H26D	110.0
C25-C26A-H26A	110.2	O8-C26A-H26B	110.2	O8-C26B-H26C	110.0	C25-C26B-H26D	110.0
H26C-C26B-H26D	108.4						

$[\mathbf{Fe^{(II)}BPAEB_{NH_2}(OAc)}]$

Computing details

Data collection: Bruker Instrument Service v2010.3.0.0; cell refinement: *SAINT* V7.68A (Bruker AXS, 2009); data reduction: *SAINT* V7.68A (Bruker AXS, 2009); program(s) used to solve structure: *SHELXS97* (Sheldrick, 2008); program(s) used to refine structure: *SHELXL97* (Sheldrick, 2008).

Geometry. All esds (except the esd in the dihedral angle between two l.s. planes) are estimated using the full covariance matrix. The cell esds are taken into account individually in the estimation of esds in distances, angles and torsion angles; correlations between esds in cell parameters are only used when they are defined by crystal symmetry. An approximate (isotropic) treatment of cell esds is used for estimating esds involving l.s. planes.

Refinement. Refinement of F^2 against ALL reflections. The weighted R-factor wR and goodness of fit S are based on F^2, conventional R-factors R are based on F, with F set to zero for negative F^2. The threshold expression of $F^2 > 2\mathrm{sigma}(F^2)$ is used only for calculating R-factors(gt) etc. and is not relevant to the choice of reflections for refinement. R-factors based on F^2 are statistically about twice as large as those based on F, and R- factors based on ALL data will be even larger.

Crystal data, data collection and refinement details for $[\mathrm{Fe}^{(\mathrm{II})}\mathrm{BPAEB}_{\mathrm{NH}_2}(\mathrm{OAc})]$

Empirical formula	$C_{22}H_{25}FeN_5O_4S$
Formula mass (g mol^{-1})	511.38
Colour, habit	clear light yellow, rhomb
Crystal dimensions (mm)	0.10 × 0.10 × 0.10 mm
Crystal system	Triclinic
Space group	*P*-1
Z	2
a (Å)	8.561 (3) Å
b (Å)	9.304 (3) Å
c (Å)	15.304 (6) Å
α (°)	105.064 (8)°
β (°)	96.915 (8)°
γ (°)	100.134 (8)°
Unit cell volume (Å^3)	1140.9 (7)
D_{calc} (Mg m^{-3})	1.489
Radiation	Mo *K*α radiation, λ = 0.71073 Å
Temperature	106 K
θ range for data collection (º)	2.3–23.3°
Collection ranges	$-9 \leq h \leq 10$
	$-10 \leq k \leq 10$
	$-17 \leq l \leq 17$
Absorption coeff. (μ) (mm^{-1})	0.79
Absorption correction	multi-scan
F(000)	532
Observed reflections	14216
Independent reflections	3853 (R_{int} = 0.055)
Data/restraints / parameters	3853 / 3 / 305
Goodness of fit on F^2	0.99
Final *R* indices (I > 2> (I))	$R_1 = 0.0372$; $wR_2 = 0.0917$
R indices (all data)	$R_1 = 0.0573$; $wR_2 = 0.1048$
Largest diff. peak and hole (e Å^{-3})	0.387and -0.411

Fractional atomic coordinates and isotropic or equivalent isotropic displacement parameters (Å^{2})

	X	*y*	*z*		*x*	*y*	*z*
Fe1	0.70869 (5)	0.42115 (5)	0.74932 (3)	H8A	0.3702	0.4013	0.8674
S1	0.51112 (10)	0.16579 (9)	0.81130 (5)	H8B	0.2641	0.3269	0.7662
O1	0.5061 (3)	0.2013 (3)	0.90861 (14)	C9	0.3421 (4)	0.0154 (3)	0.7571 (2)
O2	0.6514 (3)	0.1138 (2)	0.78273 (14)	C10	0.2532 (4)	-0.0492 (4)	0.8131 (2)
O3	0.8914 (3)	0.3289 (2)	0.70766 (14)	H10	0.2807	-0.0082	0.878
O4	0.7080 (3)	0.1674 (2)	0.59295 (14)	C11	0.1256 (4)	-0.1722 (4)	0.7753 (2)
N1	0.8690 (3)	0.5612 (3)	0.87380 (17)	H11	0.0638	-0.2142	0.8138
N2	0.5814 (3)	0.6103 (3)	0.81007 (17)	C12	0.0882 (4)	-0.2340 (4)	0.6808 (2)
N3	0.4980 (3)	0.3053 (3)	0.77220 (17)	H12	0.0024	-0.3206	0.6545
N4	0.3803 (3)	0.0197 (3)	0.60156 (18)	C13	0.1743 (4)	-0.1709 (3)	0.6248 (2)
H4B	0.365 (4)	-0.034 (3)	0.5454 (10)	H13	0.1461	-0.2145	0.5601
H4A	0.471 (2)	0.084 (3)	0.619 (2)	C14	0.3037 (4)	-0.0431 (3)	0.6606 (2)
N5	0.6851 (3)	0.5421 (3)	0.64720 (17)	C15	0.6292 (4)	0.7374 (3)	0.7714 (2)
C1	1.0255 (4)	0.5571 (4)	0.8936 (2)	H15A	0.7311	0.8043	0.8088
H1	1.0672	0.4847	0.8521	H15B	0.5454	0.7986	0.7744
C2	1.1276 (4)	0.6527 (4)	0.9710 (2)	C16	0.6519 (4)	0.6816 (3)	0.6732 (2)
H2	1.2376	0.647	0.9822	C17	0.6465 (4)	0.7720 (4)	0.6143 (2)
C3	1.0678 (4)	0.7568 (4)	1.0321 (2)	H17	0.6212	0.8694	0.634
H3	1.1355	0.8244	1.0862	C18	0.6784 (4)	0.7192 (4)	0.5269 (2)
C4	0.9074 (4)	0.7610 (4)	1.0129 (2)	H18	0.6767	0.78	0.4857
H4	0.8634	0.8315	1.0544	C19	0.7128 (4)	0.5760 (4)	0.5001 (2)
C5	0.8105 (4)	0.6633 (3)	0.9339 (2)	H19	0.7365	0.5374	0.4405
C6	0.6336 (4)	0.6577 (4)	0.9102 (2)	C20	0.7122 (4)	0.4905 (4)	0.5611 (2)
H6A	0.5716	0.5848	0.937	H20	0.7318	0.3907	0.5416
H6B	0.6117	0.7596	0.9368	C21	0.8450 (4)	0.2054 (3)	0.6413 (2)
C7	0.4081 (4)	0.5406 (4)	0.7815 (2)	C22	0.9643 (4)	0.1061 (4)	0.6239 (3)
H7A	0.3761	0.5267	0.7149	H22A	0.9198	0.0203	0.5687
H7B	0.3451	0.6091	0.8152	H22B	0.987	0.0674	0.6767
C8	0.3711 (4)	0.3865 (4)	0.8010 (2)	H22C	1.0643	0.1656	0.6147

Atomic displacement parameters (Å^2)

	U^{11}	U^{22}	U^{33}	U^{12}	U^{13}	U^{23}
Fe1	0.0136 (3)	0.0137 (2)	0.0138 (2)	0.00358 (18)	0.00287 (18)	0.00278 (18)
S1	0.0171 (5)	0.0167 (4)	0.0143 (4)	0.0016 (3)	0.0025 (3)	0.0035 (3)
O1	0.0264 (14)	0.0293 (13)	0.0147 (11)	0.0027 (11)	0.0039 (10)	0.0045 (10)
O2	0.0137 (12)	0.0229 (12)	0.0194 (11)	0.0049 (10)	0.0018 (9)	0.0048 (9)
O3	0.0168 (13)	0.0166 (12)	0.0220 (12)	0.0047 (10)	0.0038 (10)	-0.0010 (9)
O4	0.0155 (13)	0.0232 (12)	0.0187 (11)	0.0027 (10)	0.0008 (10)	0.0037 (10)
N1	0.0154 (15)	0.0172 (14)	0.0161 (13)	0.0049 (11)	0.0036 (11)	0.0041 (11)
N2	0.0156 (15)	0.0141 (13)	0.0157 (13)	0.0041 (11)	0.0033 (11)	0.0038 (11)
N3	0.0168 (15)	0.0137 (13)	0.0201 (14)	0.0053 (11)	0.0058 (11)	0.0032 (11)
N4	0.0168 (16)	0.0192 (15)	0.0156 (13)	0.0007 (12)	0.0020 (12)	0.0027 (11)
N5	0.0146 (15)	0.0158 (14)	0.0183 (14)	0.0033 (11)	0.0030 (11)	0.0032 (11)
C1	0.0182 (19)	0.0180 (17)	0.0224 (17)	0.0044 (14)	0.0049 (14)	0.0082 (14)
C2	0.0174 (19)	0.0253 (19)	0.0210 (17)	0.0025 (15)	-0.0022 (14)	0.0071 (15)
C3	0.030 (2)	0.0233 (19)	0.0237 (18)	-0.0008 (16)	-0.0103 (16)	0.0015 (15)
C4	0.033 (2)	0.0240 (19)	0.0180 (17)	0.0104 (16)	0.0013 (15)	-0.0016 (14)
C5	0.0203 (19)	0.0166 (17)	0.0164 (16)	0.0038 (14)	0.0024 (14)	0.0025 (13)
C6	0.024 (2)	0.0198 (17)	0.0193 (17)	0.0073 (15)	0.0051 (14)	0.0030 (14)
C7	0.0134 (18)	0.0226 (18)	0.0229 (17)	0.0078 (14)	0.0057 (14)	0.0057 (14)
C8	0.0145 (18)	0.0219 (18)	0.0275 (18)	0.0024 (14)	0.0036 (14)	0.0063 (15)
C9	0.0146 (18)	0.0156 (16)	0.0209 (17)	0.0060 (13)	0.0041 (13)	0.0067 (13)
C10	0.0198 (19)	0.0218 (18)	0.0229 (17)	0.0080 (15)	0.0076 (14)	0.0083 (14)
C11	0.021 (2)	0.0247 (19)	0.034 (2)	0.0044 (15)	0.0094 (16)	0.0154 (16)
C12	0.0145 (19)	0.0158 (17)	0.042 (2)	0.0021 (14)	0.0041 (15)	0.0085 (15)
C13	0.0167 (18)	0.0158 (17)	0.0253 (18)	0.0043 (14)	0.0000 (14)	0.0023 (14)
C14	0.0128 (17)	0.0117 (15)	0.0203 (16)	0.0051 (13)	0.0026 (13)	0.0034 (13)
C15	0.0192 (19)	0.0135 (16)	0.0257 (18)	0.0067 (14)	0.0045 (14)	0.0058 (13)
C16	0.0109 (17)	0.0157 (17)	0.0214 (16)	0.0005 (13)	0.0014 (13)	0.0048 (13)
C17	0.0206 (19)	0.0192 (17)	0.0309 (19)	0.0076 (15)	0.0037 (15)	0.0124 (15)
C18	0.024 (2)	0.031 (2)	0.0260 (19)	0.0052 (16)	0.0009 (15)	0.0174 (16)
C19	0.022 (2)	0.033 (2)	0.0157 (16)	0.0036 (16)	0.0019 (14)	0.0072 (15)
C20	0.0177 (18)	0.0207 (17)	0.0188 (17)	0.0051 (14)	0.0036 (14)	0.0056 (14)
C21	0.020 (2)	0.0146 (16)	0.0194 (17)	0.0051 (14)	0.0078 (14)	0.0047 (14)
C22	0.024 (2)	0.027 (2)	0.035 (2)	0.0111 (16)	0.0033 (16)	-0.0014 (16)

Geometric parameters (Å, º)

Fe1-O3	2.004 (2)	C6-H6B	0.99	O3-Fe1-N3	125.73 (10)	C8-C7-H7A	109.6
Fe1-N3	2.050 (3)	C7-C8	1.527 (4)	O3-Fe1-N1	89.34 (10)	N2-C7-H7B	109.6
Fe1-N1	2.159 (3)	C7-H7A	0.99	N3-Fe1-N1	113.55 (10)	C8-C7-H7B	109.6
Fe1-N5	2.161 (3)	C7-H7B	0.99	O3-Fe1-N5	96.75 (10)	H7A-C7-H7B	108.1
Fe1-N2	2.284 (3)	C8-H8A	0.99	N3-Fe1-N5	116.11 (10)	N3-C8-C7	107.5 (2)
S1-O2	1.445 (2)	C8-H8B	0.99	N1-Fe1-N5	111.86 (10)	N3-C8-H8A	110.2
S1-O1	1.447 (2)	C9-C10	1.392 (4)	O3-Fe1-N2	157.05 (9)	C7-C8-H8A	110.2
S1-N3	1.579 (3)	C9-C14	1.410 (4)	N3-Fe1-N2	76.51 (10)	N3-C8-H8B	110.2
S1-C9	1.770 (3)	C10-C11	1.379 (5)	N1-Fe1-N2	74.66 (10)	C7-C8-H8B	110.2
O3-C21	1.283 (4)	C10-H10	0.95	N5-Fe1-N2	74.89 (9)	H8A-C8-H8B	108.5
O4-C21	1.248 (4)	C11-C12	1.384 (5)	O2-S1-O1	116.37 (13)	C10-C9-C14	120.8 (3)
N1-C1	1.347 (4)	C11-H11	0.95	O2-S1-N3	106.07 (13)	C10-C9-S1	117.7 (2)
N1-C5	1.350 (4)	C12-C13	1.372 (5)	O1-S1-N3	112.54 (14)	C14-C9-S1	121.4 (2)
N2-C6	1.468 (4)	C12-H12	0.95	O2-S1-C9	106.94 (14)	C11-C10-C9	120.7 (3)
N2-C15	1.472 (4)	C13-C14	1.411 (4)	O1-S1-C9	105.70 (14)	C11-C10-H10	119.7
N2-C7	1.474 (4)	C13-H13	0.95	N3-S1-C9	108.95 (14)	C9-C10-H10	119.7
N3-C8	1.476 (4)	C15-C16	1.505 (4)	C21-O3-Fe1	113.2 (2)	C10-C11-C12	119.5 (3)
N4-C14	1.368 (4)	C15-H15A	0.99	C1-N1-C5	117.9 (3)	C10-C11-H11	120.2
N4-H4B	0.855 (10)	C15-H15B	0.99	C1-N1-Fe1	124.0 (2)	C12-C11-H11	120.2
N4-H4A	0.860 (10)	C16-C17	1.386 (4)	C5-N1-Fe1	118.0 (2)	C13-C12-C11	120.4 (3)
N5-C20	1.343 (4)	C17-C18	1.378 (5)	C6-N2-C15	111.0 (2)	C13-C12-H12	119.8
N5-C16	1.346 (4)	C17-H17	0.95	C6-N2-C7	113.1 (2)	C11-C12-H12	119.8
C1-C2	1.374 (4)	C18-C19	1.383 (5)	C15-N2-C7	111.9 (2)	C12-C13-C14	121.9 (3)
C1-H1	0.95	C18-H18	0.95	C6-N2-Fe1	107.41 (18)	C12-C13-H13	119.1
C2-C3	1.375 (5)	C19-C20	1.375 (4)	C15-N2-Fe1	108.12 (19)	C14-C13-H13	119.1
C2-H2	0.95	C19-H19	0.95	C7-N2-Fe1	104.94 (18)	N4-C14-C9	123.9 (3)
C3-C4	1.379 (5)	C20-H20	0.95	C8-N3-S1	115.4 (2)	N4-C14-C13	119.4 (3)
C3-H3	0.95	C21-C22	1.495 (5)	C8-N3-Fe1	120.36 (18)	C9-C14-C13	116.7 (3)
C4-C5	1.377 (4)	C22-H22A	0.98	S1-N3-Fe1	116.15 (15)	N2-C15-C16	111.8 (3)
C4-H4	0.95	C22-H22B	0.98	C14-N4-H4B	118 (2)	N2-C15-H15A	109.3
C5-C6	1.503 (5)	C22-H22C	0.98	C14-N4-H4A	123 (2)	C16-C15-H15A	109.3
C6-H6A	0.99	C19-C18-H18	120.6	H4B-N4-H4A	113 (3)	N2-C15-H15B	109.3
C2-C3-H3	120.7	C20-C19-C18	119.0 (3)	C20-N5-C16	118.1 (3)	C16-C15-H15B	109.3
C4-C3-H3	120.7	C20-C19-H19	120.5	C20-N5-Fe1	123.7 (2)	H15A-C15-H15B	107.9
C5-C4-C3	120.3 (3)	C18-C19-H19	120.5	C16-N5-Fe1	118.0 (2)	N5-C16-C17	122.0 (3)
C5-C4-H4	119.9	N5-C20-C19	122.8 (3)	N1-C1-C2	123.1 (3)	N5-C16-C15	116.3 (3)
C3-C4-H4	119.9	N5-C20-H20	118.6	N1-C1-H1	118.4	C17-C16-C15	121.7 (3)
N1-C5-C4	121.3 (3)	C19-C20-H20	118.6	C2-C1-H1	118.4	C18-C17-C16	119.3 (3)
N1-C5-C6	115.4 (3)	O4-C21-O3	122.8 (3)	C1-C2-C3	118.8 (3)	C18-C17-H17	120.3
C4-C5-C6	123.2 (3)	O4-C21-C22	120.6 (3)	C1-C2-H2	120.6	C16-C17-H17	120.3
N2-C6-C5	110.5 (3)	O3-C21-C22	116.5 (3)	C3-C2-H2	120.6	C17-C18-C19	118.8 (3)

N2-C6-H6A	109.6	C21-C22-H22A	109.5	C2-C3-C4	118.5 (3)	C17-C18-H18	120.6
C5-C6-H6A	109.6	C21-C22-H22B	109.5	H6A-C6-H6B	108.1	H22A-C22-H22C	109.5
N2-C6-H6B	109.6	H22A-C22-H22B	109.5	N2-C7-C8	110.4 (3)	H22B-C22-H22C	109.5
C5-C6-H6B	109.6	C21-C22-H22C	109.5	N2-C7-H7A	109.6		

Appendix II: Paramagnetic Susceptibility Calculations

Paramagnetic mass susceptibility of [Fe$^{(II)}$BPAEB$_{NO}$(OAc)].MeCN was calculated based on the NMR Evans method. Used formmulas and tables are as follows:

$$\chi_M^P = \sqrt{\frac{1000\ \delta\nu^P}{\nu_0 S_f m^P}} - \chi_M^{dia}$$

χ_M^P: Paramagnetic mass susceptibility (cm^{3}g^{-1})

$\delta\nu^P$: The shift in frequency (Hz) from the value found for the pure solvent: 0.473 Hz

ν_0: The operating frequency of the NMR spectrometer (Hz): 500 MHz

S_f: The shape factor of the magnet: 4π/3 for a cylindrical sample in a superconducting magnet

m^P: The concentration of the sample (g cm^{-3}): 45.9 mM

χ_M^{dia}: Diamagnetic mass susceptibility

Calculation of diamagnetic mass susceptibility (χ_M^{dia}) for [Fe$^{(II)}$BPAEB$_{NO}$(OAc)]:

C_{24}	H_{26}	N_6	O_5	S	Fe(II)
22-6	23-2.9	2(-4.6)+2(-5.6)-2.1-2.1+1.7	3(-1.7)-30	-15	-13

$$\mu_{eff} = 2.83\sqrt{\chi_M^P . T}$$

μ_{eff} : Effective magnetic moment (Bohr Magneton)

T: Temperature (K): 299.15 K

μ_{eff} = 2.56 B.M and hence the number of unpaired electrons equals 2.

Appendix III: NMR Spectra

^{1}H-NMR of $BPAEB_{NHOH}$ in $CDCl_3$

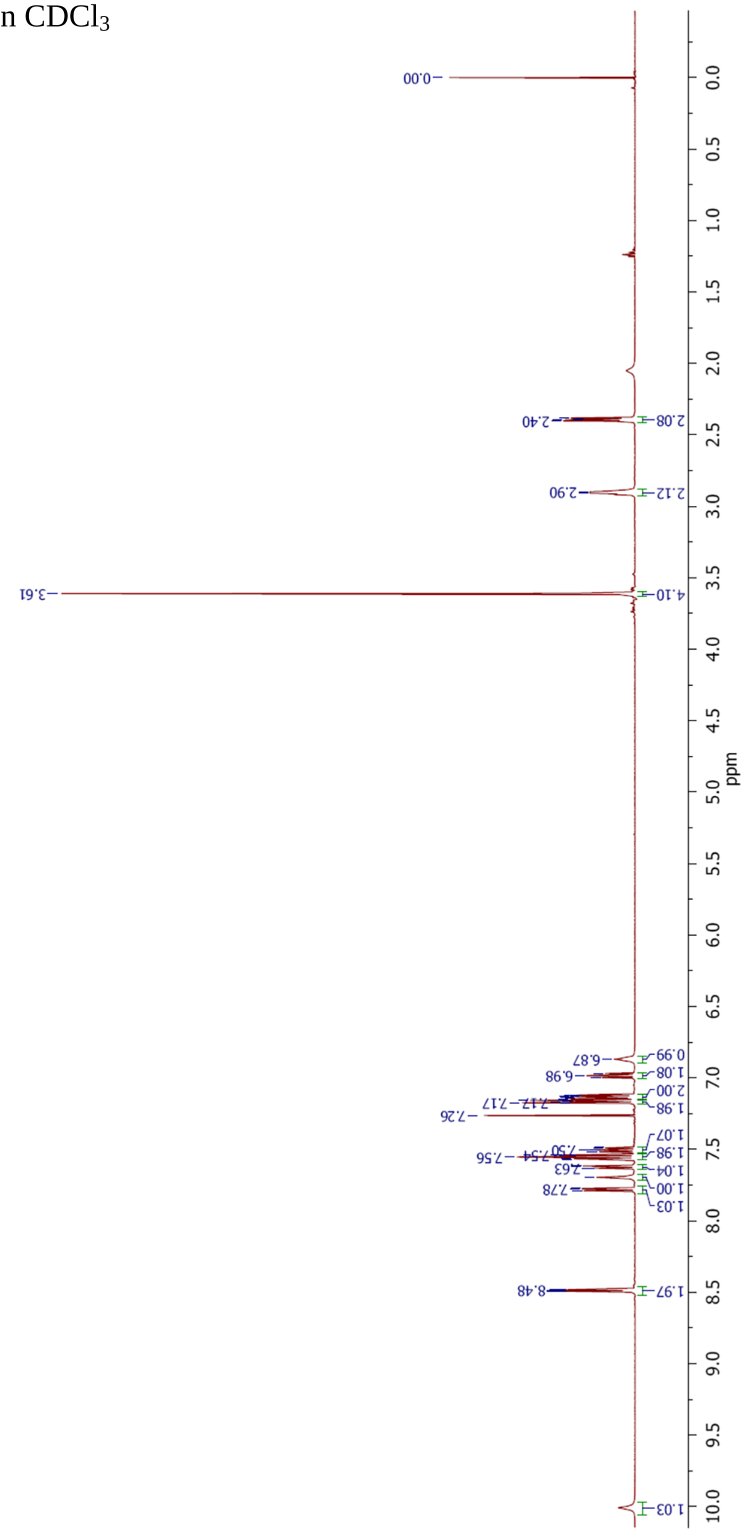

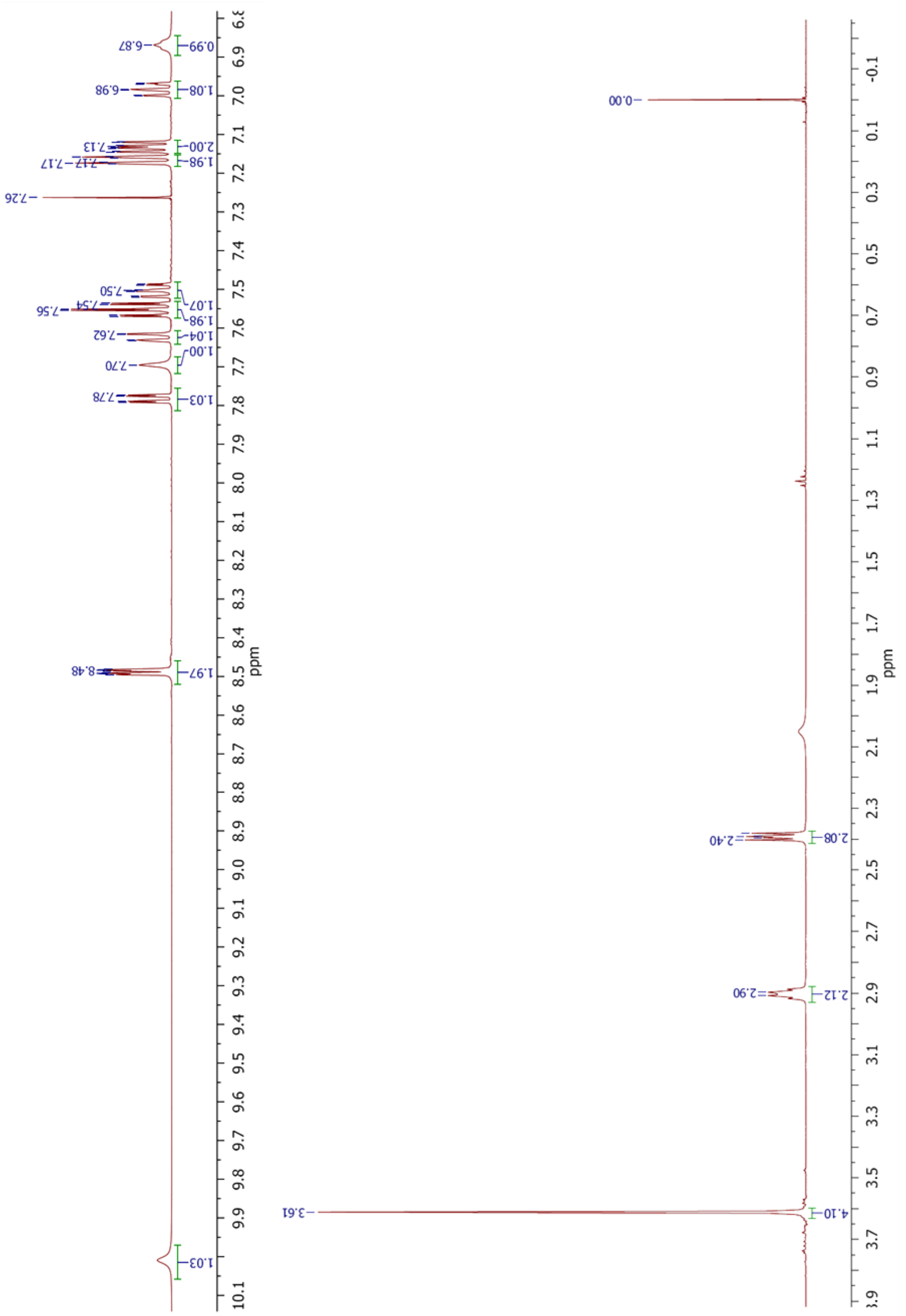
6.87
6.98
7.13
7.17
7.17
7.26
7.50
7.54
7.56
7.62
7.70
7.78
8.48
0.99
1.08
2.00
1.98
1.07
1.98
1.04
1.00
1.03
1.97
1.03
ppm
0.00
2.40
2.90
3.61
2.08
2.12
4.10
ppm

^{1}H-NMR of [Fe$^{(II)}$BPAEB$_{NO}$(OAc)] in CDCl$_3$

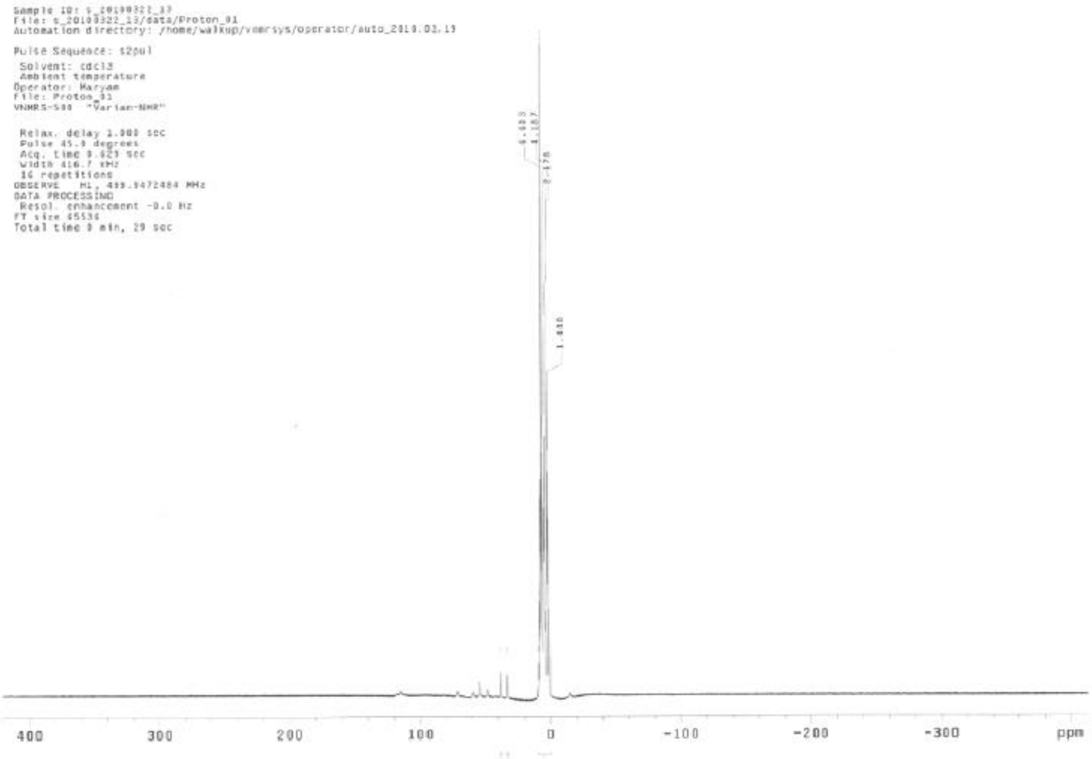

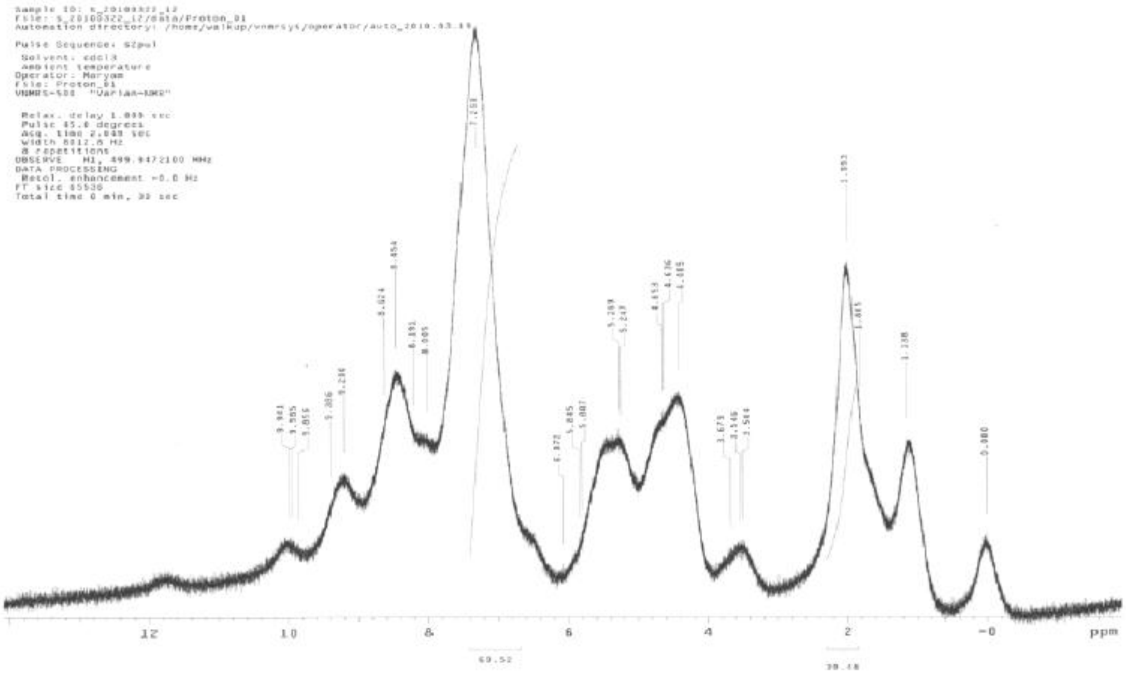

Products of the reaction of [Fe$^{(II)}$BPAEB$_{NO}$(OAc)] with PMe$_3$ in CDCl$_3$ (top: ^{1}H-NMR, bottom: ^{31}P-NMR

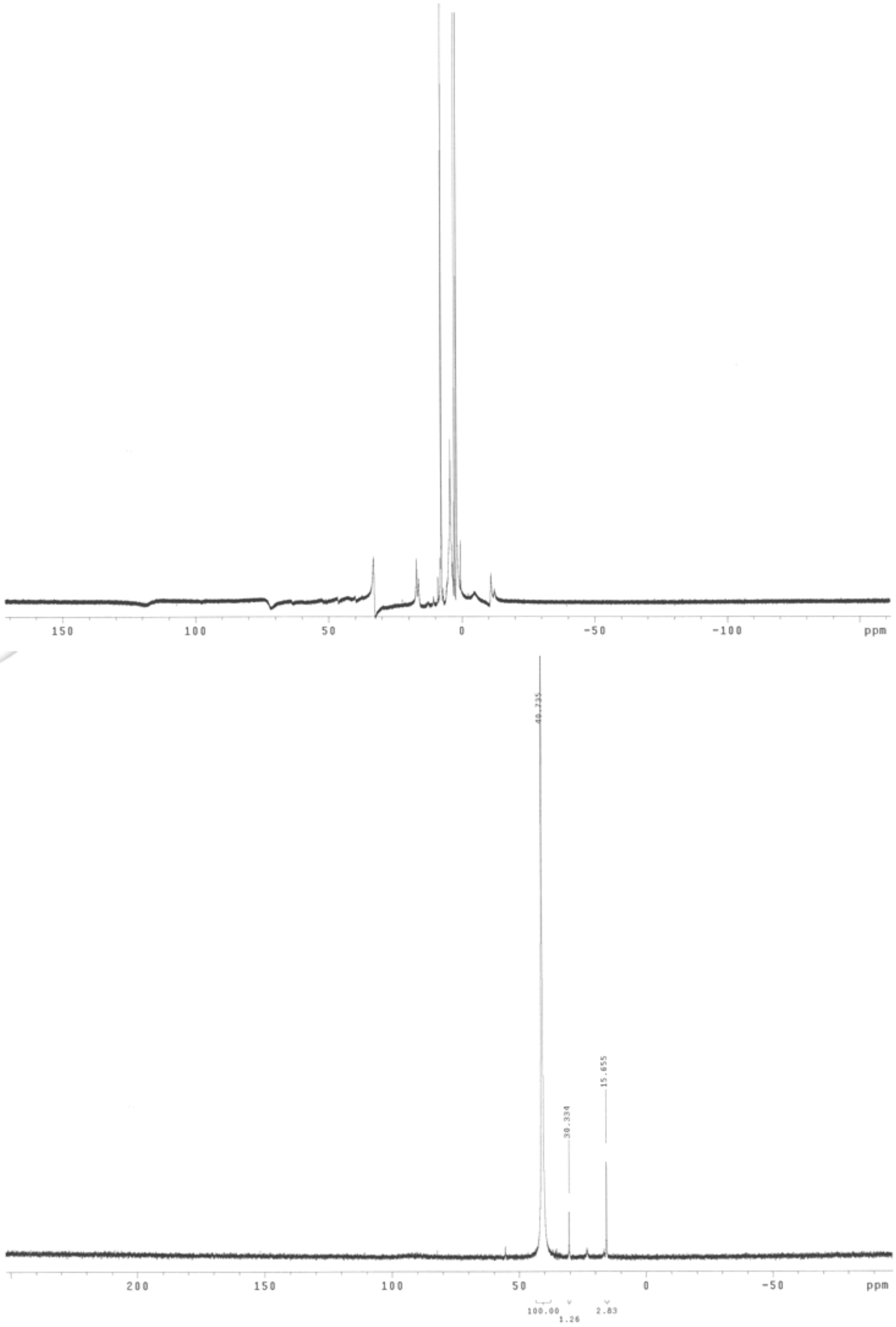

^{31}P-NMR of the reaction of [Fe$^{(II)}$BPAEB$_{NO}$(OAc)] with PMe$_2$Ph in CDCl$_3$

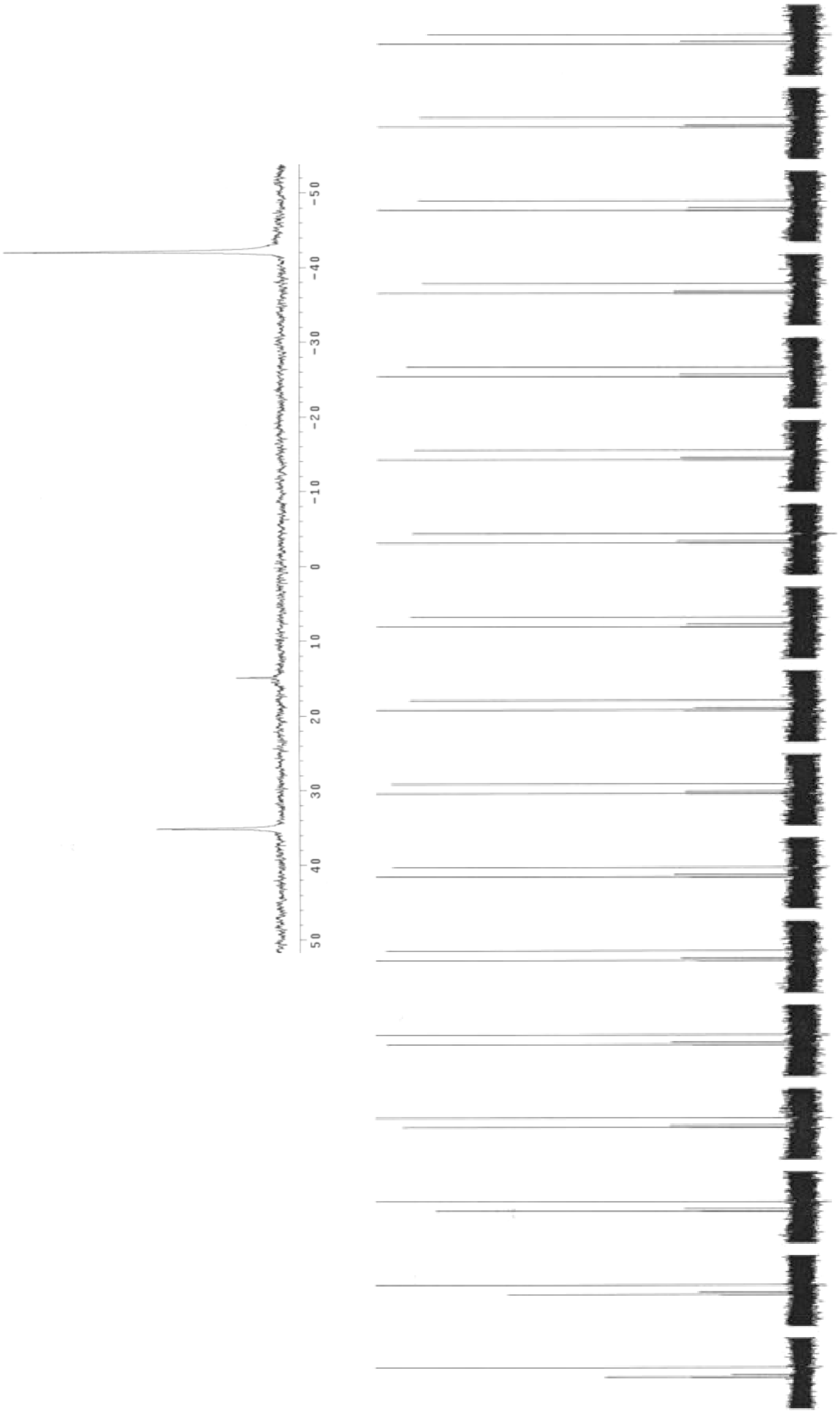

Appendix IV: ESI-Mass Spectra

ESI-Mass spectra of the reaction of [Fe$^{(II)}$BPAEB$_{NO}$(OAc)] with PEtPh$_2$ (left) and PMe$_3$(right)

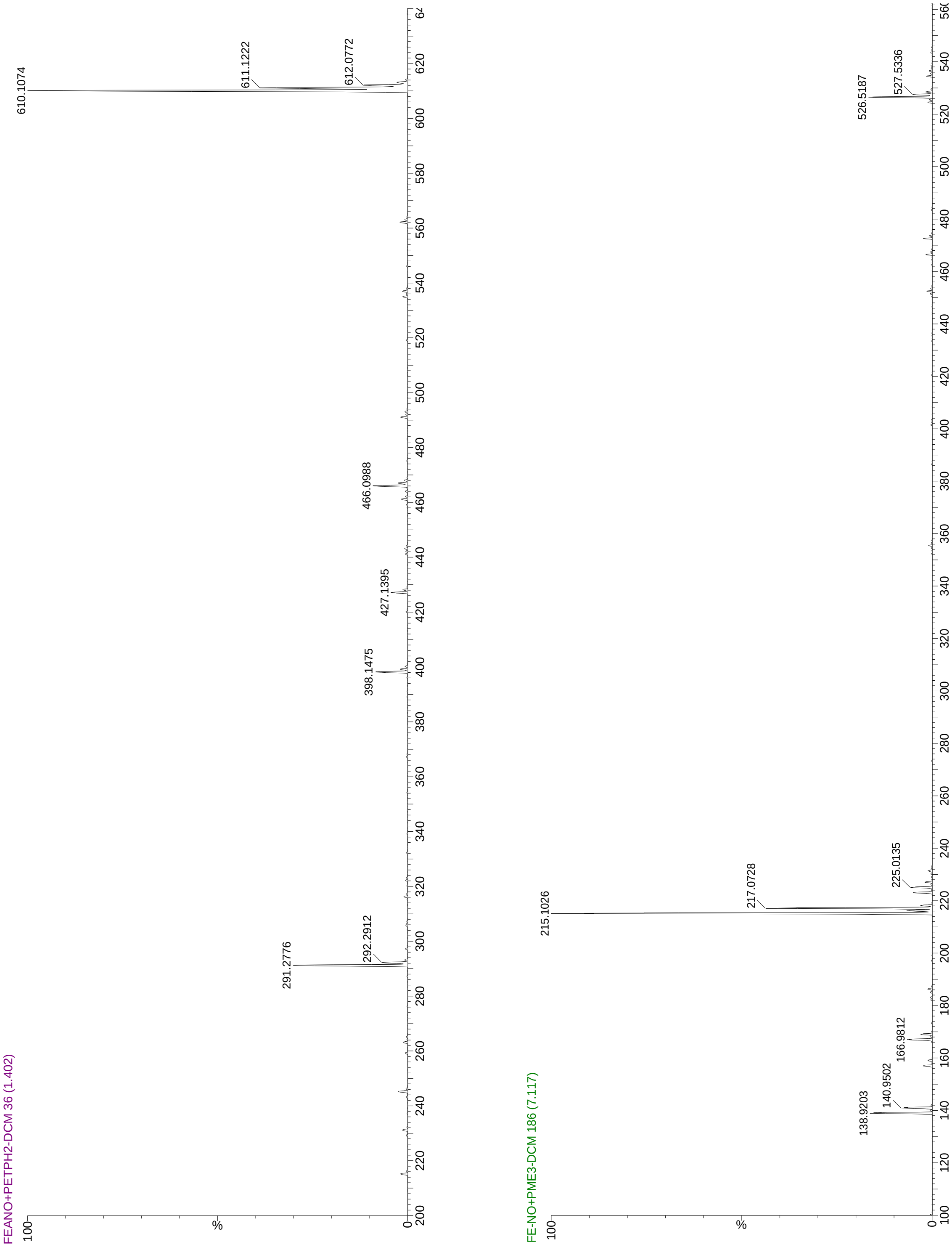

ESI-Mass spectra of the reaction of [Fe$^{(II)}$BPAEB$_{NO}$(OAc)] with PPh$_3$ (left) and PMe$_2$Ph (right)

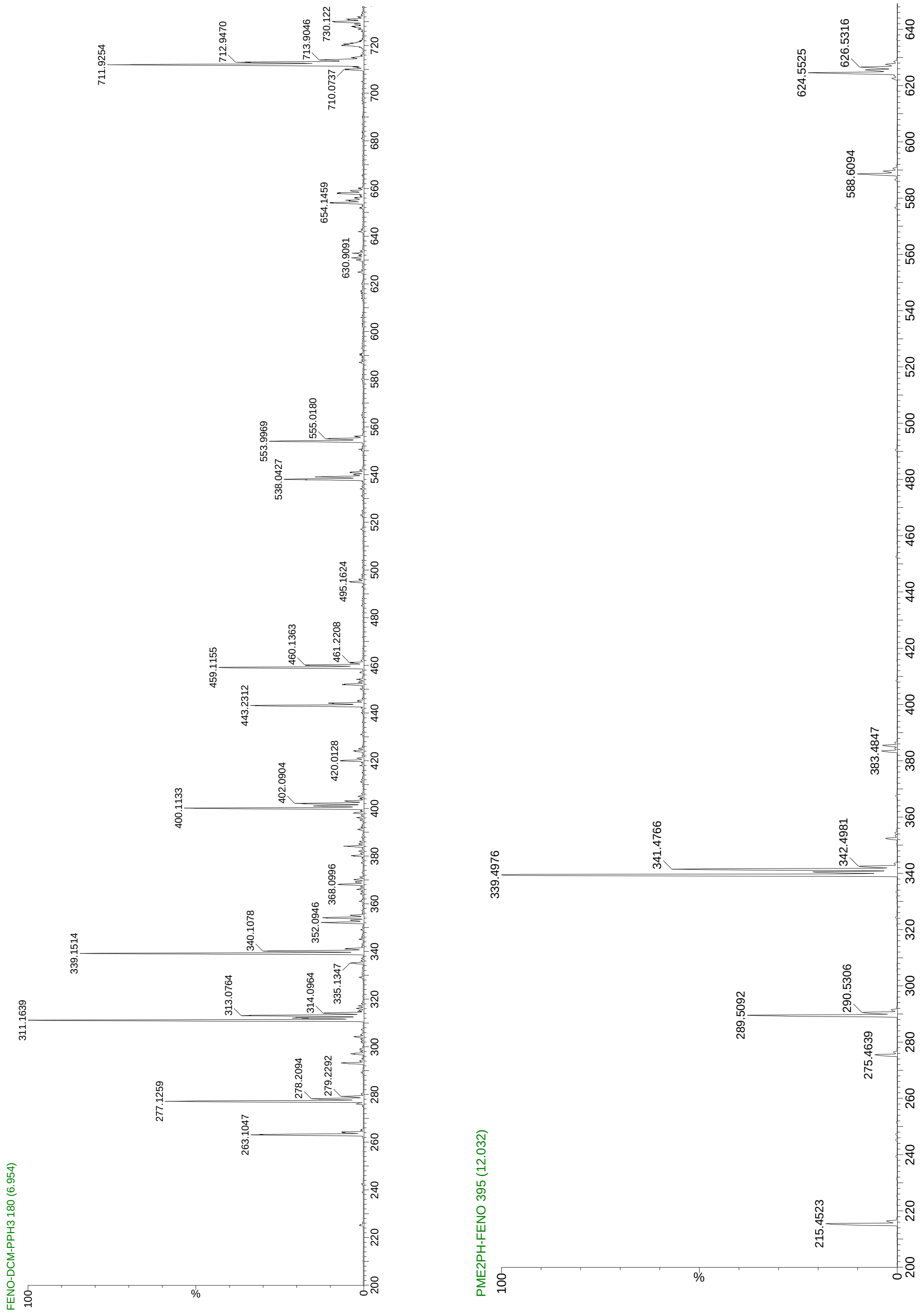

ESI-Mass spectra of [Fe$^{(II)}$BPAEB$_{NO}$(MeCN)](OTf) (left) and [Fe$^{(II)}$BPAEB$_{NO}$(OAc)] (right)

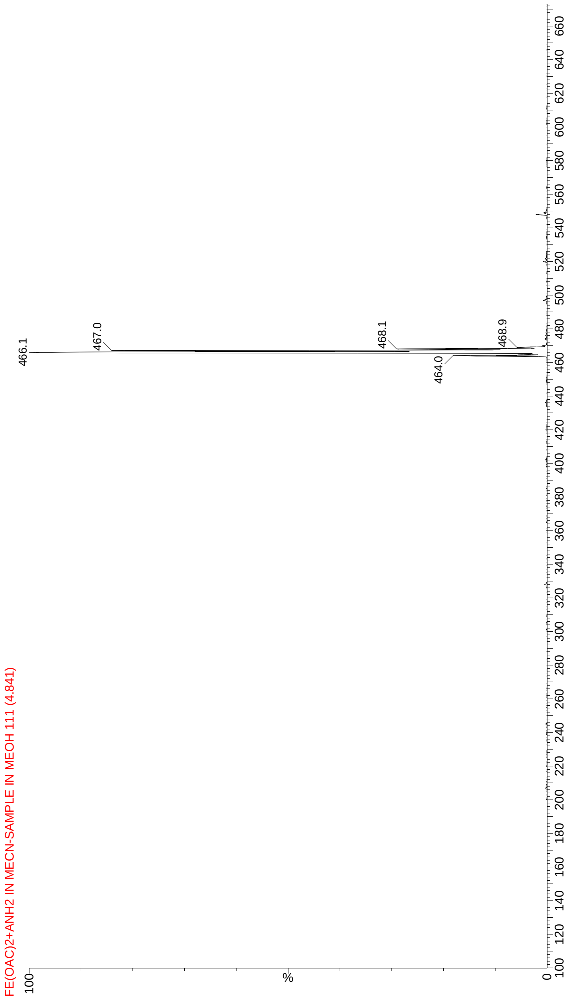

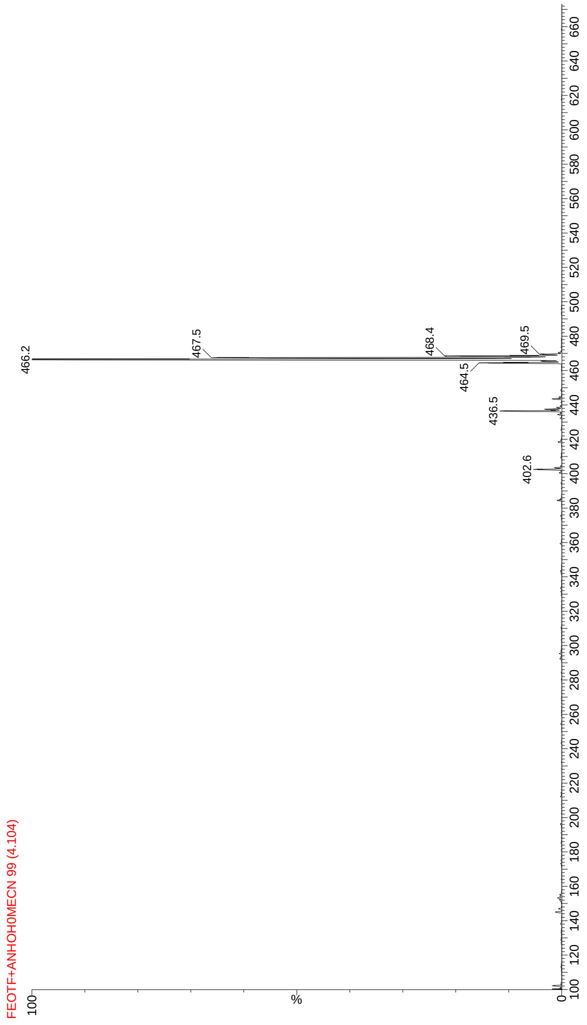

Appendix V: IR Spectra

IR spectrum of [Fe$^{(II)}$BPAEB$_{NO}$(OAc)] complex (KBr pellet)